Universität Hamburg
DER FORSCHUNG | DER LEHRE | DER BILDUNG

Estimating the impact of soil-vegetation feedbacks on the efficiency of combined pyrogenic carbon capture and enhanced weathering

Dissertation
with the aim of achieving a doctoral degree
at the Faculty of Mathematics, Informatics and Natural Sciences
Department of Biology
at University of Hamburg

submitted by

Mikita Maslouski

Hamburg, 2026

University of Hamburg, Faculty of Mathematics, Informatics and Natural Sciences (MIN),
Department of Biology, Institute of Plant Science and Microbiology (IPM)

Date of Oral Defense: 17.04.2026

Reviewers
Prof. Dr. Philipp Porada
Prof. Dr. Christian Beer

Members of the examination commission
Chair Prof. Dr. Kai Jensen
Prof. Dr. Philipp Porada
Prof. Dr. Christian Beer
Prof. Dr. Annette Eschenbach

Chair of the Subject Doctoral Committee Biology: Prof. Dr. Tobias Lenz
Dean of Faculty MIN: Prof. Dr.-Ing. Norbert Ritter

URN: urn:nbn:de:gbv:18-ediss-137215

Eidesstattliche Versicherung | Declaration on Oath

I hereby declare and affirm that this doctoral dissertation is my own work and that I have not used any aids and sources other than those indicated.

If electronic resources based on generative artificial intelligence (gAI) were used in the course of writing this dissertation, I confirm that my own work was the main and value-adding contribution and that complete documentation of all resources used is available in accordance with good scientific practice. I am responsible for any erroneous or distorted content, incorrect references, violations of data protection and copyright law or plagiarism that may have been generated by the gAI.

Ort,den | City,date
Hamburg, 01.12.2025

Unterschrift | Signature

Universität Hamburg
DER FORSCHUNG | DER LEHRE | DER BILDUNG

FACULTY
OF MATHEMATICS, INFORMATICS
AND NATURAL SCIENCES

Declaration about personal contribution to manuscripts/publications in a cumulative thesis (please submit one form per manuscript/publication)

Candidate's name: Mikita Maslouski

Manuscript (including all authors, title, and if applicable journal, year; mark all first authors with asterisk):
Mikita Maslouski*, Annette Eschenbach, Christian Beer, Simon Thomsen, and Philipp Porada (2025). " Soil and vegetation responses to biochar application in terms of its feedback on carbon sequestration under different environmental conditions - LiDELS model overview" . In: Environ. Res. Lett

Link to publication (if published):
https://iopscience.iop.org/article/10.1088/1748-9326/adbfa6

Detailed description of own contribution to this manuscript

Conceptualization and planning of project:
Mikita Maslouski, Philipp Porada and Christian Beer

Method development:
Mikita Maslouski and Philipp Porada

Data generation and analyses (including contribution to specific figures):
Mikita Maslouski, Philipp Porada, Simon Thomsen and Annette Eschenbach

Writing and editing of manuscript:
Mikita Maslouski, Philipp Porada and Annette Eschenbach

I confirm that the above information is accurate

Candidate		**Supervisor name:** Philipp Porada	
13.01.2026	Mikita Maslouski	13.1.26, Hamburg	Philipp Porada
Place, date	Signature of candidate	Place, date	Signature of supervisor

Universität Hamburg
DER FORSCHUNG | DER LEHRE | DER BILDUNG

FACULTY
OF MATHEMATICS, INFORMATICS
AND NATURAL SCIENCES

Declaration about personal contribution to manuscripts/publications in a cumulative thesis (please submit one form per manuscript/publication)

Candidate's name: Mikita Maslouski

Manuscript (including all authors, title, and if applicable journal, year; mark all first authors with asterisk):
Mikita Maslouski*, Maria Ansari, Susanne E. Hamburger, Johannes Meyer zu Drewer, Nikolas Hagemann, Annette Eschenbach, Christian Beer, Joscha N. Becker, Claudia I. Kammann, Maria-Elena Vorrath and Philipp Porada (2025). Long-term carbon dioxide removal potential from the application of wood biochar and basanite rock powder in sandy soil using the LiDELSv2 process-based modeling approach". In: Environ. Res. Lett.

Link to publication (if published):
https://iopscience.iop.org/article/10.1088/1748-9326/ae21f6

Detailed description of own contribution to this manuscript

Conceptualization and planning of project:
Mikita Maslouski, Philipp Porada and Christian Beer

Method development:
Mikita Maslouski and Philipp Porada

Data generation and analyses (including contribution to specific figures):
Mikita Maslouski, Philipp Porada, Maria Ansari, Susanne E. Hamburger, Johannes Meyer zu Drewer, Nikolas Hagemann, Annette Eschenbach and Joscha N. Becker

Writing and editing of manuscript:
Mikita Maslouski, Nikolas Hagemann, Claudia I. Kammann, Maria Ansari, Joscha N. Becker, Maria-Elena Vorrath, Philipp Porada, Susanne E. Hamburger and Annette Eschenbach

---

I confirm that the above information is accurate

Candidate		**Supervisor name:** Philipp Porada	
13.01.2026	Mikita Maslouski	13.1.26, Hamburg	Philipp Porada
Place, date	Signature of candidate	Place, date	Signature of supervisor

Contents

Chapter 1

General introduction

1.1 Pyrogenic carbon and carbonating minerals for enhanced plant growth and carbon capture and storage

Modern climate change refers to the rapid warming of Earth's climate over the past century, driven primarily by human activities such as the burning of fossil fuels, deforestation, intensive agriculture, and industrial processes (Calvin et al., 2023; Al-Ghussain, Loiy, 2019; Keerthi, 2024). This temperature increase is already amplifying weather extremes, sea-level rise and the loss of ice in polar and mountain regions (Calvin et al., 2023; Rohling et al., 2013). Without substantial and rapid reductions in greenhouse gas emissions, these impacts are expected to intensify further in the coming decades, with far-reaching consequences for ecosystems, economies, and human well-being worldwide (Calvin et al., 2023).

Mitigating climate change requires not only sharp reductions in anthropogenic greenhouse gas emissions, but also the deployment of large-scale Carbon Dioxide Removal (CDR) measures (Calvin et al., 2023; S. M. Smith et al., 2024). Integrated assessment models consistently show that negative emissions are necessary to complement emission reductions and offset residual emissions from hard-to-abate sectors (Fuhrman et al., 2019). Current pathways suggest that global CDR must scale to approximately $7 - 9$ $GtCO_2$ yr^{-1} by mid-century to reach net-zero goals (S. M. Smith et al., 2024), offsetting a significant portion of the ~ 40 $GtCO_2$ currently emitted annually by anthropogenic activities (Friedlingstein et al., 2025). Achieving this total capacity relies on a diversified portfolio of CDR methods. While conventional CDR, primarily represented by afforestation and reforestation, already contributes roughly 2 $GtCO_2$ yr^{-1}, it will need to be supplemented by novel methods such as Bioenergy with Carbon Capture and Storage (BECCS), Direct Air Capture (DACCS), Ocean Alkalinity Enhancement (OAE), Pyrogenic Carbon Capture and Storage (PyCCS), and Enhanced Rock Weathering (ERW) (S. M. Smith et al.,

2024). Among novel CDR strategies, PyCCS and ERW stand out due to their potential co-benefits, relatively low technological and economic barriers, and compatibility with agricultural systems (Amann and Hartmann, 2019; S. M. Smith et al., 2024), with a combined potential contribution estimated to around 5 $GtCO_2$ yr^{-1} (Zakkour and Cook, 2024).

The PyCCS approach relies on converting biomass into biochar, a carbon-rich material intended for long-term sequestration in soils (Zhixiang Jiang et al., 2019; Schmidt et al., 2019; Weber and Quicker, 2018). Biochar can be produced from a variety of clean biomass residues, including crop straw, green waste, fermentation residues, and animal manures (Cayuela et al., 2014). Through non-oxidative pyrolysis – thermochemical decomposition under limited oxygen – carbon fixed by plants during photosynthesis is transformed into a chemically recalcitrant form with residence times of centuries to millennia (Howell et al., 2022). Pyrolysis facilities producing biochar can be implemented across a range of scales: from modular, small-scale, farm-level units situated near feedstock sources to centralized industrial plants that leverage existing waste management infrastructure (Jesus Paula et al., 2025; Schmidt et al., 2019). Its application is highly compatible with current agricultural systems, as it follows established organic soil fertilizer practices and can be performed manually or by using standard organic spreaders and tillage machinery (Alma and Altikat, 2024; Major, 2010). Once applied to soils, biochar may alter soil organic carbon (SOC) dynamics via changes in decomposition and plant-derived carbon inputs (Schmidt et al., 2019). When produced from nutrient-rich feedstock or co-applied with fertilizers, biochar can also enhance plant growth, thereby increasing plant-derived carbon inputs (Archontoulis et al., 2016; Schmidt et al., 2021). Improvements in soil physical and chemical properties, including increased water-holding capacity, higher cation exchange capacity, and reduced nitrous oxide emissions, have been widely reported (Joseph et al., 2021).

Silicate rock weathering represents another natural pathway for long-term CO_2 sequestration. During weathering, atmospheric CO_2 is transferred into bicarbonate in the aqueous phase or precipitated as carbonate minerals (Phil Renforth and Henderson, 2017). The ERW accelerates this natural process by applying finely ground silicate rocks to soils, where they react with moisture, CO_2 and biological agents (Hartmann et al., 2013). Current agricultural systems are highly compatible with ERW as spreading rock powder can be performed using existing agricultural machinery, such as liming machines (Skov et al., 2024). The bicarbonate formed during weathering may be transported by rivers to the oceans, where it contributes to long-term carbon storage and helps buffer ocean acidification (Renforth and J. S. Campbell, 2021). In addition to carbon sequestration, rock amendments can enhance soil structure, increase nutrient availability, and support SOC stabilization, thereby improving crop yields (Buss et al., 2022; Dupla et al., 2024). Increased plant productivity enhances CO_2 uptake by vegetation and may further strengthen the net carbon sink (Dupla et al., 2024; Swoboda et al., 2022).

Co-application or co-pyrolysis of biochar and silicate rock powders (Amann and Hartmann, 2019; Buss et al., 2024) has been proposed as a promising CDR strategy. Biochar may improve soil aeration and microbial activity, potentially accelerating geochemical weathering reactions (Amann and Hartmann, 2019). However, under certain conditions, such as in compacted soils or when high application rates of fine biochar particles are used, biochar can reduce pore connectivity or induce hydrophobicity, thereby slowing water-mineral interactions and inhibiting weathering (Obia et al., 2017; Vitková et al., 2024). Recent field experiments highlight the complexity of these interactions: while Ansari et al. (in prep.) found that biochar was the primary driver of changes in soil carbon dynamics in co-pyrolyzed and co-applied systems, Honvault et al. (2024) observed that basalt amendments dominated responses in terms of nutrient availability and plant biomass. These contrasting results illustrate that outcomes depend on amendment ratios, mineralogy, pyrolysis conditions, and soil properties.

To translate these multi-process interactions into quantitative expectations over management and climate-relevant timescales, a mechanistic framework is required that links amendment-driven changes in soil physical conditions to vegetation and microbial responses, and, where applicable, to weathering microenvironments. This motivation provides the basis for the process-based modeling approach introduced in the following section.

1.2 The necessity of process-based modeling to estimate long-term soil-vegetation feedbacks

Predicting the ecosystem-level impacts of biochar and rock powder application is essential for assessing their individual and combined CDR potential. However, the complexity of soil-microbe-vegetation interactions makes it difficult or impossible to quantify these effects through experimentation alone. Process-based modeling therefore plays a central role in evaluating mechanisms and feedbacks that are challenging or impossible to measure directly. For example, Dil and Oelbermann, 2014 applied the CENTURY model to assess SOC dynamics under agricultural management practices. Soil hydraulic responses to biochar have been simulated extensively with the HYDRUS model (Filipović et al., 2020; Horel et al., 2019; Stylianou et al., 2021; Thao et al., 2023; Y. Wu et al., 2019). More recently, Bertagni et al., 2025 introduced the Soil Model for Enhanced Weathering (SMEW), a dynamic ecohydrological and biogeochemical model for quantifying alkalinity release, pH evolution, and CO_2 sequestration.

A further motivation for modeling arises from the fragmented nature of empirical studies. Field and laboratory experiments typically isolate specific processes – such as soil water retention, microbial respiration, crop performance, or mineral dissolution – without capturing the full set of interactions that jointly govern carbon cycling. Modeling

approaches help link these interdependent mechanisms, providing an integrated perspective on how soil, vegetation, microbes, and minerals collectively shape ecosystem carbon dynamics. For example, Thao et al., 2023 related biochar-induced changes in soil water content to crop yield, while Taylor et al., 2011 modeled plant-fungus interactions that enhance silicate weathering. Meanwhile, large-scale frameworks such as EPIC (Lychuk et al., 2014) and APSIM (Archontoulis et al., 2016) have linked biochar-induced changes in SOM to crop yields, soil hydrology, and greenhouse gas emissions.

Finally, modeling allow to explore temporal scales far beyond those accessible in experimental settings. Field and laboratory studies are inherently limited to years or decades (Marazza et al., 2022), while many CDR processes – including mineral weathering, biochar aging, and slow changes in SOC stocks – operate over centuries to millennia. Models such as RothC have been used to explore long-term biochar decomposition under changing environmental conditions (Lefebvre et al., 2020). Global models of silicate weathering explore present and future weathering fluxes (C. Li et al., 2022; Taylor et al., 2016).

Despite the wide range of available biochar (Ronix et al., 2025) and enhanced weathering models (Taylor et al., 2017), no explicit process-based modeling framework exists that jointly represents the interactions among soil physics, microbial dynamics, vegetation productivity, and mineral dissolution while quantifying their combined effects on long-term carbon sequestration. For instance, the SMEW model provides high-resolution geochemical insights into alkalinity release and a novel method for calculating plant nutrient uptake, yet it excludes microbial dynamics and employs simplified representations of soil physics and Net Primary Production (NPP) processes. Similarly, while HYDRUS remains the "gold standard" for simulating soil water and heat transport, it primarily treats vegetation as a passive "water sink" (transpiration) and lacks carbon cycle integration, such as SOC dynamics and NPP, which is essential for long-term CDR accounting. Furthermore, while agricultural and carbon models like CENTURY and RothC have been instrumental in assessing SOC variations and biochar decomposition, and more complex frameworks like EPIC and APSIM have successfully linked biochar application to crop yields and soil hydrology, these models generally lack the capacity to simulate the specific geochemical pathways of mineral weathering or long-term biochar stabilization.

This gap is critical because, at the ecosystem scale, the carbon balance emerges from the interplay between plant carbon uptake, microbial decomposition, and soil physical and chemical processes. Vegetation determines the primary carbon input to soils through NPP and litter deposition, while root systems influence soil structure, water uptake, and rhizosphere conditions (Maaroufi, 2016). Microbial communities control the turnover of soil organic carbon through respiration, with activity strongly regulated by soil moisture, temperature, and aeration (E. M. Ryan et al., 2018). Consequently, amendment-induced changes in soil physical properties, such as porosity, water retention, and thermal regimes, can propagate through plant and microbial responses to alter ecosystem-scale CO_2 fluxes

and long-term carbon storage (Maslouski et al., 2025b). In addition, biotic processes may influence mineral weathering and alkalinity generation through root exudation, microbial metabolism, and vegetation-driven hydrological fluxes, thereby linking biological activity to inorganic carbon removal pathways (Wild et al., 2022). Although not all of these feedbacks are explicitly represented in existing models, their existence motivates the need for a mechanistic framework that couples soil processes with vegetation and microbial dynamics.

This thesis therefore requires an intermediate-complexity framework that couples soil physics, vegetation carbon processes, and soil CO_2 dynamics and remains computationally feasible for long-term simulations. To address this gap, I developed and applied the LiBry-DETECT Layer Scheme (LiDELS) model. The LiDELS couples vertical soil water and energy dynamics with vegetation carbon assimilation and soil CO_2 production and transport, which is essential because soil moisture and soil CO_2 jointly regulate microbial activity, plant carbon inputs, and weathering microenvironments. The model is intentionally kept at intermediate complexity to remain computationally feasible for transient multi-decadal to millennial simulations and systematic scenario analysis. Model implementation details and parameterization are provided in Chapters 2 and 3.

1.3 Thesis objectives and structure

This dissertation was conducted within the framework of the Pyrogenic Carbon and Carbonating Minerals for Enhanced Plant Growth and Carbon Capture and Storage (PyMiCCS) project, which aims to investigate the carbon dioxide removal potential of biochar-silicate mineral systems (Hartmann et al., 2021) using laboratory, lysimeter, and field experiments.. Within this broader project, process-based modeling is required to integrate experimentally observed changes in soil properties with vegetation and microbial responses and to extrapolate these interactions beyond experimentally accessible temporal and spatial scales. The present thesis contributes to PyMiCCS by developing and applying the LiDELS model, a mechanistic modeling framework designed to quantify soil–vegetation feedbacks and their implications for long-term CDR efficiency of biochar and rock powder amendments. In this thesis, CDR is evaluated primarily through changes in SOC (including persistent pyrogenic carbon), changes in ecosystem CO_2 fluxes, and through the potential generation/export of alkalinity from silicate weathering proxied by calcium leaching.

The specific objectives of this thesis are: (i) to develop and validate a process-based ecosystem model (LiDELS) capable of simulating soil-vegetation feedbacks in amended soils under northern German climate conditions; (ii) to mechanistically assess how biochar-induced changes in soil hydraulic and thermal properties influence NPP, evapotranspiration, and soil respiration in sandy soils; (iii) to quantify the millennial-scale carbon sequestration potential of wood biochar, basanite rock powder, and their combined ap-

plication strategies (co-application and co-pyrolysis) in temperate sandy soils; (iv) to evaluate the synergies and trade-offs between physical soil improvements and chemical weathering processes in determining the net ecosystem carbon balance (NEE); (v) to outline pathways for the spatial upscaling of LiDELS toward assessments of the regional to global CDR potential of biochar and rock amendments under present and future climate conditions.

Structure of the Thesis

This cumulative dissertation is organized into four chapters, comprising a general introduction, two peer-reviewed manuscripts, and a general conclusion.

Chapter 1 (General Introduction) outlines the scientific context of climate change mitigation, terrestrial CDR strategies (PyCCS and ERW), and soil-vegetation-microbe feedbacks. It defines the motivation for using process-based models to overcome the limitations of empirical studies.

Chapter 2 presents the study *"Soil and vegetation responses to biochar application in terms of its feedback on carbon sequestration under different environmental conditions - LiDELS model overview"*, published in *Environmental Research Letters*. This chapter introduces the LiDELSv1 model, validates it using soil and climate data from Hamburg, and investigates medium-term impacts of biochar on soil water retention, soil temperature, microbial respiration, and vegetation productivity.

Chapter 3 presents the study *"Long-term carbon dioxide removal potential from the application of wood biochar and basanite rock powder in sandy soil using the LiDELSv2 process-based modeling approach"*, published in *Environmental Research Letters*. This chapter extends the framework to LiDELSv2 by incorporating modules for silicate weathering (calcium leaching), a biochar decomposition function, and improved representation of soil evaporation. It expands the temporal scope to 1,000 years to quantify long-term CDR outcomes for biochar, basanite rock powder, and their combined application strategies.

Chapter 4 (General Conclusions) synthesizes insights from the preceding chapters, linking mechanistic medium-term soil-vegetation feedbacks with long-term carbon sequestration projections. It discusses limitations of the modeling approach, identifies key processes requiring further refinement, and outlines future research directions. In particular, it describes ongoing efforts toward global upscaling of LiDELS and the development of a model emulator suitable for integration into Earth System Models.

Chapter 2

Soil and vegetation responses to biochar application in terms of its feedback on carbon sequestration under different environmental conditions – LiDELS model overview

Abstract

Biochar application to soil shows promise for enhancing soil properties, increasing crop yields, improving water retention, and promoting carbon sequestration. While the direct effects of biochar on soil properties have been studied to some extent, the overall impact on ecosystem carbon balance remains uncertain, as field and lab studies typically do not account for interactions with vegetation. The LiDELS (LiBry-DETECT Layer Scheme) model offers a process-based approach to assess these soil-vegetation interactions and the potential for carbon sequestration in response to biochar application under diverse environmental conditions. This study presents an overview of the LiDELS model and its application to a sandy soil profile under the climate conditions of northern Germany. LiDELS simulates the impacts of biochar on key soil functions, including water retention, thermal properties, evapotranspiration rates, and net primary production (NPP). Model validation shows strong agreement with observed data for soil moisture, temperature, and CO_2 flux, confirming LiDELS's applicability across varying soil textures, vegetation types, and biochar treatments. Results indicate that biochar application to sandy soil in Hamburg enhances soil water availability by 35%, increases NPP by 6%, raises soil CO_2 by 21%, and has no significant impact on soil respiration or soil temperature. LiDELS thus represents a valuable predictive tool for evaluating environmental feedback of biochar in agriculture and carbon management, supporting sustainable land use practices.

2.1 Introduction

Biochar, a stable form of carbon produced through the pyrolysis of organic material, has several potential benefits. It enhances soil properties for agricultural productivity by improving nutrient availability and increasing water retention (Joseph et al., 2021). Moreover, a primary goal of biochar application is carbon sequestration, thereby aiding in the reduction of greenhouse gas emissions (Zhixiang Jiang et al., 2019; Weber and Quicker, 2018).

The properties of specific biochar types vary based on several factors, including the used raw organic material (feedstock), pyrolysis method, post-pyrolysis modifications, application rate, and environmental conditions (Blanco-Canqui, 2021; Weber and Quicker, 2018). For instance, Acharya et al., 2024 reported significant variability in saturated hydraulic conductivity (K_{sat}), soil water holding capacity (WHC), infiltration rates, and plant-available water (PAW) depending on biochar feedstocks and pyrolysis temperatures across different soil types. The impacts of biochar application can range from increases in these indicators to no effects or even decreases. Blanco-Canqui, 2021 also highlighted considerable variability in carbon sequestration, soil gas emissions, microbial activity, and crop yields, all influenced by the type of biochar treatment, soil properties, and production methods. Such wide variations create uncertainty around the local benefits of biochar applications.

Predicting the outcomes of biochar application is crucial for assessing its potential for carbon sequestration and its broader implications for climate change mitigation. This complexity necessitates the use of modeling studies to evaluate certain effects that are challenging or impossible to measure directly. For instance, Dil and Oelbermann, 2014 utilized the CENTURY model to forecast soil organic carbon (SOC) variations under different agroecosystem management techniques. The RothC model has been applied for long-term biochar decomposition modeling at a regional scale, accounting for varying environmental conditions (Lefebvre et al., 2020). Similarly, the Environmental Policy Integrated Climate (EPIC) model evaluated the impacts of biochar on SOC, cation exchange capacity, pH, and bulk density (Lychuk et al., 2014). The Agricultural Production Systems Simulator (APSIM) further extended the EPIC model by integrating crop yields, CO_2 and N_2O emissions, and changes in plant-available water as feedback to biochar's effects on SOC and crop dynamics across diverse soils and environmental conditions (Archontoulis et al., 2016). Direct changes in soil hydraulic properties due to biochar application have also been extensively investigated using the 1D-HYDRUS model (Filipović et al., 2020; Horel et al., 2019; Stylianou et al., 2021; Thao et al., 2023; Y. Wu et al., 2019).

These altered properties are represented by model parameters describing the soil water retention curve (SWRC) parameters (Van Genuchten, 1980) and/or alterations in K_{sat}. The specific combinations of SWRC parameters changes vary depending on the

measurement data available. For example, Thao et al., 2023 determined hydraulic parameters by fitting them to measured SWRCs before and after biochar treatment, while estimating K_{sat} using soil textural input data and changes in soil bulk density (ρ_{bulk}) via the Rosetta pedotransfer function (Schaap et al., 2001). In contrast, Stylianou et al., 2021 estimated the SWRC for control soil with the Rosetta model, applying measured values of K_{sat} and saturated water content (θ_{sat}) for various biochar treatments. In their pot experiment, Horel et al., 2019 assumed no significant changes in SWRC parameters due to soil homogenization, relying solely on measured changes in K_{sat}. Conversely, Y. Wu et al., 2019 assumed a constant K_{sat} while applying measured SWRC parameters. Filipović et al., 2020 managed to measure changes in both SWRC parameters and K_{sat} in their study.

While various modeling approaches have been applied to assess the effects of biochar on soil hydraulic properties, many studies focus less on the impacts on vegetation, which could benefit from these changes. Vegetation, in turn, influences the carbon sequestration potential of biochar through alterations in soil hydrology and CO_2 emissions. Only Thao et al., 2023 attempted to link cumulative changes in soil water content following biochar application with crop yield. However, their model has limited meteorological input, relying solely on precipitation and evapotranspiration data. This limitation may affect the broader applicability of the model, particularly regarding its ability to address one of the key functions of biochar application: carbon sequestration.

This paper aims to address a key gap in biochar research by examining the impacts of biochar on vegetation and the feedback of vegetation on biochar-associated soil properties, processes, and carbon sequestration. Unlike previous models, our LiDELS (LiBry-DETECT Layer Scheme) model integrates direct changes in the soil water retention curve to assess how soil and vegetation respond to biochar addition. By capturing these dynamics, LiDELS can evaluate feedback loops related to carbon sequestration, including shifts in soil carbon. This model provides a versatile tool for exploring the broader environmental impacts of biochar under varying climate conditions and soil types, making it particularly useful for developing effective carbon management strategies within agricultural systems.

2.2 Model description

The LiDELS (LiBry-DETECT Layer Scheme) model is based on two pre-existing models: LiBry, presented by Porada et al., 2013, and DETECT, introduced by E. M. Ryan et al., 2018. The connection between these models is established through a dynamic soil-vegetation Layer Scheme, as shown in Figure 2.1.

LiDELS is a simple 1D process-based ecosystem model. Soil-atmosphere exchange, as surface energy and water balance, are solved by the LiBry model. Soil is represented as several independent pools (layers), which interact with each other through gas, water,

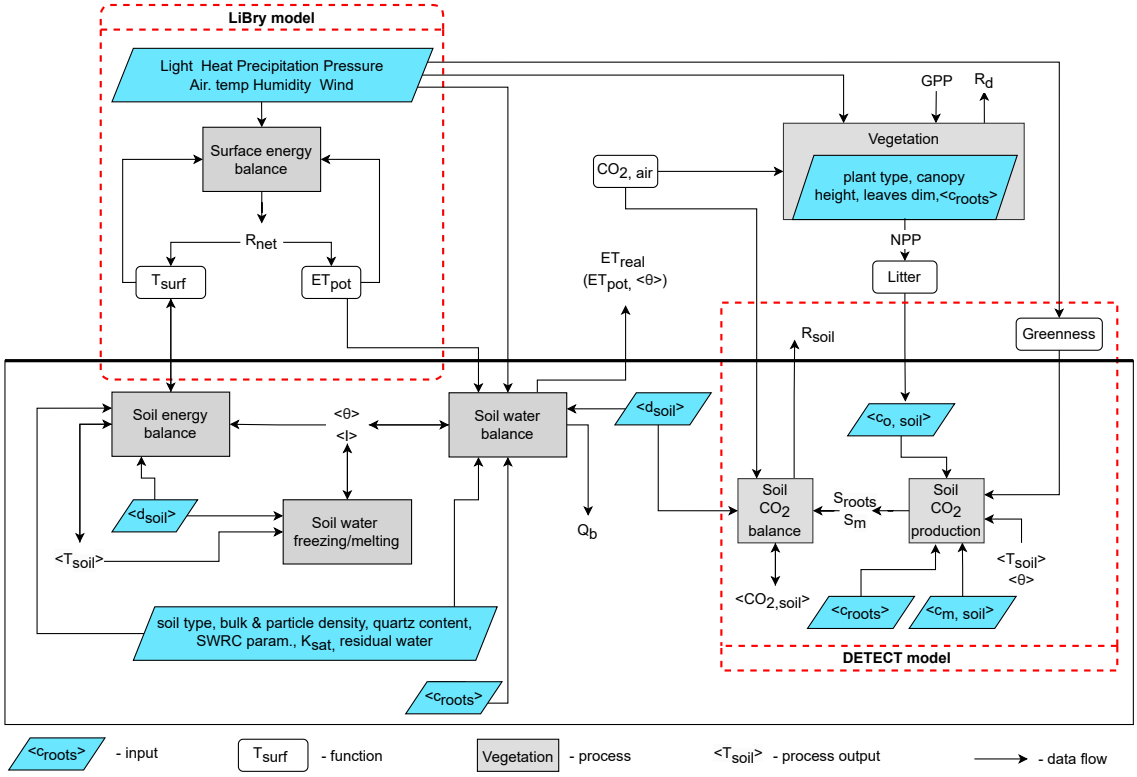

Figure 2.1: Basic LiDELS model process scheme. <> brackets represent value for each soil layer as a vector. R_{net} - net radiation at the top of the soil surface. T - temperature at surface $(_{surf})$ or in soil layer; ET - evapotranspiration potential $(_{pot})$ or real; R - whole plant $(_d)$ or soil CO_2 respiration corresp.; CO_2 - air or soil layer gas concentration; Q_b - seepage; Q_C - weathering rate; θ - soil water content; I - soil ice content; d - soil layer thickness; c - distribution function of soil organic matter $(_o)$, microbes $(_m)$ or roots. For a more detailed scheme see Figure 2.12 in Appendix.

and heat exchange. Vegetation is presented as a photosynthetic CO_2 assimilation process with light and CO_2 limitations (Farquhar et al., 1980). Soil CO_2 production and CO_2 diffusive transport between soil layers is solved by the DETECT model. The model requires the following input parameters:

- **Climate-forcing data**, such as short- and long-wave radiation, precipitation, air pressure, air temperature, humidity, and wind speed.
- **Soil properties**, including soil layer dimensions, soil type, particle and bulk density, quartz/organic/microbe content. A soil layer refers to a part of the soil column with the same soil properties.
- **Vegetation data**, such as plant type, root distribution, canopy height, and leaf dimensions.

2.2.1 LiBry model

LiBry is a process-based dynamic vegetation model designed to simulate soil/surface/atmosphere energy balance interactions involving non-vascular vegetation species such as lichens, bryophytes, and cyanobacteria. It is used to calculate the dynamics of non-vascular vegetation from local to global scale (Y. Ma et al., 2024; Porada et al., 2013), under both current climate conditions and those of the geological past (Porada et al., 2016). The model has also served as the foundation for a process-based vascular vegetation model (Halder et al., 2022).

LiBry calculates potential evaporation and surface temperature based on the approach of Monteith, 1981, utilizing continuous time series data for climate variables such as downwelling shortwave and longwave radiation, precipitation, air temperature, relative humidity, and wind speed, along with site-specific boundary conditions such as roughness length and soil thermal conductivity. The key variables required for these calculations include net radiation, saturation vapor pressure, and aerodynamic resistance to heat transfer (Porada et al., 2013). The detailed connections between these variables are illustrated in Figure 2.12 in Appendix. It should be noted that the LiDELS model employs only the energy and water exchange relationships between the atmosphere, surface, and soil derived from the LiBry model, without incorporating vascular vegetation. For further details on the vegetation modeling approach, see Section 2.2.3.

2.2.2 DETECT model

The DETECT model (DEconvolution of Temporally varying Ecosystem Carbon componenTs) is designed to simulate soil carbon dioxide (CO_2) production and transport within a soil column (E. M. Ryan et al., 2018). It also provides a means to evaluate how total soil respiration can serve as a proxy for total soil CO_2 production (Samuels-Crow et al., 2018). A similar approach to estimating root respiration and gas flux through the soil surface is employed in the MAIZSIM process-based maize crop model (Beegum et al., 2023).

The DETECT model is based on a non-homogeneous partial differential equation that captures the dynamics of CO_2 production and transport in the soil. This mathematical framework allows for a detailed representation of how CO_2 concentrations vary over time and depth in the soil profile. The model simulates CO_2 production from both root respiration and microbial decomposition, accounting for variations in soil water content and temperature that significantly influence these processes.

In contrast to DETECT, the LiDELS model uses a layered or "pool-based" logic instead of a continuous soil profile with fine spatial resolutions. For more information on the layer-based approach, see Section 2.2.3. LiDELS also generates soil water and temperature data internally for each time step, using a distinct methodology for calculating antecedent soil variables compared to the approach employed in DETECT. For further

details on the DETECT model implementation, refer to Section 2.6.1.

2.2.3 Soil-vegetation scheme

In LiDELS, soil is represented as a series of independent layers (pools), each corresponding to a portion of the soil column with uniform soil properties. Using discrete soil layers instead of a continuous profile allows for more efficient numerical calculations and simplifies the application of boundary conditions, enabling adaptive grid refinement and improving accuracy where needed.

For simplicity, equations used in the model are summarized in Table 2.9. For a more detailed representation scheme see Figure 2.12 in Appendix.

Heat transport between soil layers is modeled using the Crank–Nicolson method on a non-uniform grid, as outlined by Bonan, 2019. The surface temperature, calculated by the LiBry model at each time step, serves as the upper boundary condition. To simulate conditions at the lower boundary, an additional layer with identical parameters and temperature to the deepest layer is added, ensuring no heat exchange at that boundary.

Dynamic heat conductivity is implemented following the model by Xiong et al., 2023, which improves upon the original model proposed by G. S. Campbell, 1985. This conductivity dynamically depends on soil physical properties (such as porosity, composition, and texture) and adjusts according to changes in soil water and ice content. The dynamic heat capacity of the soil is calculated as a weighted average of the heat capacities of solids, water, and ice.

Water transport, similarly to the 1D-HYDRUS model (Simunek et al., 2005), is implemented using the Richards equation and the Van Genuchten, 1980 model to calculate the hydraulic conductivity and potential of the soil layers. For each time step, the water balance is calculated based on precipitation and potential evaporation reduced by the amount of available water in the layer (ET_{pot} and ET_{real} in Figure 2.1), along with the remaining water exchange between layers. The model requires the definition of the groundwater level, i.e., the saturated layer, as a boundary condition.

The soil heat and water balance are interconnected through the process of soil water freezing and melting, which depends on the amount of ice and water content in the soil layer, as well as the soil layer's temperature and heat capacity. Additional details can be found in Section 2.6.2 in Appendix.

Vegetation is simulated as a dynamic biomass pool that changes due to the balance of photosynthesis and respiration. Leaf photosynthesis is represented by a widely used mathematical model proposed by Farquhar et al., 1980. The photosynthetic CO_2 assimilation process is limited by light and CO_2, and the photosynthetic capacity of the plant depends on amounts of chlorophyll and Rubisco. Temperature dependencies for light and CO_2 assimilation are based on Bernacchi et al., 2003, 2001. Additionally, the vegetation requires the calculation of two conductances for water vapor - leaf boundary

layer conductance and stomatal conductance. The first is assumed to be proportional to leaf boundary layer conductance for heat, as commonly used (Bonan, 2019). It is calculated based on leaf dimensions and wind speed. Stomatal conductance to water is represented by a soil moisture stress factor that reduces maximum conductance as root zone soil water decreases. Net photosynthesis, or NPP, is estimated by subtracting plant autotrophic respiration from total photosynthesis (GPP).

Carbon assimilated through the photosynthesis process enters the soil organic carbon pool via falling leaves and dead roots. It is assumed that the plant biomass pool is in a steady state, which means that all assimilated carbon finally ends up in the soil organic pool. The litter function redistributes positive cumulative NPP as a constant hourly flux over the next 24 hours to maintain non-negative photosynthesis input. For more details, see Section 2.6.2 in Appendix.

The air CO_2 time trend is based on National Oceanic and Atmospheric Administration (NOAA) measurements in Hawaii, fitted to Gartow, Germany, CO_2 measurements. The function represents seasonal CO_2 changes (sinus part of the function) and can simulate a growing trend if needed (parabolic part of the function). The fits for the air CO_2 function are shown in Figure 2.9 in Appendix.

2.2.4 Model validation

Model validation was conducted by comparing the model outputs with existing published research, focusing on the region of Hamburg, Germany.

For the dependencies of soil water and temperature, we utilized the study by Thomsen, 2018. Using a soil profile and 2-year meteorological data as input, the model predicted soil moisture with reasonable accuracy ($R^2 > 0.55$) and soil temperature with high accuracy ($R^2 > 0.95$). Results are presented in Figure 2.11 in Appendix.

The mean actual evapotranspiration rate (ET_{real}) generated by the model corresponded to the range of $500 - 600$ mm yr^{-1}, as predicted by several studies for this region (Elnashar et al., 2021; Pan et al., 2020).

The mean Gross Primary Production (GPP) predicted by the model was consistent with the estimates for Northern Germany provided by L. Ma, 2020. For the sample model based on Hamburg's meteorological conditions and soil data, the mean GPP value was approximately 1 kgC m^{-2} yr^{-1}, with a GPP/NPP ratio of 0.58.

Verifying soil CO_2 profiles and production is challenging due to the limited number of available studies. The closest comparison comes from the study by Wordell-Dietrich et al., 2020, which investigated forest soils with much higher water retention capacity. The reported annual soil CO_2 flux of 700 gC m^{-2} yr^{-1} was comparable to the LiDELS model prediction for Hamburg conditions (935 gC m^{-2} yr^{-1}). While these values are within the same general range, the comparison remains too coarse to capture short-term variations, such as changes occurring over the past few years. Additionally, soil CO_2 concentrations

were several times higher, reaching up to 40,000 ppm at near-surface depths.

To illustrate the uncertainty in soil CO_2 flux estimates, we also reference a study by Poyda et al., 2016, which reported CO_2 fluxes around 2000 gC m^{-2} yr^{-1} for fen soils used for forage production in northern Germany.

To validate soil CO_2 production under Hamburg conditions, we referred to the study by E. M. Ryan et al., 2018, which applied the DETECT model to sandy soil (80 % sand, 10 % clay). The resulting CO_2 production rates were similar for comparable soil water content and organic content, confirming the model's accuracy for this soil type.

Table 2.1: Parameters from Šurda et al., 2024 used in our modeling study

Name	Product of origin	Porosity [-]	K_{sat} [cm h^{-1}]	α [cm^{-1}]	n [–]
Control	-	0.371	48.93	0.157	1.76
B300	willow	0.411	39.18	0.211	1.49
B520	willow	0.398	34.65	0.193	1.52
B550	fiber sludge and grain husks	0.403	45.18	0.229	1.49

2.2.5 Simulation setup

In their study, Šurda et al., 2024 show how biochar produced at different temperatures (from 300 °C to 550 °C) and different feedstocks (willow or fiber sludge and grain husks) changes the sandy soil SWRC and K_{sat} parameters for application rate 1% weight/weight. The soil they used (91 % sand, 1.5 % clay) is very similar to the upper soil layers found in Hamburg, as presented by Thomsen, 2018. By modifying these parameters for the upper layer of the simulated soil profile, we aim to study how they influence the model outputs. See Table 2.1. for a summary of the data used.

For the sample soil profile, we use the suburban dry grassland soil profile measured by Thomsen, 2018. To calculate the soil profile's SWRC and K_{sat} parameters, we used the Rosetta model. Data are summarized in Table 2.2. For calculating the dynamic heat conductivity, we chose $R = 1.2$, as proposed for sandy soils by the Xiong et al., 2023 model. The R parameter refers to the physical properties of the soil. We assumed that biochar would be applied and mixed with the second layer of our sample soil profile ($4 - 25$ cm). Therefore, the properties of this layer were adjusted to match those of the soil used by Šurda et al., 2024.

For the DETECT model parameters, we followed those proposed by E. M. Ryan et al., 2018 in their original model for mixed-grass prairie with mixed C3 and C4 vegetation. This includes measured values for total soil microbes, root biomass profile, and empirical parameters in production functions. We adjusted the total soil carbon amount from 712 mgC in a 1 cm^2 column of soil 1 m deep to 1000 mgC, as it is a more characteristic local value (Poeplau et al., 2020). For the vegetation component, we used sample parameters

Table 2.2: Sample soil profile used in model simulation. Physical soil profile data based on measurements by Thomsen, 2018. Soil water retention parameters astimated by Skaggs and Ghane, 2017 Rossetta model and Bonan, 2019.

Depth	Soil texture [%]			Porosity	ρ_{bulk}	α	n	K_{sat}
[cm]	Sand	Silt	Clay	[%]	[g cm^{-3}]	[cm^{-1}]	[-]	[cm h^{-1}]
4	92.6	6.4	1.0	31.6	1.3	0.167	1.906	31.6
25	91.0	7.5	1.5	48.9	1.6	0.157	1.761	48.9
50	90.0	8.3	1.7	47.8	1.4	0.157	1.875	21.6
100	94.5	2.2	3.4	43.1	1.5	0.124	2.228	28.4
300	96.2	2.8	1.1	43.6	1.5	0.128	2.440	39.9

for C3 vegetation (Bernacchi et al., 2003, 2001; Bonan, 2019), which matched the regional GPP.

For the model run, we used the ECMWF ERA-5 40-year climate dataset (Hersbach et al., 2020) with a temporal resolution of one hour. In the Hamburg region, this dataset provides uniform climate data for an area of approximately 580 km^2. Since the LiDELS model does not incorporate a biochar degradation function, we are unable to simulate the long-term effects of biochar application. However, given the variability in long-term meteorological conditions, we are able to model the middle-term impact of biochar on seasonal fluctuations in the model outputs. The hourly data outputs were first aggregated into daily values, and then, for each day of the year, an average value was calculated by comparing it with the corresponding days across all 40 years of the simulation. This approach effectively downscales high-frequency data outputs while simultaneously reducing noise and potential anomalies thereby enhances model reliability.

While the model simulates the entire soil column described in Table 2.2, only the top 1 m (first four layers) is shown, as it exhibits the most significant variations and is most relevant for the analysis.

2.3 Results

2.3.1 Soil water

The impacts of biochar on soil water content are shown in Figure 2.2 and summarized for the application layer (θ_2) and the layer above it (θ_3) in Table 2.3. Biochar addition significantly increases water availability in the application layer, retaining more water. For low-temperature willow biochar (B300), the maximum change in mean water content is 0.14±0.01, compared to 0.104±0.006 in the control, representing an approximately 35% increase in mean annual layer water content. The maximum amount of plant-available water is also shifted from the third layer to the second, where biochar is applied. Although biochar addition increases water availability within the soil profile, it does not affect the

total amount of water stored in the soil column. Statistically, only the low-temperature biochar (SB300) differs from the others, while SB520 and SB550 have similar effects on mean annual water content.

Table 2.3: Mean annual soil water content for the application layer (θ_2) and the layer above (θ_3). Standard deviations represent the variability of these variables over a 40-year simulation. Different letters within a column indicate significant differences between samples ($p < 0.05$)

	$\langle\theta_2\rangle$ [-]	$\langle\theta_3\rangle$ [-]
Control	$0.104 \pm 0.006^{\,a}$	$0.134 \pm 0.007^{\,a}$
B300	$0.140 \pm 0.010^{\,b}$	$0.124 \pm 0.007^{\,b}$
B520	$0.135 \pm 0.010^{\,c}$	$0.125 \pm 0.007^{\,b}$
B550	$0.135 \pm 0.010^{\,c}$	$0.125 \pm 0.007^{\,b}$

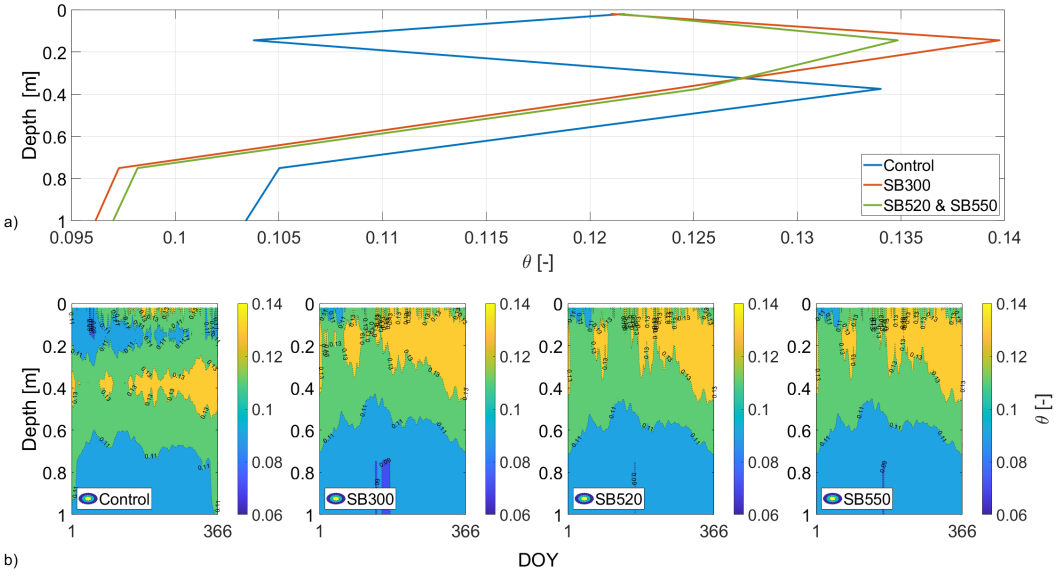

Figure 2.2: Mean annual soil water content for control soil and three biochar treatments. Profile a) represents the mean value for an average year, while the contour plots b) represent seasonal changes during the average year. For the SB520 and SB550 biochar treatments, the changes are not distinguishable at this scale.

2.3.2 Soil temperature

The impacts on soil temperature are shown in Figure 2.3 and summarized for the application layer (T_2) and the layer above (T_3) in Table 2.4.

Biochar addition slightly increases soil temperature in the application layer and the layer below during the middle of the average year, but for annual temperatures, there are no significant differences between treatments. The temperature increase can be attributed

Table 2.4: Mean annual soil temperatures for the application layer (T_2) and the layer above (T_3). Standard deviations represent the variability of these variables over a 40-year simulation. Different letters within a column indicate significant differences between samples ($p < 0.01$)

	$\langle T_2 \rangle$ [deg C]	$\langle T_3 \rangle$ [deg C]
Control	$9.7 \pm 1.0^{\,a}$	$9.7 \pm 0.9^{\,a}$
B300	$10.1 \pm 1.1^{\,a}$	$10.0 \pm 1.0^{\,a}$
B520	$10.1 \pm 1.1^{\,a}$	$10.0 \pm 1.0^{\,a}$
B550	$10.1 \pm 1.1^{\,a}$	$10.0 \pm 1.0^{\,a}$

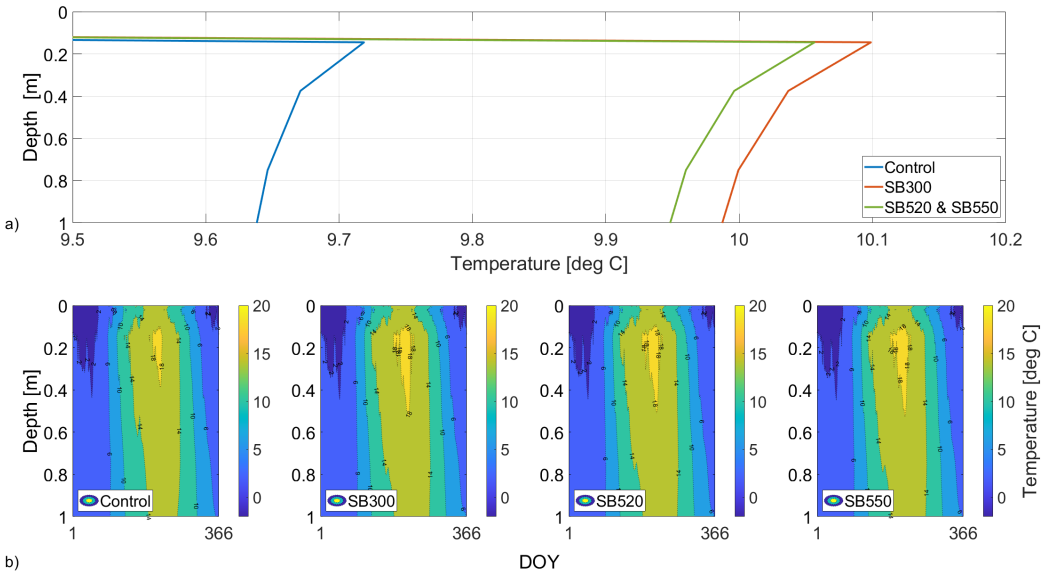

Figure 2.3: Mean annual soil temperature for control soil and three biochar treatments. Profile a) represents the mean value for an average year, while the contour plots b) represent seasonal changes during the average year. For the SB520 and SB550 biochar treatments, the changes are not distinguishable at this scale.

to the higher thermal capacity of the soil resulting from increased soil water content, which enhances the soil's ability to store heat more effectively.

2.3.3 Soil CO_2

Effects of biochar on soil CO_2 concentration are shown in Figure 2.4 and summarized for the application layer ($CO_{2,2}$) and the layer above ($CO_{2,3}$) in Table 2.5. Biochar addition significantly increases soil CO_2 concentration, starting from the application layer and extending deeper. The increase, comparing B550 and control soil, was 1215 ± 172 ppm and 1005 ± 108 ppm, respectively, for the $4-25$ cm layer - representing an increase of more than 21%. The increased amount of soil water enhances microbiological activity in the DETECT model, stimulating CO_2 production. On the other hand, more water in

the soil layer decreases soil gas diffusion. As a result, CO_2 produced by microbial and root respiration accumulates below the saturated soil, leading to higher CO_2 concentrations.

Table 2.5: Mean annual soil water temperatures for the application layer ($CO_{2,2}$) and the layer above ($CO_{2,3}$). Standard deviations represent the variability of these variables over a 40-year simulation. Different letters within a column indicate significant differences between samples ($p < 0.01$)

	$\langle\ CO_{2,2}\ \rangle$ [ppm]	$\langle\ CO_{2,3}\ \rangle$ [ppm]
Control	$1005 \pm 108^{\,a}$	$1117 \pm 125^{\,a}$
B300	$1211 \pm 177^{\,b}$	$1303 \pm 189^{\,b}$
B520	$1210 \pm 174^{\,b}$	$1304 \pm 191^{\,b}$
B550	$1215 \pm 172^{\,b}$	$1309 \pm 189^{\,b}$

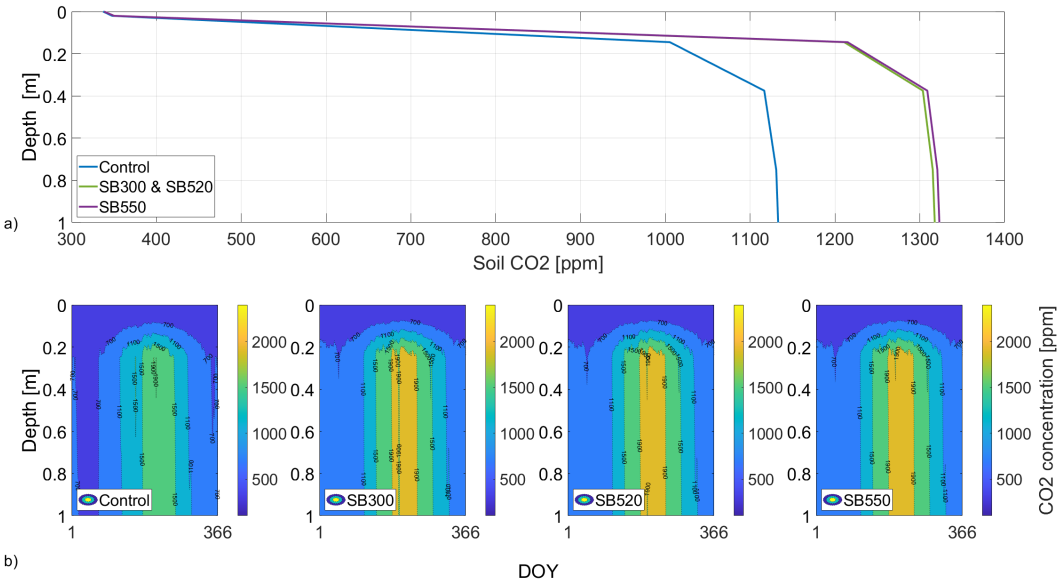

Figure 2.4: Mean annual soil CO_2 concentration for control soil and three biochar treatments. Profile a) represents the mean value for an average year, while the contour plots b) represent seasonal changes during the average year. For the SB300 and SB520 biochar treatments, the changes are not distinguishable at this scale.

Higher soil CO_2 concentrations do not significantly lead to higher soil CO_2 emissions, as shown in Figure 2.5 and summarized in Table 2.6. Since the exchange between the soil and the atmosphere occurs due to differences in carbon dioxide concentration near the surface, the soil profile indicates that the CO_2 concentration at the surface has not changed significantly, which does not result in a notable increase in CO_2 emissions.

Table 2.6: Mean annual soil CO_2 flux for control soil and three biochar treatments. Standard deviations represent the variability of these variables over a 40-year simulation. Different letters indicate significant differences between samples ($p < 0.01$)

	$\langle\ R_{soil}\ \rangle$ [gC m^{-2} y^{-1}]
Control	$935 \pm 101\,^{a}$
B300	$945 \pm 118\,^{a}$
B520	$942 \pm 115\,^{a}$
B550	$943 \pm 114\,^{a}$

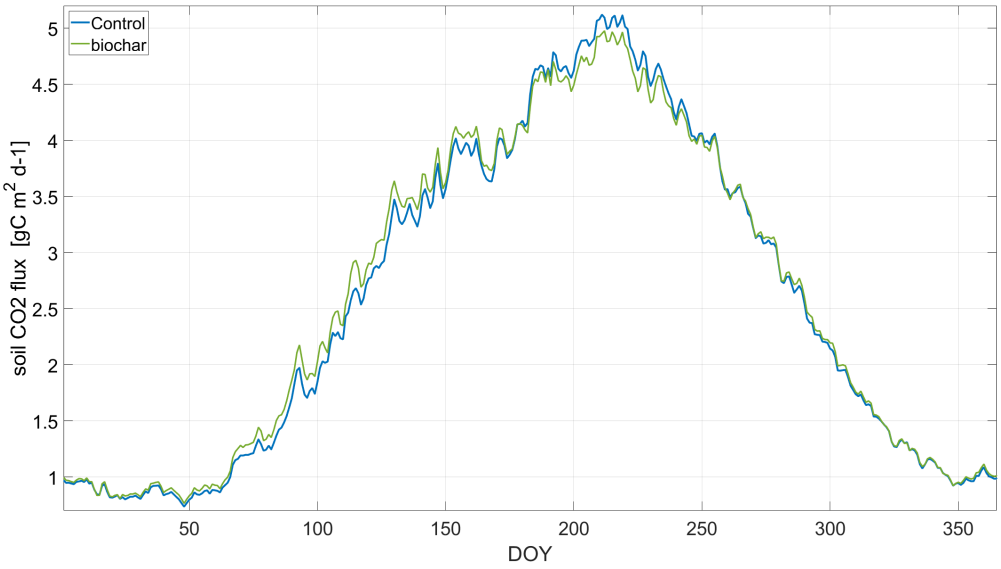

Figure 2.5: Mean annual soil CO_2 flux for control soil and three biochar treatments. All biochar treatments lead to very similar changes at this scale.

2.3.4 Seepage and evapotranspiration

The impacts on annual seepage rate and evapotranspiration are shown in Figures 2.6 and 2.7 and summarized in Table 2.7.

Biochar addition significantly increases evapotranspiration rates and decreases seepage across all three treatments. For high-temperature willow biochar (B520), the change is an increase in evapotranspiration of approximately 109 mm yr^{-1}, with an equivalent decrease in seepage rate from 274 mm yr^{-1} in the Control soil to 165 mm yr^{-1}. Although biochar addition does not impact the total amount of water stored in the soil column, as noted earlier, the proportions of fluxes out of the system are shifted. With biochar treatment, more water is retained in the second layer, where a large amount of root mass is prescribed, making it more available to plants and enhancing their productivity and transpiration rates. While there is a significant difference between the control and biochar-amended soils, the different biochar treatments do not show statistically significant differences from

each other.

Table 2.7: Mean annual seepage and evapotranspiration for control soil and three biochar treatments. Standard deviations represent the variability of these variables over a 40-year simulation. Different letters within a column indicate significant differences between samples ($p < 0.01$)

	$\langle\, Q_b \,\rangle$ [mm yr^{-1}]	$\langle\, ET_{real} \,\rangle$ [mm yr^{-1}]
Control	$274 \pm 73\,^{a}$	$505 \pm 49\,^{a}$
B300	$165 \pm 54\,^{b}$	$614 \pm 66\,^{b}$
B520	$177 \pm 56\,^{b}$	$603 \pm 64\,^{b}$
B550	$176 \pm 57\,^{b}$	$603 \pm 64\,^{b}$

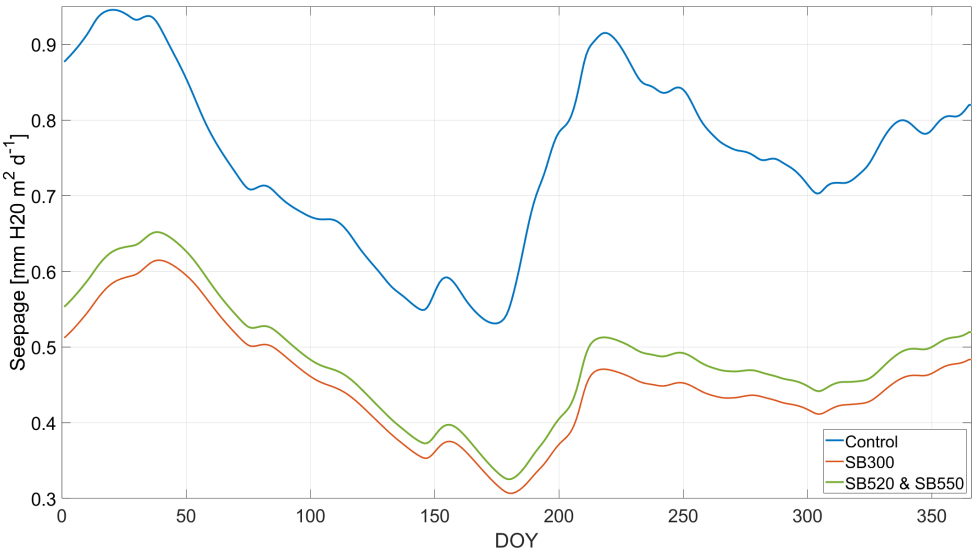

Figure 2.6: Mean annual seepage rate for control soil and three biochar treatments. For the SB520 and SB550 biochar treatments, the changes are not distinguishable at this scale.

2.3.5 Net primary production

The impacts on annual net primary production (NPP) are shown in Figure 2.8 and summarized in Table 2.8. All biochar treatments significantly increase NPP rates. For instance, the increase from 629 ± 41 gC m^{-2} y^{-1} in the Control soil to 664 ± 39 gC m^{-2} y^{-1} for B550 biochar represents more than 6% increase for the sample year. Although biochar amendments make more water available to plants throughout the year, the real impact on NPP is observed primarily during the vegetation period (from 80 to 290 DOY). Statistically, different types of biochar do not show significant differences in mean annual NPP from each other. An increase in NPP without a significant rise in soil CO_2 results in soil carbon accumulation of approximately 20 gC m^{-2} yr^{-1}, which represents about a 2% increase compared to the initial soil carbon content.

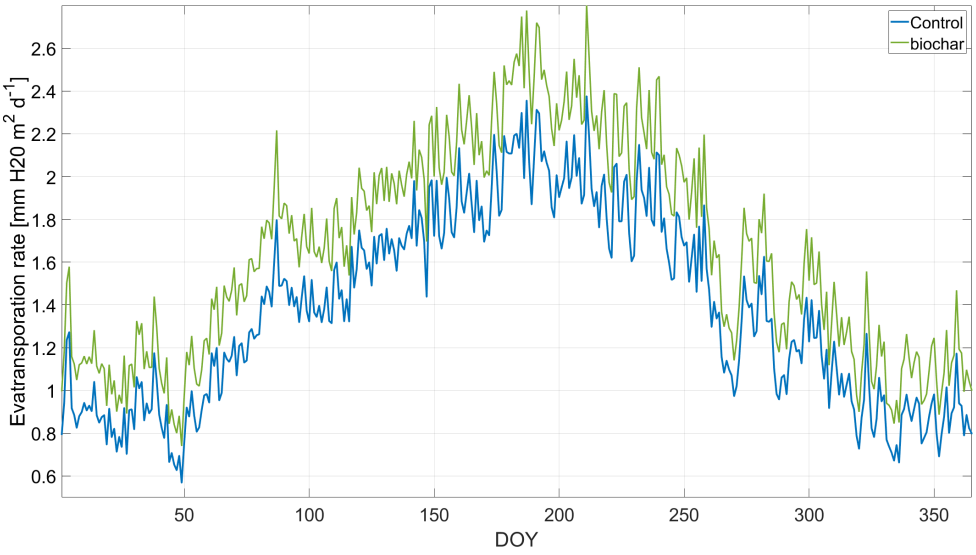

Figure 2.7: Mean annual evapotranspiration for control soil and three biochar treatments. All biochar treatments lead to very similar changes at this scale.

Table 2.8: Mean annual NPP for control soil and three biochar treatments. Standard deviations represent the variability of these variables over a 40-year simulation. Different letters indicate significant differences between samples ($p < 0.01$)

	$\langle$ NPP $\rangle$ [gC m^{-2} y^{-1}]
Control	$629 \pm 41^{\,a}$
B300	$664 \pm 39^{\,b}$
B520	$661 \pm 40^{\,b}$
B550	$662 \pm 39^{\,b}$

2.4 Discussion

2.4.1 Biochar application rates and pyrolysis temperature representation in the LiDELS Model

The choice of biochar application rates and pyrolysis temperatures is critical in evaluating its effects on soil and vegetation. In this study, we selected an application rate of 1% weight/weight (w/w) based on findings from Šurda et al., 2024, who investigated biochar amendments in sandy soils similar to those found in Hamburg. This rate corresponds to approximately 30 tons of biochar per hectare, assuming a 20 cm incorporation depth and a soil bulk density of 1.6 g cm^{-3}. The chosen rate corresponds to a commonly studied biochar application level (Bekchanova et al., 2024).

Higher application rates in sandy soils generally lead to greater increases in soil water retention, mainly due to reductions in bulk density, increases in porosity, surface area, and enhanced soil aggregation (Blanco-Canqui, 2017; Vitková et al., 2024). These

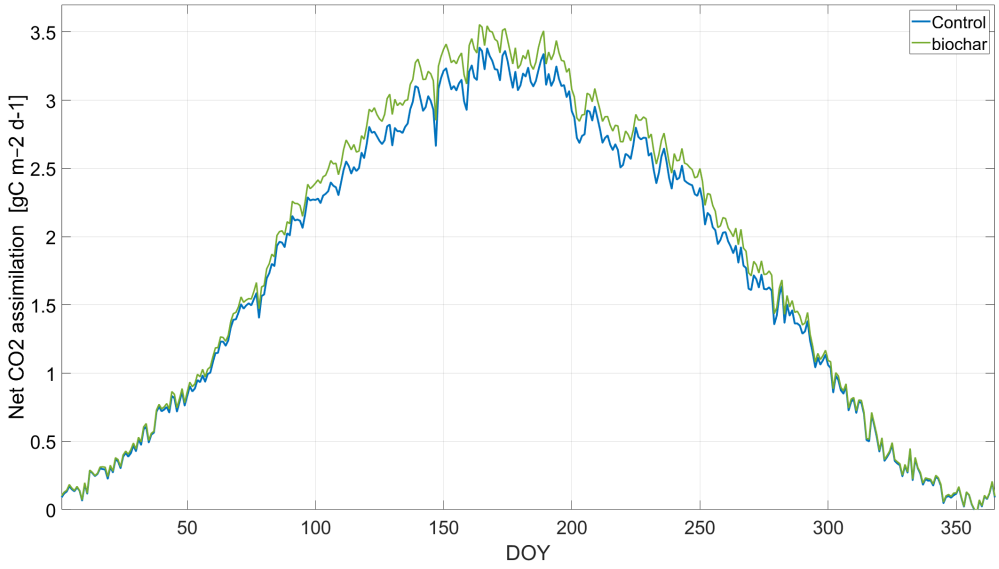

Figure 2.8: Mean annual NPP for control soil and three biochar treatments. All biochar treatments lead to very similar changes at this scale.

effects generally last longer at higher application rates, as a larger amount of biochar remains effective over time, even as aging and degradation gradually reduce its functionality (Baronti et al., 2022). However, increased biochar content can also raise the soil's contact angle (CA), leading to more hydrophobic soil behavior, potentially reducing water infiltration at the surface (Vitková et al., 2024). In essence, while higher biochar application improves the soil's water-holding capacity, it may simultaneously reduce water infiltration due to its hydrophobic nature.

The pyrolysis temperature of biochar also influences its hydrophilic/hydrophobic properties and overall soil behavior. Low-temperature biochar has the potential to be more water-repellent than high-temperature biochar (Blanco-Canqui, 2017). In their research, Šurda et al., 2024 demonstrated that biochar created at 520 °C did not lose its ability to repel water and, in fact, enhanced it when compared to biochar produced at 300 °C. Because of the variable feedstock and greater pyrolysis temperature, only 550 °C biochar displayed a decrease in water repellency.

Lower-temperature biochars tend to retain more nutrients and labile organic compounds, which are often lost at higher temperatures, potentially enhancing microbial activity and plant growth (Joseph et al., 2010; Tomczyk et al., 2020). Medium-temperature biochars ($400 - 500\,°C$) are particularly effective at increasing cation exchange capacity (CEC), improving nutrient retention in soil (Tomczyk et al., 2020)

However, the LiDELS model currently only considers impacts on vegetation and microbes that result from changes in soil temperature and hydrology. It does not account for nutrient cycling or the decomposition of labile biochar components, which could play a significant role in long-term soil fertility and microbial dynamics.

2.4.2 Biochar impact on water balance

Biochar application to sandy soils has generally decreased both saturated and unsaturated hydraulic conductivity in the majority of applied soils (Blanco-Canqui, 2017), which leads to a reduction in seepage in the soil layer where biochar is applied (T. Wang et al., 2017). A decrease in seepage often means that the soil is able to retain more water within that layer rather than allowing it to percolate downwards. This concept is well predicted by the LiDELS model, as presented in Figure 2.2. For applied willow biochar (Table 2.1), saturated hydraulic conductivity in the soil decreases by 25% for B300 and by 42% for B520, which is consistent with the literature (Blanco-Canqui, 2017). For B550 biochar, the decrease is only 8%, yet similar results are achieved. It appears that the soil water retention curve (SWRC) parameters in our model have a more significant influence on soil water retention, and these parameters are within a similar range for all three biochar types. This is expected, as modeled sandy soil often remains at a low water content, far from saturation.

A meta-study by Blanco-Canqui, 2017 shows that biochar application increases water retention, and this parameter is the most consistent compared to other soil hydraulic properties. The increased water retention can lead to an increase in plant available water content (PAWC). The LiDELS model can predict changes in mean soil layer water content, which in our case would refer to the change in the amount of water available for plants. For low-temperature biochar, the increase in the mean soil layer water content after biochar application was predicted to be 35%. Głab et al., 2016, after the application of biochar produced from a mixture of miscanthus and winter wheat, reported a 29%−51% increase in PAWC for an identical application rate (1% w/w) and pyrolysis temperature (300 °C). Manickam et al., 2015, after the application of rice husk biochar, achieved a change of around 33% and 44%−74% in PAWC for twice and five times higher application rates, respectively. Zong et al., 2016, however, reported a significant enhancement of water-holding capacity, while not increasing the PAWC of the soil.

Biochar application in sandy soil is found to reduce evaporation losses (Bohara et al., 2019) and increase transpiration rates (Mollinedo et al., 2015). In the LiDELS model, the significant increase in evapotranspiration rates (by approx. 20%) is primarily attributed to enhanced plant transpiration, as more water is retained within the root-rich layer (by 30% − 35%), promoting greater root water uptake. A similar finding can be found in Ghanem et al., 2022, where increasing irrigation by 40% increased evapotranspiration from biochar-amended soil by approx. 18%. Overall, this has a positive effect on NPP and consistently reduces seepage within the model.

2.4.3 Biochar impact on temperature balance

The effect of biochar on the thermal properties of soil is primarily considered through changes in bulk density and moisture status (Usowicz et al., 2016). Biochar often de-

creases bulk density in sandy soils, which results in greater amounts of air in the pore spaces, lower connectivity between soil particles, and poorer thermal exchange (Blanco-Canqui, 2017). Biochar itself typically has lower thermal conductivity, which additionally contributes to this effect. Despite the aforementioned factors, several studies on changes in soil temperature following biochar treatment in sandy soils showed no significant influences (Usowicz et al., 2016; Q. Zhang et al., 2013). The LiDELS model also predicts no significant differences between control and biochar-amended soils. The slight increase in soil temperature observed in our modeling study, as mentioned earlier, can be attributed to the increase in water content within the soil layer. Water has a much greater thermal capacity than soil, which may lead to enhanced heat storage in the soil layer.

2.4.4 Biochar impact on carbon sequestration

Our model study demonstrates a positive impact of biochar on carbon (C) sequestration. First, biochar itself is a highly recalcitrant form of organic C, with a long mean residence time, making it a stable addition to soil C stocks. Second, biochar application increases net primary production (NPP), primarily through enhanced soil water retention in the root zone. Third, we observe no significant increase in soil CO_2 emissions. Finally, there is a slight increase in soil organic matter, largely attributable to the previously mentioned points: increased input (higher NPP) and minimal change in output (stable soil respiration).

There is a confirmed positive impact of biochar addition on carbon assimilation by plants in low-fertility soils (Blanco-Canqui, 2021), mainly due to improved water retention characteristics, its role as a carbon source for soil, and increased nutrient availability. Ye et al., 2020 report a 15% increase in plant growth for biochar plus fertilizer application compared to fertilizer alone. Bekchanova et al., 2024 in their meta analysis observed a 20% increase in food crop yields, with no effect on biomass production after biochar treatment of sandy-textured soils. Our model predicts a positive impact on NPP, with an increase of 6%, considering only changes in plant-available water. As mentioned earlier, this estimate does not account for changes in nutrient content, which are crucial for NPP estimations.

The most uncertain aspect of this result concerns soil respiration. Different studies report contrasting outcomes: some document a significant increase in soil CO_2 flux in sandy soils (He et al., 2017), while others observe no significant effect (S. Liu et al., 2016). However, studies reporting increased CO_2 emissions primarily focus on laboratory incubation experiments that assess short-term effects—typically spanning a few days to weeks—during which the labile fraction of biochar decomposes relatively quickly as it becomes readily available to microorganisms. Sagrilo et al. (2015) suggest that elevated CO_2 emissions in coarse-textured soils can be linked to the relative content of labile biochar compared to existing soil organic carbon. Furthermore, El-Naggar et al. (2015)

found that biochar addition, when co-applied with poultry manure, can reduce soil CO_2 emissions compared to applying poultry manure alone.

In our LiDELS model, the lack of a significant increase in soil CO_2 flux is primarily due to increased soil water content following biochar application. While biochar enhances root and microbial respiration—as anticipated in the DETECT model—it simultaneously reduces the mean annual soil CO_2 diffusivity, retaining more CO_2 within the soil beneath the application layer.

2.5 Conclusions

Our modeling study reveals that biochar application positively influences vegetation by enhancing net primary production through improved water retention in the root zone. This increase in NPP, combined with the lack of a significant rise in soil CO_2 emissions, leads to a net carbon accumulation in the soil, supporting biochar's potential for carbon sequestration in sandy soils.

Validation of the LiDELS model confirms its utility as a versatile tool for forecasting environmental feedback across various types of biochar, soil and vegetation types, and environmental conditions within specific agricultural contexts.

Looking forward, our findings suggest that vegetation plays a crucial role in moderating the effects of biochar on soil moisture and microbial activity. In the absence of vegetation, reduced transpiration would likely result in even greater soil water retention, potentially stimulating microbial activity and soil respiration due to increased moisture availability. This could lead to carbon loss from the system, as there would be no concurrent NPP increase to offset the rise in soil respiration. Therefore, the interaction between biochar, vegetation, and microbial processes is essential for understanding the long-term carbon dynamics of biochar-amended soils and the sustainability of its sequestration benefits.

Acknowledgments

We would like to thank to ICDC, CEN, University of Hamburg for providing ERA data for running the model. We acknowledge the assistance of AI tools (e.g., OpenAI's ChatGPT) in refining the publication language and improving the clarity of the manuscript. We would like to thank Weronika Stanek-Maslouska for text editing and language corrections.

The data that support the findings of this study are openly available following an embargo at the following https://zenodo.org/records/14849558.

2.6 Appendix

2.6.1 Details about the DETECT Model Integration

Soil CO_2 Respiration

Soil CO_2 respiration is calculated using the following equation:

$$CO_{2,\text{out}} = \sum \left(S_{\text{roots}} + S_{\text{m}} + \left(C_{\text{int}} - C_{\text{fin}} \right) \cdot d_{\text{soil}} \right), \tag{2.1}$$

where C_{int} and C_{fin} represent the initial and final CO_2 concentrations in the soil, respectively, for each time step, with summation over all soil layers. This formula is consistent with the approach proposed by E. M. Ryan et al., 2018 in the supplementary material.

Antecedent Dataset

Antecedent soil water and soil temperature are calculated as proposed by E. M. Ryan et al., 2018 in Eq. 13. An exception is made for the beginning of the simulation, before the predefined antecedent period is reached. For these time periods, a secondary weight is defined, representing the number of available data points for the corresponding period. For example, for soil water for the roots, the antecedent period is defined as 4 weeks with weights $w = (0.2, 0.6, 0.2, 0)$. After 1.5 weeks, we have $7 \cdot 24 = 168$ model outputs for the first week and only 84 for the second. Additionally, until the total period is reached, the w-weights should be normalized. The new weights are given by:

$$\begin{aligned} w_1 &= 0.2 \cdot 168 \cdot (0.2 \cdot 168 + 0.6 \cdot 84)^{-1} &= 40, \\ w_2 &= 0.6 \cdot 84 \cdot (0.2 \cdot 168 + 0.6 \cdot 84)^{-1} &= 60. \end{aligned}$$

In the next step, the weight w_1 will be multiplied by the mean value for water content over the last 168 values ($\theta(i, 84:252)$), and w_2 will be multiplied by the mean over the first 84 values ($\theta(i, 1:84)$). Summing these values gives us the antecedent value at step 252 for soil layer i.

Vegetation Greenness

Vegetation greenness is calculated following the approach proposed by E. M. Ryan et al., 2018 for the $G(t)$ function in the supplementary material but is applied here to R_{short}. Since vegetation greenness reflects seasonal changes in root respiration within the DETECT model, we assumed that substituting it with shortwave radiation measurements would be sufficient, as these are expected to exhibit a similar seasonal pattern.

2.6.2 Details about the LiDELS Model

Soil Ice Content in the LiDELS Model

The maximum amount of melted soil ice or frozen soil water is defined by the following formula:

$$W_{fX} = P \cdot d_{\text{soil}} \cdot c_{\text{soil}} \cdot (273.15 - T_{\text{soil}}) \cdot (\lambda_{H2O} \cdot \rho_{H2O})^{-1} \tag{2.2}$$

where λ_{H2O} is the latent heat of fusion for water, and ρ_{H2O} is the density of water. Subsequently, the soil water content $\langle\theta\rangle$, ice content $\langle I\rangle$, and soil temperature $\langle T_{\text{soil}}\rangle$ are updated based on the amount of water available for freezing or the amount of ice that has melted.

Air CO_2 Concentration

The air CO_2 concentration is described by the following empirical time dependence:

$$\begin{aligned} CO_{2,\text{air}} \qquad (t) &= 0.012 \cdot (1979 + t'/c_{\text{hyr}})^2 \\ &\quad -46.68 \cdot (1979 + t'/c_{\text{hyr}}) + 45200 \\ &\quad +9.36 \cdot \sin\left(2\pi \cdot (1979 + t/c_{\text{hyr}}) + 6.66\right). \end{aligned} \tag{2.3}$$

Typically, $t' = t$, but for this model run, only the seasonal (sinusoidal) dependence was used, so $t' = 0$. A sample fit is presented in Figure 2.9.

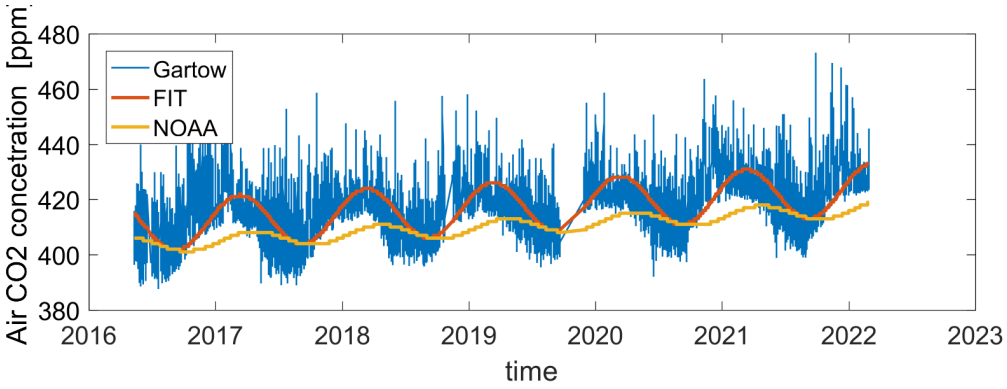

Figure 2.9: Fitting Results for the air CO_2 Function. The function was initially fitted to NOAA measurements starting from 1974. Parameters were then adjusted to fit CO_2 measurements at Gartow. For NOAA data, the fit achieved $R^2 = 0.998$, while for Gartow data, the fit resulted in $R^2 = 0.54$.

Plant Litter

The litter function is implemented through a simple algorithm that sums the daily net primary production (NPP). When this cumulative sum becomes positive, it redistributes this total evenly as a constant hourly flux over the next 24 hours. This ensures that the plant litter flux remains non-negative and effectively reflects the available NPP. A sample output is presented in Figure 2.10.

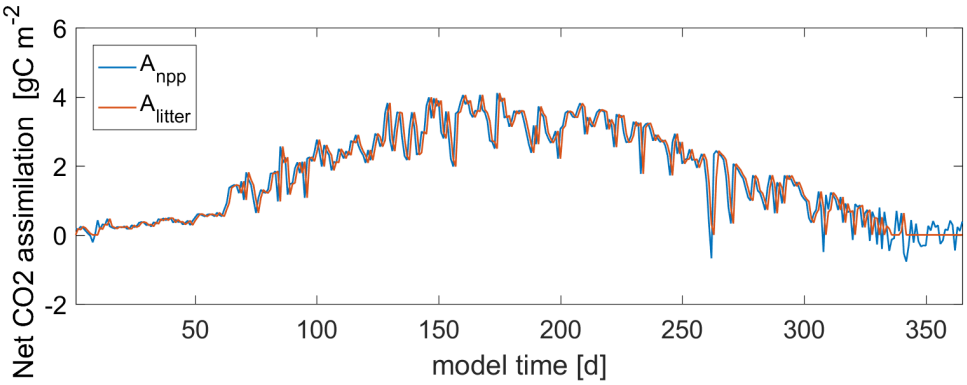

Figure 2.10: Demonstration of Litter Function Output Compared to NPP in the Model. For this sample run, the total net primary production (A_{NPP}) was 634.95 gC m^{-2}, while the total litter output (A_{litter}) was 635.00 gC m^{-2}.

2.6.3 Supplementary Materials

Table 2.9: List of variables and parameters with references used in LiDELS model

Parameter	**Definition**	**Reference**
LiBry model		
wind	wind speed [m s^{-1}]	ECMWF ERA dataset (Hersbach et al., 2020)
R_{long}	near infrared (longwave) radiation [W m^{-2}]	–
R_{short}	visible (shortwave) radiation [W m^{-2}]	–
T_{a}	air temperature [K]	–
rhum	relative humidity [-]	–
rain	precipitation [mm m^{-2} s^{-1}]	–
g_{ac}	aerodynamic conductance [m s^{-1}]	Bonan, 2019, eq. 6.26
e_{sat}	saturation vapor pressure [Pa]	Huang et al., 2023, eq. 5
VPD	vapor pressure deficit [Pa]	$e_{\mathrm{sat}} \cdot (1 - \mathrm{rhum})$
ET_{pot}	potential evapotrasporation [m s^{-1}]	Porada et al., 2013, eq. B30
T_{surf}	surface temperature [K]	Porada et al., 2013, eq. B31
R_{net}	downling net radiation [W m^{-2}]	Porada et al., 2013, eq. B25
DETECT model		

Continued on next page

Table 2.9: List of variables and parameters with references used in LiDELS model (Continued)

$\langle c_{\mathrm{o,soil}} \rangle$	soil organic distribution in layers [-]	E. M. Ryan et al., 2018, $f_s(z)$ function in Supplement
$\langle c_{\mathrm{m,soil}} \rangle$	soil microbes distribution in layers [-]	E. M. Ryan et al., 2018, $f_m(z)$ function in Supplement
$\langle c_{\mathrm{roots}} \rangle$	soil roots distribution in layers [-]	E. M. Ryan et al., 2018, $f_r(z)$ function in Supplement
$\langle S_{\mathrm{roots}} \rangle$	soil CO_2 production by roots [gC m^{-3} hr^{-1}]	E. M. Ryan et al., 2018, eq. 3
$\langle S_{\mathrm{m}} \rangle$	soil CO_2 production by microbes [gC m^{-3} hr^{-1}]	E. M. Ryan et al., 2018, eq. 5
R_{soil}	soil CO_2 flux [gCO_2 m^{-2} hr^{-1}]	see section 2.6.1
Greenness	vegetation greenness [-]	see section 2.6.1
$\langle CO_{2,\mathrm{soil}} \rangle$	soil CO_2 concetration [mg CO_2 m^{-3}]	E. M. Ryan et al., 2018, eq. 10
Soil-vegetation scheme: soil		
$\langle d_{\mathrm{soil}} \rangle$	soil layer thickness [m]	based on Thomsen, 2018 soil profiles
$\langle c_{\mathrm{q,soil}} \rangle$	soil layer quartz content [-]	based on Thomsen, 2018 soil profiles
$\langle \rho_{\mathrm{b,soil}} \rangle$	soil layer bulk density [g m^{-3}]	based on Thomsen, 2018 soil profiles
$\langle \rho_{\mathrm{s,soil}} \rangle$	soil layer particle density [g m^{-3}]	$\langle \rho_{\mathrm{b,soil}} \rangle / (1 - \langle P \rangle)$
$\langle P \rangle$	soil layer porosity [-]	based on Thomsen, 2018 soil profiles
$\langle SWRC \rangle$	soil layer water retention curve parameters	based Šurda et al., 2024 & Skaggs and Ghane, 2017 & Bonan, 2019, Table 8.3
$\langle K_{\mathrm{sat}} \rangle$	soil layer saturated conductivity [cm h^{-1}]	–
$\langle \theta_{\mathrm{res}} \rangle$	soil layer residual water content [-]	based on Thomsen, 2018 soil profiles
$\langle \theta \rangle$	soil layer water content [-]	Bonan, 2019, eq. 8.13

Continued on next page

Table 2.9: List of variables and parameters with references used in LiDELS model (Continued)

$\langle I \rangle$	soil layer ice content [-]	See section 2.6.2
$\langle K(\theta) \rangle$	soil layer hydraulic conductivity [m s^{-1}]	Van Genuchten, 1980, modified eq. 8
$\langle \psi(\theta) \rangle$	soil layer water potential [m]	Van Genuchten, 1980, modified eq. 3
$\langle \theta_{WP} \rangle$	soil layer permanent wilting point [m]	Van Genuchten, 1980, eq. 21
$\langle c_{soil} \rangle$	soil layer heat capacity [J m^{-3} K^{-1}]	Bonan, 2019, eq. 5.32
$\langle \kappa_{soil} \rangle$	thermal conduct. in layers borders [W m^{-1} K^{-1}]	Bonan, 2019, eq. 5.16 and Xiong et al., 2023
$\langle Q_b \rangle$	water inflitrated throw the soil [m h^{-1}]	Bonan, 2019, eq. 8.21 & eq. 8.22
$\langle T_{soil} \rangle$	soil layer temperature [K]	Bonan, 2019, eq. 5.11 & Table 5.1
$\langle D_{CO_2,soil} \rangle$	soil layer CO_2 diffusion coef. [m^2 s^{-1}]	Fang and Moncrieff, 1999, eq.12
Soil-vegetation scheme: atmosphere		
press	air pressure [Pa]	DWD, n.d.
$D_{CO_2,air}$	air diffusion coef. [m^2 s^{-1}]	Risk et al., 2002, eq.4, & Fang and Moncrieff, 1999, eq.12
ET_{real}	real evapotrasporation [m s^{-1}]	Bonan, 2019, eq. 9.39 and own fit for S_{dot} from Entekhabi and Eagleson, 1989 Fig. 7
$CO_{2,air}$	air CO_2 concentration [ppm]	see section 2.6.2
Soil-vegetation scheme: vegetation		
g_{bw}	boundary layer conductance [mol m–2 s–1]	Bonan, 2019, Table 10.1 for forced convection

Continued on next page

Table 2.9: List of variables and parameters with references used in LiDELS model (Continued)

GPP	gross primary production [gC m^{-2} hr^{-1}]	Bonan, 2019, Table 11.5, temp. dependencies based on Bernacchi et al., 2003, 2001
Rd	whole plant respiration [gCO_2 m^{-2} hr^{-1}]	Bernacchi et al., 2001, Table 1
NPP	net assimilation [gC m^{-2} hr^{-1}]	Bonan, 2019, Table 11.5
Litter	plant litter [gC m^{-2} hr^{-1}]	see section 2.6.2
g_{sw}	stomatal conductance [mol m^{-2} s^{-1}]	Bonan, 2019, eq. 12.56. Reducing factor based on roots available water content. Assumed $g_{sw,max}$ = 0.1 mol m^{-2} s^{-1}
h	canopy height [m]	assumed to be 1 m
d_l	leaf size [m]	assumed to be 0.1 m

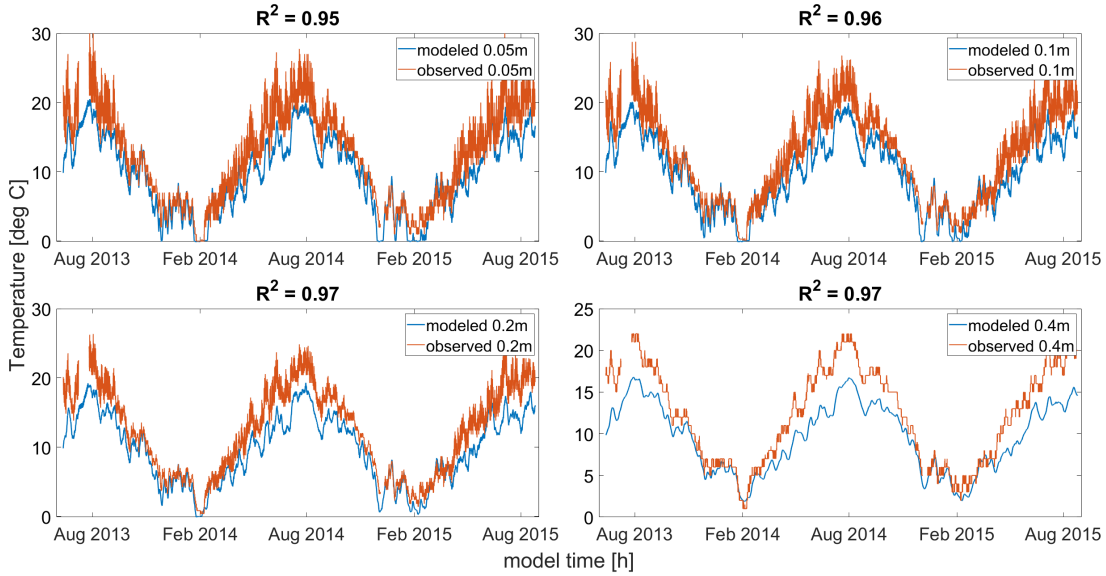

(a) for soil temperature

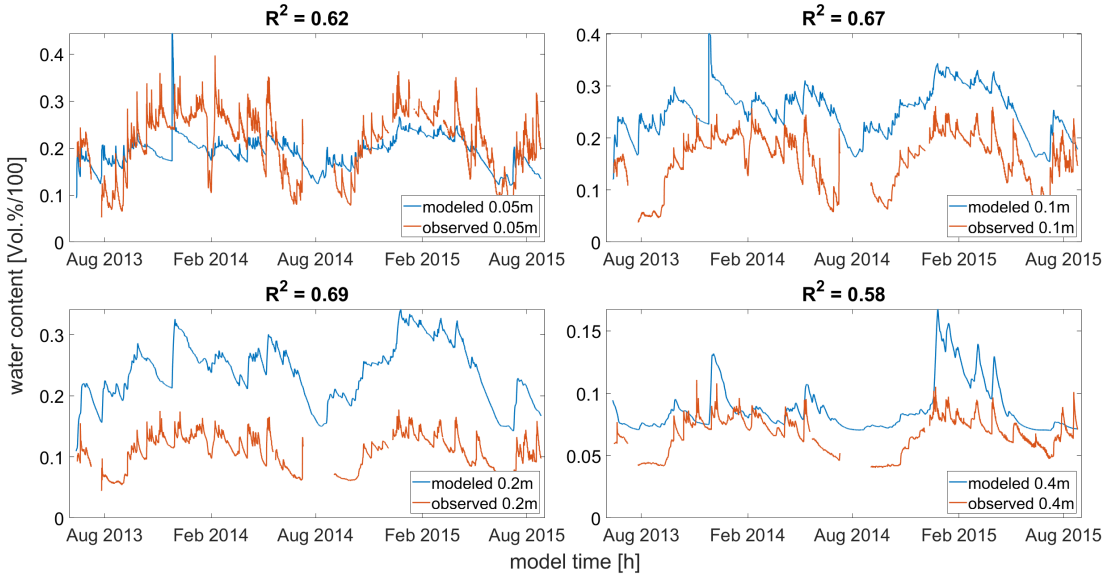

(b) for volumetric water content

Figure 2.11: Result of the model validation using soil data measurements from Thomsen, 2018 for Hamburg suburban wet soil, grassland area

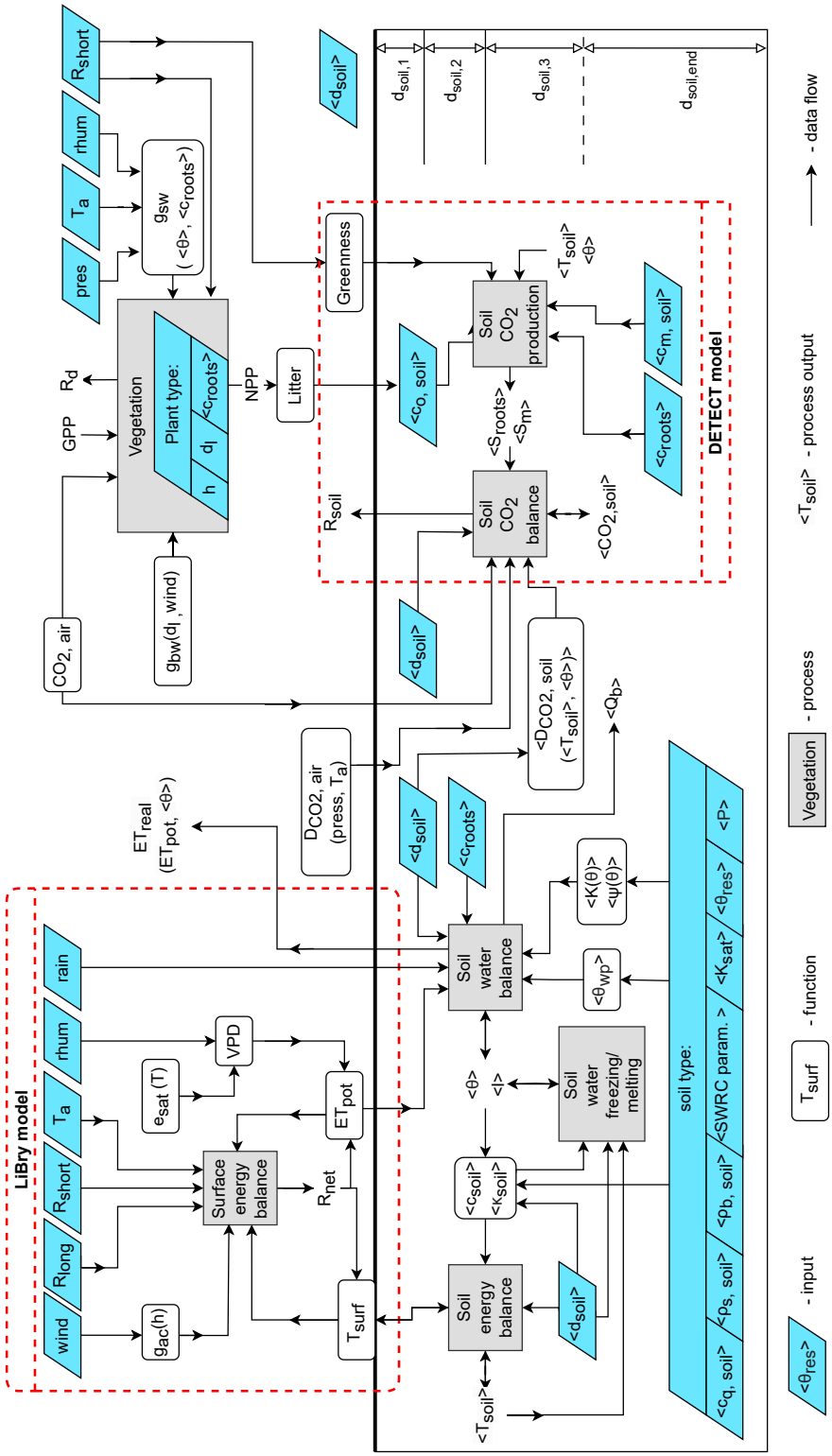

Figure 2.12: Precise LiDELS model process scheme. For parameters explanation and references see Table 2.9

Chapter 3

Long-term carbon dioxide removal potential from the application of wood biochar and basanite rock powder in sandy soil using the LiDELSv2 process-based modeling approach

Abstract

The rise in atmospheric carbon dioxide (CO_2) concentrations requires scalable and effective carbon dioxide removal (CDR) strategies. Pyrogenic carbon capture and storage (PyCCS) relies on the pyrolysis of biomass and the non-oxidative use of biochar, e.g., in soils. Enhanced rock weathering (ERW) captures CO_2 by forming dissolved bicarbonate. In addition to CDR, both methods may offer soil improvement as a co-benefit. However, their interaction and combined CDR potential remain largely unexplored.

Here, we investigate their individual and combined effects on carbon dynamics in a temperate agricultural soil. Using the process-based LiDELSv2 model calibrated against data from the lysimeter experiment, we simulate 1,000-year impacts of applying 4.2 wt% wood biochar (WB), 2 wt% basanite rock powder (RP), their co-application, and co-pyrolyzed material (rock-enhanced biochar, RE-biochar) on soil organic carbon (SOC), net primary production (NPP), net CO_2 ecosystem exchange (NEE), and calcium (Ca^{2+}) leaching in a northern German sandy soil.

Biochar alone led to the highest increase in SOC and achieved a modeled NEE of -200 g C ha^{-1} yr^{-1} per ton of biochar throughout 1,000 years, acting as a long-term carbon sink. Co-application and RE-biochar increased SOC too, but to a lesser extent.

Rock powder alone reduced SOC by 7%. Although RP enhanced Ca^{2+} leaching, this did not result in net CO_2 removal. Ecosystem respiration and NPP remained stable in the long term.

Our results suggest that, when accounting for assumed application rates, biochar is the primary driver of long-term soil-based CDR, while ERW provides only minor co-benefits. This highlights the need to tailor interventions to specific soil and climate conditions.

3.1 Introduction

Climate change is primarily driven by the increase in atmospheric carbon dioxide (CO_2), resulting largely from anthropogenic activities such as fossil fuel combustion, deforestation, and industrial processes. During the past two centuries, CO_2 emissions have far exceeded the Earth's natural capacity to absorb them, leading to global warming and wide-ranging impacts on biodiversity, human health, food security, and ecological stability (Calvin et al., 2023; Al-Ghussain, Loiy, 2019; Keerthi, 2024).

Although emission reduction is and will remain critical, carbon dioxide removal (CDR) approaches are increasingly recognized as an essential additive strategy to limit the global rise in temperature (Calvin et al., 2023; S. M. Smith et al., 2024). These approaches aim to actively remove CO_2 from the atmosphere and securely store it over long timescales (Calvin et al., 2023; Keerthi, 2024).

Within CDR strategies, Pyrogenic Carbon Capture and Storage (PyCCS) involves the production of biochar, a stable, carbon rich product derived from biomass non-oxidative pyrolysis, and its application to soils for long-term carbon sequestration. In the soil, biochar might stabilize carbon and prevents rapid decomposition (Schmidt et al., 2019). Hence, biochar application increases soil organic carbon (SOC) stocks by stabilizing biomass-derived carbon and, potentially, by increasing plant-derived C inputs by stimulating plant growth and yields (Schmidt et al., 2021). The labile carbon fraction of biochar (3–30%) is decomposed by soil microorganisms, releasing nutrients that support plant growth when produced from nutrient-rich feedstock (Archontoulis et al., 2016). Moreover, biochar can improve soil water retention, and overall soil fertility, potentially enhancing CO_2 uptake through increased biomass productivity (Acharya et al., 2024; Lehmann et al., 2021; Schmidt et al., 2021) and it can also reduce agricultural emissions of non-CO_2 greenhouse gases (Lehmann et al., 2021). First long-term studies in biochar-amended agricultural soils reported an increase in overall SOC stocks (Blanco-Canqui et al., 2020; Guo et al., 2024; Weng et al., 2022). However, findings from Gross et al. (2024) report no increase in SOC stock.

Enhanced Rock Weathering (ERW) is another CDR process that accelerates the natural weathering of silicate minerals to capture atmospheric CO_2 and form bicarbonate in the aqueous phase or carbonate minerals in the solid phase, both stable for at least 10,000 years (Hartmann et al., 2013; Phil Renforth and Henderson, 2017). Beyond carbon se-

questration, this approach can also improve soil structure, enhance nutrient availability, and contribute to SOC stabilization (Buss et al., 2022; Dupla et al., 2024). Like biochar, ERW may support increased CO_2 uptake by vegetation through improved soil fertility and plant growth (Dupla et al., 2024; Swoboda et al., 2022).

Although the individual effects of biochar and rock powder on soil and carbon dynamics are well documented (Hartmann et al., 2013; Schmidt et al., 2021), their combined application remains relatively understudied. Biochar may enhance rock weathering by improving soil aeration and stimulating microbial activity, potentially accelerating geochemical reactions (Amann and Hartmann, 2019). In contrast, under certain conditions – such as in compacted soils or when biochar with fine particle size is applied at high rates - it can suppress weathering by clogging pore spaces and increasing soil hydrophobicity, thus limiting water-mineral interactions (Obia et al., 2017; Vitková et al., 2024). A nine-week field lysimeter experiment showed that, when co-applied with basanite, biochar was the dominant driver of changes in soil carbon content and microbial activity (Ansari et al., in prep.). In contrast, Honvault et al. (2024) suggest that while plant biomass production and nutrient availability were generally additive under co-application, these effects were largely driven by the basalt amendment. In both cases (Ansari et al., in prep. Honvault et al., 2024), the dominant role of either amendment may also be linked to its considerably higher application rate, potentially influencing the relative strength of biochar or rock powder effects.

Most existing experimental studies have focused on short-term responses of biochar–rock powder combinations and their potential additive or synergistic CDR effects (Ansari et al., in prep. Hamburger et al., in prep. Honvault et al., 2024; Vorrath et al., 2025). However, the stability of these amendments and their interactions must be understood over much longer timescales to reliably assess their net CDR potential. To address this gap, we employed the LiBry-DETECT Layers Scheme version 2 (LiDELSv2) – a process-based model that simulates the effects of biochar and rock powder on soil properties, both individually and in combination, over centennial to millennial timescales.

In this study, we used LiDELSv2 to investigate the cumulative carbon removal potential over 1,000 years from the sole, co-application and co-pyrolysis of wood-derived biochar and basanite rock powder in a sandy soil under northern German climatic conditions.

3.2 Materials and Methods

3.2.1 Geisenheim experiment

The calibration of the LiDELSv2 was based on a lysimeter experiment conducted on the grounds of Hochschule Geisenheim University, Germany (49°59′1″N, 7°57′22″E). The experiment used a sandy agricultural topsoil of northern Germany, sourced from Gräflich Bernstorff'sche Betriebe, Gartow (53°1′10″N, 11°30′1″E), with a texture comprising 93.8%

sand and 2.5% silt. The soil was placed in lysimeter pots and amended with different combinations of biochar and/or basanite rock powder (Ansari et al., in prep. Hamburger et al., in prep.). Cabbage turnip (*Brassica oleracea* var. *gongylodes* L.) was cultivated as the test crop (Hamburger et al., in prep.).

The biochar used in this experiment was produced from wood chips at 650 °C (hereafter referred to as WB, wood biochar). The basanite rock powder (commercial name: *Eifelgold*) was sourced from Rheinische Provinzial-Basalt- und Lavawerke, Sinzig, Germany (hereafter referred to as RP, rock powder). Rock-enhanced biochar (RE-biochar) was produced from a mixture of wood chips and basanite in a weight ratio of 80:20, followed by pelletization and pyrolysis at 650 °C at industrial scale. The resulting RE-biochar consisted of approximately 68% biochar and 32% basanite by weight. The same ratio (2.1:1) was assumed for the co-application of biochar and basanite. Further details on the (RE-)biochars are provided in Meyer zu Drewer and Hagemann (2025), while the properties of the basanite rock powder are described in Meyer zu Drewer et al. (2025).

The soil in the lysimeter pots was mixed with WB at a 4.2% weight-to-weight ratio (wt%), corresponding to an application rate of approximately 120 t ha^{-1}. For the sole RP treatment, the application rate was 2 wt%, equivalent to 57 t ha^{-1}. The RE-biochar treatment was applied at 6.2 wt%, corresponding to 177 t ha^{-1}. In the co-application treatment, the soil was mixed with 4.2 wt% of biochar and 2 wt% of basanite rock powder (Ansari et al., in prep. Hamburger et al., in prep.).

At the end of the experiment, Ansari et al. (in prep.) measured soil water retention parameters, bulk density (Table 3.1), soil organic carbon (SOC) content, microbial biomass (MB) and Hamburger et al. (in prep.) measured cumulative crop yield. These measurements were subsequently used for model calibration (see sections 3.6.1-3.6.1 in Appendix).

3.2.2 LiDELSv2 process-based modeling approach

LiBry-DETECT Layer Scheme version 2 (LiDELSv2, Figure 3.1) is a one-dimensional, process-based ecosystem model that integrates soil–plant–atmosphere interactions under biochar and mineral amendment scenarios (Maslouski et al., 2025a). It is based on two earlier models: LiBry (Porada et al., 2013), which simulates energy and water fluxes at the soil-atmosphere interface, and DETECT (E. M. Ryan et al., 2018), which calculates soil CO_2 production and vertical transport. The soil is modeled in discrete layers, allowing for dynamic simulation of heat and water transport, soil carbon dynamics, changing hydraulic conductivity, and thermal capacity due to amendments. Vegetation processes are modeled via light- and CO_2-limited photosynthesis (Farquhar et al., 1980) and stomatal regulation based on root-zone water availability (Bonan, 2019). The model has been previously validated for sandy soils under northern German climatic conditions and accurately reproduces key biogeophysical processes (Maslouski et al., 2025a).

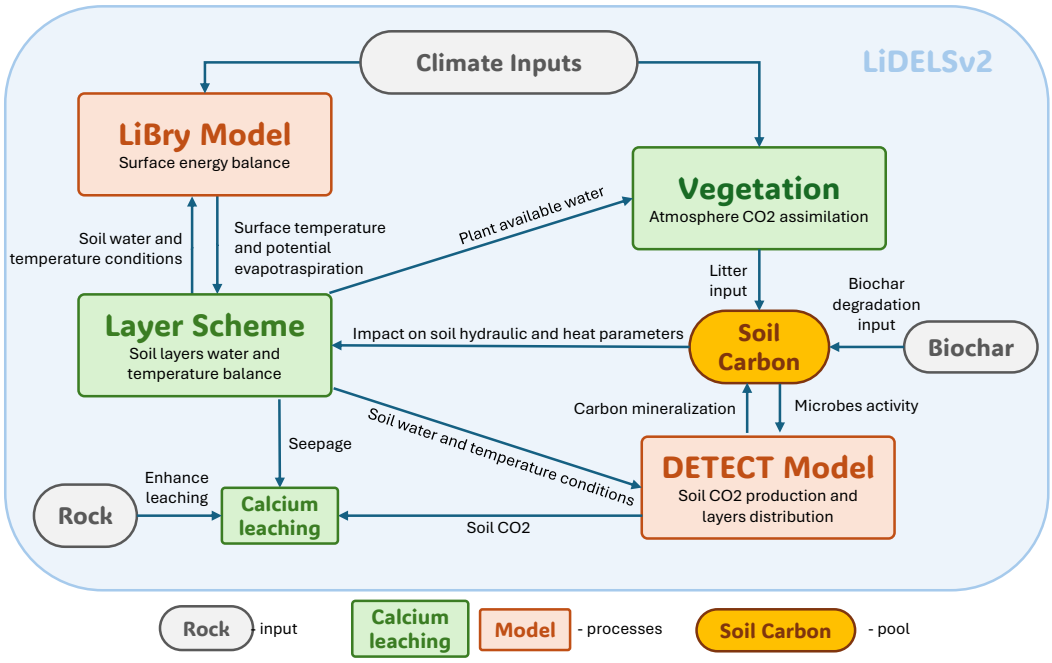

Figure 3.1: Schematic representation of the LiDELSv2 structure. For more detailed scheme see Figure 3.10 in Appendix.

Compared to previous version by Maslouski and Porada (2024), LiDELSv2 now includes several key developments. First, a soil evaporation module based on Bonan (2019) was implemented, allowing for a more realistic representation of soil water fluxes beyond transpiration alone. In the reference scenario, this component accounted for ∼11% of evapotranspiration, consistent with regional observations (Miralles et al., 2025). Second, a weathering module based on Arens and Kleidon (2008) was added to estimate calcium ion (Ca^{2+}) leaching from silicate minerals. The modeled Ca^{2+} leaching rate was approximately 0.7 g m^{-2} yr^{-1}, which matches empirical estimates for the region (Arens and Kleidon, 2011). Finally, a biochar degradation module was incorporated to simulate the gradual breakdown of labile biochar fractions, using decay rates for oak biochar produced at 650 °C from Zimmerman (2010). This module affects soil carbon dynamics, hydrology, thermal properties (Lawrence and Slater, 2008), and microbial activity (Liddle et al., 2020).

3.2.3 Model setup

For the model simulations, we used the ECMWF ERA5 climate dataset (Hersbach et al., 2020) for Hamburg in Germany, which provides 40 years of hourly meteorological data starting from 1 Jan 1979. For spin up period, model was run for 500 years, repeating the ERA5 dataset, in order to achieve stable state. To simulate long-term dynamics, the dataset then was repeated 25 times to construct a continuous 1,000-year climate input for all scenarios, which extrapolate the present climate into the future.

The long-term LiDELSv2 simulations were initialized using measured data from the Geisenheim experiment, which contained soil water retention parameters estimated using the LABROS software based on retention curve measurements from soil samples and information about applied amendments (Table 3.1)

Table 3.1: Soil and amendment parameters used as model inputs. Values obtained from the Geisenheim experiment (Ansari et al., in prep.) are presented as treatment means ± standard deviation ($n = 0.05$). Different letters within a row indicate statistically significant differences between treatments ($p < 0.05$). Note that Meyer zu Drewer and Hagemann (2025) did not report statistical analyses for the carbon (C) content of the amendments. The persistent carbon fraction (PAC) was not measured for the (RE-)biochar used in this study and was therefore assumed from the BC_{HyPy} fraction of a comparable material (same rock type and amendment rate, similar feedstock and pyrolysis conditions at pilot scale, Meyer zu Drewer et al. (2025)). This values is also consistent with recently published PAC dependencies on production conditions by Hagemann et al. (2025).

Treatment / Parameter	Control	Rock Powder (RP)	Wood Biochar (WB)	Co-application RP + WB	Co-pyrolysis (RE-biochar)
Bulk density [g/cm^3]	1.26 ± 0.03^a	1.26 ± 0.04^a	1.14 ± 0.03^b	1.17 ± 0.04^c	1.21 ± 0.03^d
Porosity [–]	0.51 ± 0.01^a	0.52 ± 0.02^a	0.56 ± 0.01^b	0.55 ± 0.02^b	0.53 ± 0.01^c
Saturated conductivity [cm/h]	43 ± 4^a	50 ± 18^b	47 ± 4^a	52 ± 7^a	47 ± 4^a
van Genuchten α [1/cm]	0.031 ± 0.005^{ab}	0.029 ± 0.001^a	0.029 ± 0.003^a	0.027 ± 0.001^b	0.028 ± 0.002^{ab}
van Genuchten n [–]	4.9 ± 0.6^a	5.3 ± 0.1^a	4.9 ± 0.4^a	5.6 ± 0.6^a	5.3 ± 0.6^a
C content [–]	0.0124	0.0124**	0.494*	0.494*	0.336*
PAC fraction [–]	n.d	n.d	0.908*	0.908*	0.911*

(*) indicates the content in the amendments. The soil content value accounts to the sum of Control soil and the application rate, which is 4.2 wt% for biochar-related treatments.

(**) indicates the carbon content in the Control

The modeled soil column had a depth of 4 m, with uniform soil parameters corresponding to the Control treatment (Table 3.1). For the biochar and/or rock powder treatments, soil parameters were changed in the top two layers, comprising a cumulative depth of 25 cm, based on the values specified in Table 3.1.

Soil carbon, microbes, and root distributions followed the vertical profiles proposed by E. M. Ryan et al. (2018) in DETECT model. The majority of SOC and MB were concentrated within the top 1 m of the soil profile. Initial SOC values for all scenarios were based on measurements from the Geisenheim experiment and amounted to 67 Mg ha^{-1}. Initial MB was estimated using the calibration relationship described in Appendix

3.6.1 section and was set to 8 kg ha^{-1}.

For the biochar degradation, its carbon content and the persistent aromatic carbon (PAC) fraction were used (Table 3.1). PAC is defined as the fraction of biochar carbon that remains stable in the soil for over 1,000 years (Schmidt et al., 2024). From a modeling perspective, only the labile fraction of (RE-)biochar – calculated as (1 - PAC) – contributes to degradation. Within this labile part, only the (RE-)biochar's carbon content (Table 3.1) contributes to the SOC pool.

For the calcium leaching module, we applied the sandstone lithology class proposed by Arens (2013) (after Nockolds (1954)) for the Control treatment. For treatments containing rock powder, the Control lithology was adjusted using a weighted average with the basalt lithology class from Arens (2013).

To approximate the effects of lower, more agronomically realistic biochar application rates, we scaled the amendment-induced changes in soil parameters (Table 3.1) linearly relative to the Control. Specifically, the difference between the Control and a given treatment was reduced in proportion to the assumed application rate. For example, the porosity in the WB treatment ($\rho = 0.56$) differs from the Control ($\rho = 0.51$) by 0.05 at the applied rate of 4.2 wt%. At half this rate, the adjustment was reduced to 0.025, yielding a porosity of 0.535, while at one-quarter of the rate it was 0.0125, resulting in 0.5225. The same procedure was applied to saturated conductivity, bulk density, and the van Genuchten parameters.

3.3 Results

3.3.1 Effects on soil organic carbon pool

For the Control treatment, LiDELSv2 applies a steady-state approach, where SOC remains nearly constant throughout the simulation (Table 3.2). For treatments containing biochar, we distinguish between total SOC (SOC_{total}), representing the sum of soil organic carbon and biochar, and non-biochar SOC (SOC_{nonBC}), which excludes both the persistent aromatic carbon (PAC) fraction and the labile portion of biochar that has not yet decomposed (turned into SOC_{nonBC}) at a given point in time. Only SOC_{nonBC} (denoted as $c_{o,soil}$ in Figure 3.10 in the Appendix) affects the dynamic processes in the model, including soil heat fluxes, water balance, and microbial activity.

The highest cumulative increase in SOC_{nonBC} of approximately 52% compared to the Control was observed for the sole application of WB (Figure 3.2) in 1,000 years. When normalized by application rate, this corresponds to an increase in SOC_{nonBC} by $\sim$ 308 kg C ha^{-1} yr^{-1} per ton of applied biochar. This was followed by the WB+RP and RE-biochar treatments, which resulted in SOC_{nonBC} increases of 17% and 10%, respectively. These changes were most pronounced during the first 500 years of the simulation, with the accumulation rate gradually declining thereafter. In contrast, the sole application

Table 3.2: Mean non-biochar (nonBC) and total soil organic carbon in kg C m^{-2} for each treatment, averaged over specific time intervals and expressed relative to the Control soil column. Values represent treatment means ± standard deviation. All treatments within a column differ significantly from one another ($p < 0.05$).

Timeframe	0-50 yrs		51-100 yrs		101-500 yrs		501-1,000 yrs	
Treatment	nonBC	total	nonBC	total	nonBC	total	nonBC	total
Control	6.9 ± 0.2		6.7 ± 0.2		6.2 ± 0.2		7.1 ± 0.6	
Rock Powder (RP)	6.8 ± 0.2		6.5 ± 0.2		5.8 ± 0.3		6.6 ± 0.6	
vs. Control [%]	−1		−3		−6		−7	
Wood Biochar (WB)	7.7± 0.3	14.3± 0.3	8.5± 0.2	15.0± 0.2	9.4± 0.3	15.6± 0.3	10.8± 0.7	17.0± 0.7
vs. Control [%]	+13	+109	+27	+123	+52	+154	+52	+138
Co-application (RP + WB)	7.3± 0.2	13.9± 0.2	7.5± 0.1	14.0± 0.2	7.3± 0.2	13.6± 0.3	8.3± 0.6	14.5± 0.7
vs. Control [%]	+7	+103	+12	+108	+19	+121	+17	+104
Co-pyrolysis (RE-biochar)	7.1± 0.2	11.6± 0.2	7.2± 0.1	11.6± 0.2	6.9± 0.2	11.1± 0.3	7.8± 0.6	12.1± 0.6
vs. Control [%]	+4	+69	+7	+73	+11	+81	+10	+70

of RP led to a consistent reduction in SOC_{nonBC}, reaching a decrease of 7% over the 1,000-year period.

Sole WB application and its co-application with RP resulted in the largest increases in SOC_{total} of approximately 154% and 121% above Control levels after 500 years, respectively (Figure 3.3). The RE-biochar treatment, characterized by a lower carbon content, produced a more moderate increase of 81% after 500 years. For the Control and RP-only treatments, SOC_{total} corresponds directly to SOC_{nonBC}, due to the absence of biochar.

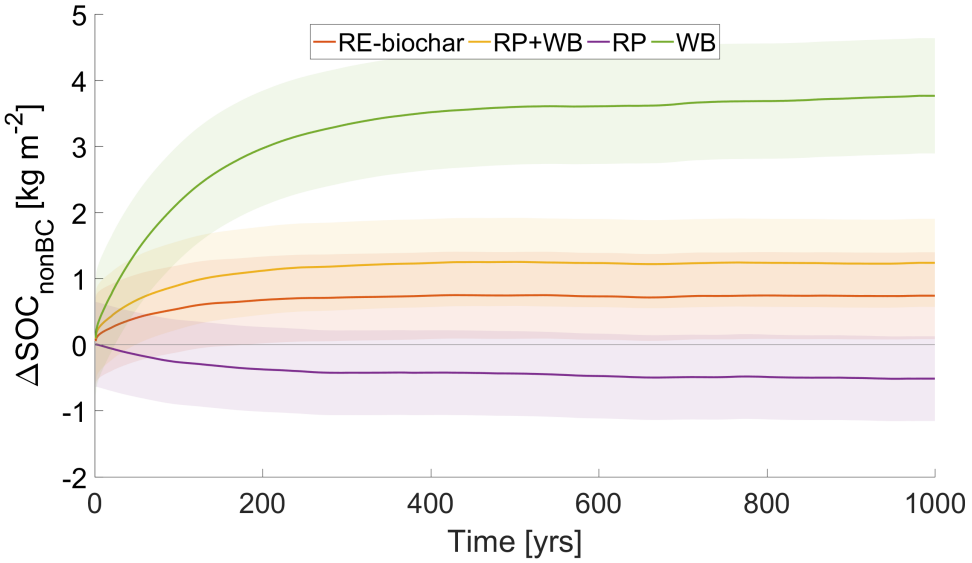

Figure 3.2: Change in mean non-biochar soil organic carbon relative to the modeled Control treatment (ΔSOC_{nonBC}) for wood biochar (WB), rock powder (RP), their co-application (RP+WB), and co-pyrolysis (RE-biochar). Solid lines represent smoothed trends, while shaded areas represent the standard deviation caused by natural ecosystem variability.

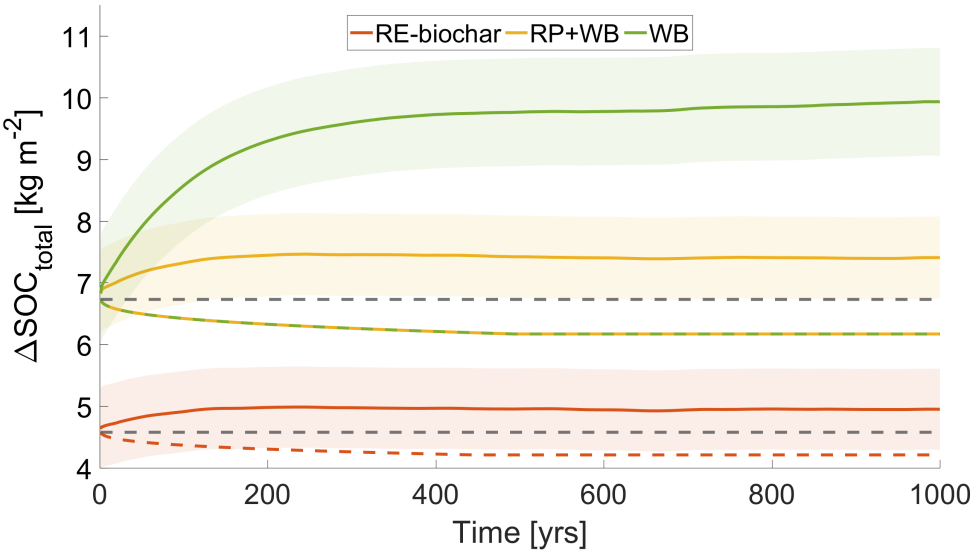

Figure 3.3: Smoothed mean trends of total soil organic carbon relative to the modeled Control treatment (ΔSOC_{total}, solid lines) for wood biochar (WB), co-application with rock powder (RP+WB), and their co-pyrolysis (RE-biochar). Shaded areas represent the standard deviation caused by natural ecosystem variability. Dashed colored lines indicate the modeled contribution of biochar to SOC_{total}, while the dashed gray lines show the initial biochar carbon input at the time of application.

3.3.2 Effects on CO_2 fluxes

As mentioned earlier, SOC in LiDELSv2 remains nearly constant, reflecting a long-term balance between CO_2 assimilation and ecosystem respiration (R_{eco}) in the Control treatment. Since LiDELSv2 does not account for changes in nutrient dynamics, modeled CO_2 fluxes may vary as a result of changes in soil temperature and hydrology, which in turn affect microbial and plant activity.

The most notable change in Net Primary Production (NPP) occurred during the early years following biochar application (Figure 3.4). Over time, changes in SOC and soil properties had only minor impacts on vegetation productivity (Table 3.3), and NPP remained relatively stable across all treatments. Biochar sole treatment showed a modest 1% increase in NPP, while RP-alone decreased NPP by 0.4%. Co-application and co-pyrolysis treatments showed negligible changes (±0.1%) relative to the Control.

Table 3.3: Mean net primary production (NPP) for each treatment, averaged over specific time intervals, and expressed compared to the Control soil column. Values represent treatment means ± standard deviation. All treatments within a column do not differ significantly from one another ($p > 0.05$).

NPP [g C m^{-2} yr^{-1}] / Treatment	0-50 yrs	51-100 yrs	101-500 yrs	501-1,000 yrs
Control	577 ± 49	574 ± 49	572 ± 50	585 ± 51
Rock Powder (RP)	575 ± 48	571 ± 48	570 ± 49	583 ± 50
vs. Control [%]	−0.3	−0.4	−0.4	−0.4
Wood Biochar (WB)	583 ± 55	577 ± 50	576 ± 52	589 ± 54
vs. Control [%]	+1.0	+0.6	+0.7	+0.6
Co-application RP + WB	578 ± 52	573 ± 48	572 ± 50	585 ± 52
vs. Control [%]	+0.2	−0.2	−0.1	−0.1
Co-pyrolysis (RE-biochar)	578 ± 50	574 ± 49	573 ± 50	586 ± 51
vs. Control [%]	+0.2	+0.1	+0.1	+0.1

Model results did not show significant changes in R_{eco} (Table 3.4). Biochar-related treatments initially decreased CO_2 release, with the largest reduction observed in the WB-only scenario – a 1.3% decrease during the first 50 years compared to Control. However, this effect diminished over time, resulting in up to 0.3% over 1,000 years (Figure 3.5). The RP-only treatment showed a 0.1% increase in CO_2 respiration in the first 50 years, followed by a 0.2% decrease compared to Control over the next 500 years.

To estimate the net CO_2 balance of the modeled ecosystem with and without amendments, we calculated the net ecosystem exchange (NEE) as the difference between R_{eco} and gross primary production (Table 3.5). In the first $300-400$ years, all biochar-related treatments reduced NEE relative to the Control (Figure 3.6). However, over longer timescales, NEE in both the co-application and co-pyrolysis scenarios became indistinguishable from the Control, making their long-term impact comparable to the baseline.

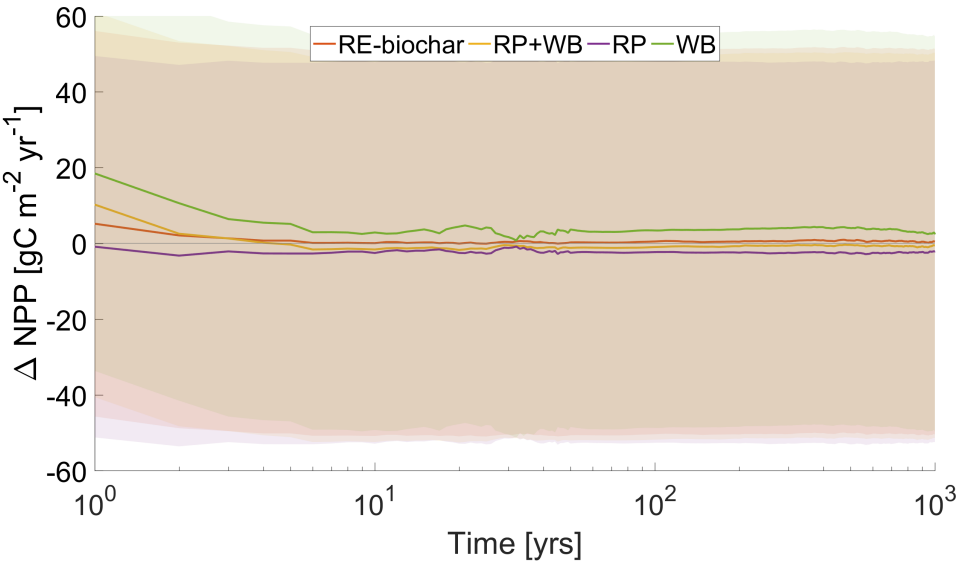

Figure 3.4: Change in mean net primary production over time compared to the modeled Control soil column (Δ NPP) for wood biochar (WB), rock powder (RP), their co-application (RP+WB), and co-pyrolysis (RE-biochar). Solid lines represent smoothed trends, while shaded areas represent the standard deviation caused by natural ecosystem variability.

Table 3.4: Mean ecosystem respiration (R_{eco}) for each treatment, averaged over specific time intervals, and expressed compared to the Control soil column. Values represent treatment means ± standard deviation. All treatments within a column do not differ significantly from one another ($p > 0.05$).

R_{eco} [g C m^{-2} yr^{-1}] / Treatment	0-50 yrs	51-100 yrs	101-500 yrs	501-1,000 yrs
Control	1190 ± 76	1201 ± 71	1200 ± 72	1210 ± 72
Rock Powder (RP)	1192 ± 76	1201 ± 71	1198 ± 72	1208 ± 72
vs. Control [%]	+0.1	0.0	−0.2	−0.2
Wood Biochar (WB)	1174 ± 75	1191 ± 71	1201 ± 72	1213 ± 72
vs. Control [%]	−1.3	−0.8	+0.1	+0.3
Co-application RP + WB	1184 ± 76	1197 ± 71	1199 ± 72	1210 ± 72
vs. Control [%]	−0.5	−0.3	−0.1	−0.1
Co-pyrolysis (RE-biochar)	1187 ± 76	1200 ± 71	1200 ± 72	1211 ± 72
vs. Control [%]	−0.2	−0.1	0.0	0.0

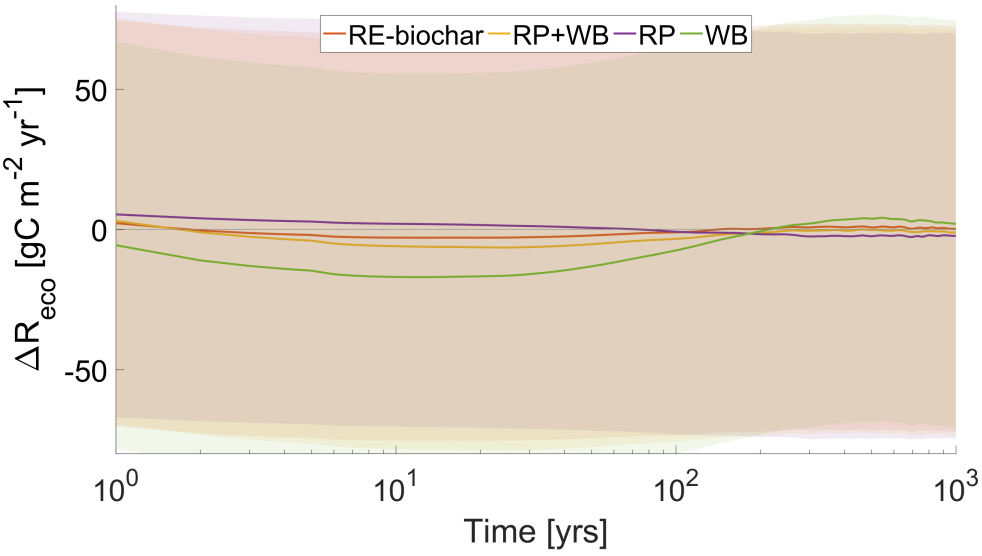

Figure 3.5: Change in mean ecosystem respiration over time compared to the modeled Control soil column (Δ R_{eco}) for wood biochar (WB), rock powder (RP), their co-application (RP+WB), and co-pyrolysis (RE-biochar). Solid lines represent smoothed trends, while shaded areas represent the standard deviation caused by natural ecosystem variability.

Table 3.5: Mean net ecosystem exchange (NEE) for each treatment, averaged over specific time intervals, and expressed compared to the Control soil column. Values represent treatment means ± standard deviation. All treatments within a column do not differ significantly from one another ($p > 0.05$).

NEE [g C m^{-2} yr^{-1}] / Treatment	0-50 yrs	51-100 yrs	101-500 yrs	501-1,000 yrs	1,000-yrs mean
Control	−6 ± 73	3 ± 71	1 ± 71	−2 ± 72	−1 ± 71
Rock Powder (RP)	−3 ± 72	5 ± 70	2 ± 70	−2 ± 71	0 ± 70
vs. Control	+3	+2	+1	0	+1 ± 70
Wood Biochar (WB)	−28 ± 79	11 ± 71	−1 ± 73	−3 ± 75	−3 ± 74
vs. Control	−22	−14	−2	−1	−2 ± 74
Co-application RP + WB	−13 ± 76	0 ± 70	1 ± 71	−2 ± 72	−1 ± 71
vs. Control	−7	−3	0	0	0 ± 71
Co-pyrolysis (RE-biochar)	−10 ± 74	1 ± 71	1 ± 71	−2 ± 72	0 ± 71
vs. Control	−4	−2	0	0	0 ± 71

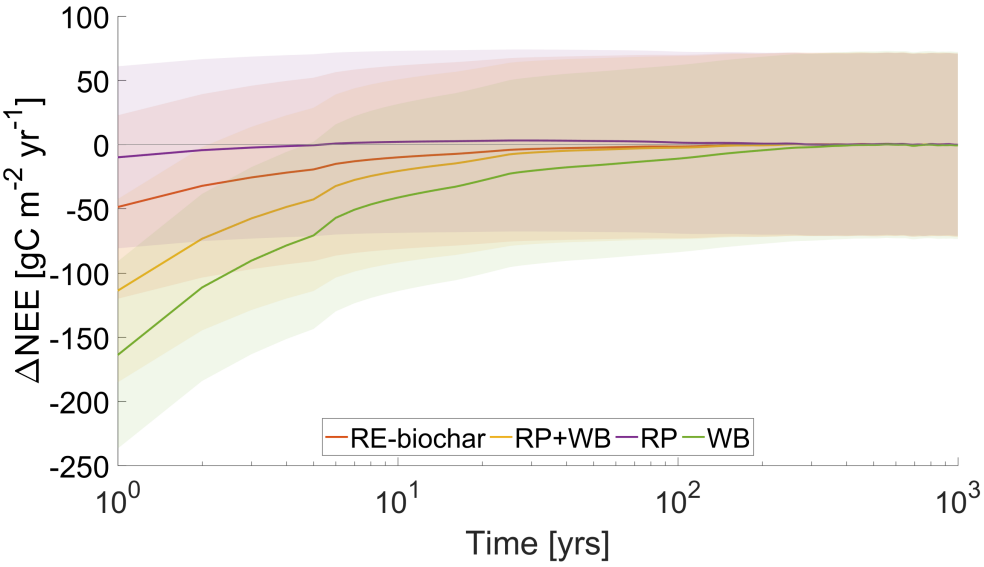

Figure 3.6: Change in net ecosystem exchange over time compared to the modeled Control soil column (Δ NEE) for wood biochar (WB), rock powder (RP), their co-application (RP+WB), and co-pyrolysis (RE-biochar). Solid lines represent smoothed mean trends, while shaded areas represent the standard deviation caused by natural ecosystem variability.

In contrast, the WB-only treatment consistently maintained lower NEE values than the Control, resulting in a net CO_2 removal of approximately 24 kg C ha^{-1} yr^{-1} over the 1,000-year period. When normalized by application rate, this corresponds to $\sim$ 200 g C ha^{-1} yr^{-1} per ton of applied biochar. The RP-only treatment resulted in higher NEE values, primarily due to reduced carbon assimilation caused by lower soil moisture. These results suggest that, under the modeled conditions, RP does not meaningfully contribute to long-term reductions in CO_2 emissions.

3.3.3 Effects on calcium leaching

In our weathering model, Ca^{2+} as the dominant cation released during the dissolution of basanite was assumed to be mobilized into soil groundwater and exported via drainage, representing a potential long-term CDR pathway. While the model focused on Ca^{2+}, other cations such as Mg^{2+}, K^+, and Na^+ may also participate in weathering reactions and enhance CO_2 removal, although they were not explicitly modeled.

Calcium leaching increased in all RP-containing treatments, indicating enhanced weathering activity (Table 3.6). The strongest response (Figure 3.7) was seen in the RP-only treatment, with a 21% increase in Ca^{2+} release in the short-term that gradually declined over time to 19%. Assuming the formation of 2 moles of HCO_3^- per mole of Ca^{2+} leached, the additional CDR potential from leaching may reach up to $\sim$ 3 g CO_2 ha^{-1} yr^{-1}, representing a theoretical upper bound.. Co-application and co-

pyrolysis scenarios showed similar but slightly weaker effects ($\sim$ 14% short-term, declining to $\sim$ 8% in the long term). In contrast, WB-only treatment led to a reduction in Ca^{2+} leaching – up to 26% at 1,000 years – mainly due to reduced soil water movement, which is a key driver of calcium leaching in the LiDELSv2.

Table 3.6: Mean calcium ions leaching (Ca^{2+}) for each treatment, averaged over specific time intervals, and expressed compared to the Control soil column. Values represent treatment means ± standard deviation. Different letters within the same column indicate statistically significant differences between treatments ($p < 0.05$).

Ca^{2+} [g m^{-2} yr^{-1}] Treatment	0-50 yrs	51-100 yrs	101-500 yrs	501-1,000 yrs
Control	0.69 ± 0.14^a	0.68 ± 0.15^a	0.70 ± 0.15^a	0.67 ± 0.15^a
Rock Powder (RP)	0.83 ± 0.17^b	0.83 ± 0.18^b	0.84 ± 0.18^b	0.80 ± 0.18^b
vs. Control [%]	+21	+21	+20	+19
Wood Biochar (WB)	0.59 ± 0.13^c	0.56 ± 0.14^c	0.5 ± 0.13^c	0.50 ± 0.13^c
vs. Control [%]	−15	−18	−23	−26
Co-application RP + WB	0.79 ± 0.16^b	0.78 ± 0.17^b	0.78 ± 0.17^d	0.73 ± 0.17^d
vs. Control [%]	+15	+13	+10	+8
Co-pyrolysis (RE-biochar)	0.77 ± 0.16^b	0.76 ± 0.17^b	0.77 ± 0.17^d	0.73 ± 0.17^d
vs. Control [%]	+13	+12	+10	+8

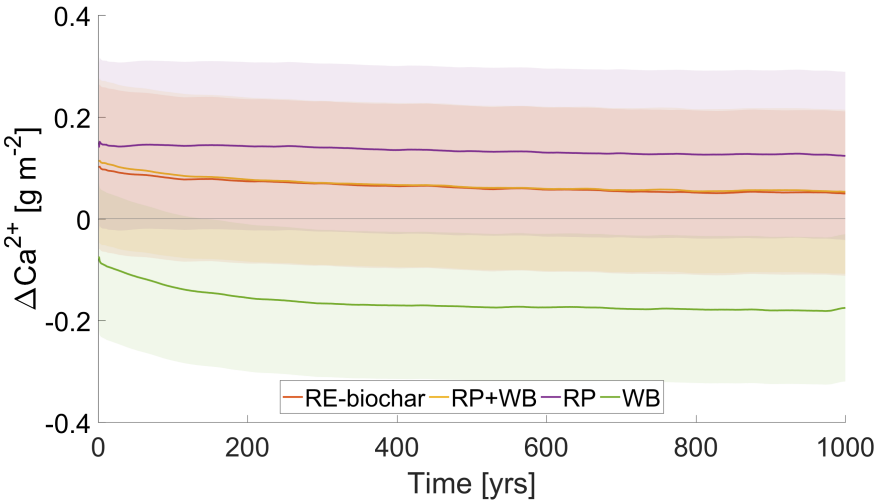

Figure 3.7: Change in calcium ions leaching over time compared to the modeled Control soil column (Δ Ca^{2+}) for wood biochar (WB), rock powder (RP), their co-application (RP+WB), and co-pyrolysis (RE-biochar). Solid lines represent smoothed mean trends, while shaded areas represent the standard deviation caused by natural ecosystem variability.

3.3.4 Sensitivity to biochar application rates

Under the assumed conditions, all biochar-amended treatments exhibited an approximately linear dependence of SOC change on application rate after 100 years (Figure 3.8), with a slight quadratic tendency. For net ecosystem exchange (Figure 3.9), a quadratic response was observed only for the co-application treatment, whereas the WB and RE-biochar treatments showed only small deviations from linearity.

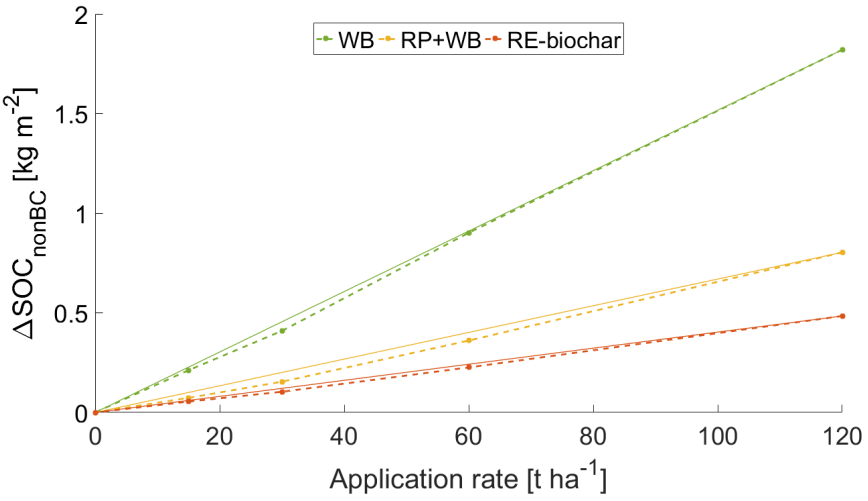

Figure 3.8: Change in non-biochar soil organic carbon (ΔSOC_{nonBC}) relative to the Control after 100 years for wood biochar (WB), co-application with rock powder (RP+WB), and co-pyrolysis (RE-biochar). Solid lines connect the Control (0 t ha^{-1}) and Geisenheim (120 t ha^{-1}) experiments; dashed lines with points show intermediate model outputs.

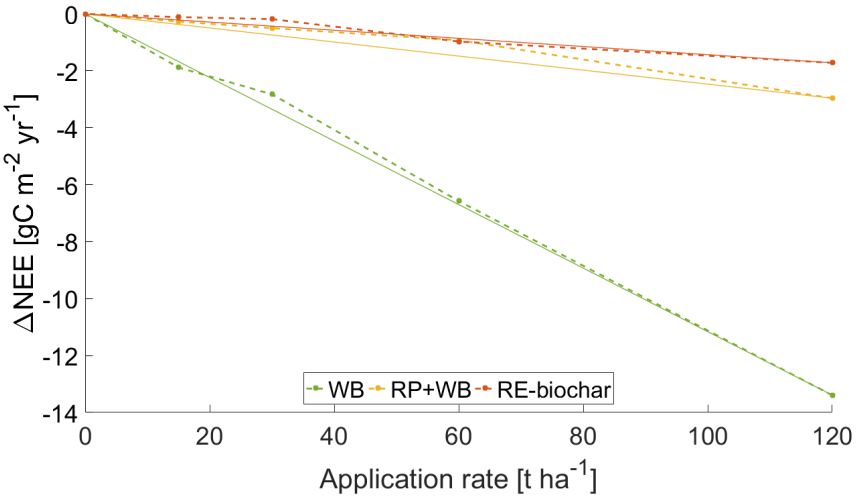

Figure 3.9: Change in net ecosystem exchange over time compared (Δ NEE) relative to the Control after 100 years for wood biochar (WB), co-application with rock powder (RP+WB), and co-pyrolysis (RE-biochar). Solid lines connect the Control (0 t ha^{-1}) and Geisenheim (120 t ha^{-1}) experiments; dashed lines with points show intermediate model outputs.

3.4 Discussion

3.4.1 Model validity and relevance of application rates

The Control scenario assumes a steady-state system with minimal change in SOC over the 1,000-year simulation period. The initial SOC stock was set to 67 t ha^{-1} based on measurements from the Geisenheim experiment and reached a mean of 71 ± 6 t ha^{-1} during the final 500 years. This value is slightly lower than the mean SOC reported for German mineral soils, which typically ranges from 90 to 100 t ha^{-1} (Poeplau et al., 2020).

Simulated values for NPP in the Control scenario averaged $572 - 585$ g C m^{-2} yr^{-1}, aligning well with reported ranges of $590-680$ g C m^{-2} yr^{-1} for temperate croplands under comparable climatic conditions (L. Ma, 2020). The Control treatment was constrained to be approximately NEE-neutral (-1 g C m^{-2} yr^{-1}) in order to maintain a steady state, where ecosystem respiration balances gross primary production in long-term. In real-world systems, however, European croplands tend to exhibit slightly positive NEE values (approximately +17 g C m^{-2} yr^{-1}), indicating a gradual loss of SOC over time (Ciais et al., 2010).

Taken together, the consistency between modeled, observed, and literature-based values for SOC, NPP, and NEE supports the plausibility of the Control simulation and strengthens confidence in the model's capacity to simulate treatment effects.

While the modeled biochar and rock powder application rates in this study were selected to match those used in the Geisenheim experiment, their real-world applicability should be carefully contextualized. The applied rate of 56 t ha^{-1} for rock powder lies at the upper end of what is considered agronomically feasible (Beerling et al., 2020; Dietzen et al., 2018). In contrast, the modeled biochar application rate of 121 t ha^{-1} is well above typical field applications, which generally fall in the range of 10–30 t ha^{-1} (Bekchanova et al., 2024), which in practice rather will be the result of repeated application of biochar-treated manure or biochar-based fertilizers (Grafmüller et al., 2024). High biochar application rates can lead to the accumulation of potentially toxic trace elements originating from both biochar and rock powder and may pose risks when applied to soils (Dupla et al., 2023; Kujawska, 2023). In the RE-biochars comparable to those used in this study, most trace element concentrations (e.g., Zn, Cu) were within EU fertilizer safety standards, although some elements such as Ni approached threshold values (Meyer zu Drewer et al., 2025). In addition, high application rates may induce hydrophobic soil behavior, potentially reducing surface water infiltration (Vitková et al., 2024).

These considerations underscore the mechanistic nature of our study: the selected application rates are not intended as direct field recommendations but rather to illustrate long-term system behavior and treatment interactions. While relative changes compared to the Control treatment provide meaningful insight, we also present maximum CDR effects normalized to per-ton application rates of biochar, to improve comparability and guide future implementation strategies.

Within this framework, our assumption of linear scaling in soil parameters with decreasing biochar application rates produced nearly linear long-term responses of SOC and NEE across all treatments. This outcome reflects the simplified parameterization procedure, rather than a mechanistic representation of biochar-soil interactions. In practice, experimental evidence suggests that biochar effects on soil properties and ecosystem fluxes are often nonlinear. Several meta-analyses report near-linear responses of bulk density and porosity to application rate (Blanco-Canqui, 2017; Zhen Jiang et al., 2025), but mixed or site-specific effects on saturated conductivity. Blanco-Canqui (2017) further noted that small application rates (<10 t ha^{-1}) may produce no measurable change, while high rates (>2 wt%) do not further reduce soil bulk density. Similarly, Altdorff et al. (2019) found nonlinear responses of van Genuchten parameters and saturated conductivity across different application levels or repeated application.

Thus, while our model-based results help contextualize potential outcomes at agronomically relevant rates, they should be interpreted as first-order approximations that do not capture the full range of nonlinear feedbacks reported in experimental studies.

3.4.2 Comparison of (RE-)biochar and rock powder (co-)application

All biochar treatments contributed to increases in modeled SOC_{nonBC} through inputs from labile biochar degradation and from litter derived from increased plant carbon assimilation. It should be noted that the SOC_{nonBC} pool in the model does not retain information about the origin of carbon inputs; whether derived from biochar or litter, all inputs contribute equally. Subsequent microbial decomposition of SOC_{nonBC} produces CO_2 without distinction of carbon origin. This represents a simplification compared to empirical observations, where biochar degradation may follow distinct oxidation pathways (Zimmerman, 2010).

We observed an initial reduction in SOC_{nonBC} losses via soil respiration, until soil carbon stocks grew large enough that R_{eco} increased due to the expanded carbon reservoir (Figure 3.5). In the WB sole scenario, SOC_{nonBC} increased by an average of 13% over the first 50 years and by 52% after 1,000 years, relative to the Control (Table 3.2).

Most empirical studies cover shorter timescales (typically up to 10 years), a meta-analysis by Gross et al. (2021) reported a comparable trend, with average SOC increases of 1.3 g C m^{-2}, with higher values observed for longer durations and higher application rates. The slightly lower SOC_{nonBC} and higher SOC_{total} gains in our simulation may reflect the conservative degradation assumptions embedded in the LiDELS model, as well as the properties of high-temperature biochar, which typically contains a smaller labile fraction than low-temperature variants (Tomczyk et al., 2020).

In contrast, RP application did not directly increase SOC, as it does not introduce carbon into the system. Under field conditions, RP can indirectly enhance SOC by increasing

soil pH and nutrient availability, thereby promoting plant growth and litter inputs (Swoboda et al., 2022; Vienne et al., 2022). However, these mechanisms are not represented in our model. Instead, the RP treatment was defined by higher saturated hydraulic conductivity and a van Genuchten n parameter, along with a lower van Genuchten α compared to the Control (Table 3.1). These properties made the soil slightly more conductive to water flow, reducing water retention in the root zone. As a result, plant-available water decreased, leading to reduced carbon assimilation and ultimately a 7% decline in SOC over the 1,000-year simulation period.

The co-application of WB and RP, as well as the use of RE-biochar, resulted in intermediate outcomes. Both treatments led to increases in SOC relative to the Control, but their performance was significantly lower than that of WB alone, despite identical biochar application rates. Even when combining the individual effects of WB and RP, the resulting SOC increase remained higher than that of the WB+RP and RE-biochar treatments. This divergence widened over time, suggesting that co-application or co-pyrolysis may dilute the long-term carbon sequestration benefits of biochar.

Due to the addition of the PAC fraction, SOC_{total} increased substantially under all biochar-related treatments. The high-temperature biochar used in our simulations contained over 90% PAC, resulting in nearly a 100% additional increase in SOC_{total} compared to SOC_{nonBC} for WB and WB+RP treatments, and approximately 60% for RE-biochar. These substantial SOC_{total} gains are expected to remain stable in soil for over a thousand years (Howell et al., 2022). For low-temperature biochar, a lower fraction of PAC is expected (Hagemann et al., 2025), resulting in higher proportions of labile carbon that are more rapidly degraded. This would likely lead to greater short-term increases in SOC_{nonBC}, but a reduced potential for long-term carbon storage compared to the high-temperature biochar considered here (J. Wang et al., 2016).

All biochar treatments contributed to an increase in NPP, primarily during the first 10 years, driven by improved soil water availability. Over time, as vegetation adapted to the new conditions – represented in the model by changes in mean annual soil water content – NPP stabilized. Subsequently, the expanded soil carbon reservoir led to an increase in R_{eco}. For WB+RP and RE-biochar, NEE became slightly positive after 300–400 years, offsetting their initial climate benefits over the 1,000-year simulation. In contrast, the WB-only treatment consistently maintained lower NEE values than the Control, making it the only treatment with a net negative NEE under the modeled conditions.

Our results show that calcium leaching alone does not fully offset the positive NEE observed in the RP-only treatment. However, it provides a modest additional carbon removal effect when RP is co-applied with WB or incorporated into RE-biochar. Findings from Vorrath et al. (2025), who studied the same basanite rock, suggest that significant contributions to CDR can also arise from other ions present in basanite. These additional weathering reactions may bring the NEE of RP-based treatments closer to that of the Control.

Overall, our modeling results align with experimental findings (Ansari et al., in prep. Hamburger et al., in prep. Vorrath et al., 2025), showing that WB-based scenarios offer the highest CDR potential. Solo biochar application emerges as the primary driver, while weathering-related processes play a secondary, supportive role – mainly through their influence on soil physical and hydrological properties. Vorrath et al. (2025) also reported that biochar may have up to eight times higher CDR potential than rock powder. When accounting for applied application rates, this impact could be up to 16 times higher. This disproportion may help explain why our modeling study shows a clear dominance of biochar in terms of long-term carbon sequestration.

3.4.3 Model limitations

While LiDELSv2 provides a robust and flexible framework for simulating long-term soil carbon dynamics under amendments such as rock powder and biochar, important mechanistic limitations remain that should be acknowledged and addressed in future model developments.

The model does not represent key processes associated with biochar surface chemistry, such as cation exchange capacity, sorption of organic and inorganic species, or reduction–oxidation reactions. These mechanisms can strongly influence nutrient availability, soil fertility, kinetics of mineral weathering, microbial activity, and influence SOC formation (Antonangelo et al., 2024; Joseph et al., 2021; Lee et al., 2021). Moreover, LiDELSv2 simplifies the weathering module by considering only Ca^{2+} release from basanite, thereby neglecting contributions from other base cations (e.g. Mg^{2+}, K^{+}, Na^{+}) and omitting potential interactions between biochar and rock powder that are mediated by aqueous-phase geochemistry and reactive transport. As a result, the model likely underestimates or misrepresents the synergistic or antagonistic effects of combined amendments, and our estimates of rock powder's CDR potential should not be interpreted as a full evaluation of geochemical pathways.

The current version of LiDELSv2 does not simulate nutrient dynamics. In real-world ecosystems, increased nutrient availability can stimulate plant growth and carbon assimilation, potentially enhancing NPP and SOC formation (Z.-L. Li et al., 2021). As a result, our simulations likely provide a conservative estimate of the CDR potential of the tested amendments, as they focus solely on hydrological and structural soil properties.

Moreover, LiDELSv2 does not account for non-CO_2 greenhouse gas emissions that may be associated with biochar or basalt applications (Chiaravalloti et al., 2023; Joseph et al., 2021). These emissions could either offset or enhance the net climate benefit, depending on site-specific conditions and amendment characteristics.

The impact of PAC in the model is represented solely through static soil input parameters. These are assumed to remain unaffected by changes in soil properties, microbial interactions, or long-term weathering processes. In reality, PAC degrades very slowly

over centuries, primarily through the gradual breakdown of aromatic structures. This process can alter soil structure and influence modeled soil parameters over time (Mia et al., 2017), which is not captured in the LiDELSv2.

Finally, the current model run does not include seasonal harvesting, which would in reality increase NEE and reduce SOC stocks over time (Ciais et al., 2010). Other agricultural practices, such as irrigation, tillage, and fertilization, also influence soil carbon dynamics by altering decomposition rates, microbial activity, and plant productivity (Han et al., 2024), but are also not represented in the current simulations.

Taken together, these limitations mean that the model results should be interpreted as idealized scenarios that isolate the effects of soil physical and hydrological changes. The exclusion of nutrient cycling, reactive transport, electrochemical processes, management practices, and non-CO_2 emissions implies that the modeled CDR potentials may underestimate or misrepresent real-world outcomes, depending on site conditions. Therefore, while the model provides valuable insights into long-term trends and relative treatment performance, the absolute values of SOC and NEE should be viewed with caution and complemented by empirical data and more comprehensive models in future work.

3.5 Conclusions

Our long-term simulations using the LiDELSv2 process-based model demonstrate that the application of biochar to temperate sandy agricultural soil offers the highest potential for CDR and carbon sequestration. Biochar led to persistent increases in both total and non-biochar SOC over a 1,000-year period. While co-application with rock powder and co-pyrolysis also improved SOC stocks, their effectiveness was lower than biochar alone, suggesting that combining biochar with RP may reduce its long-term CDR performance. Rock powder application alone had no positive effect on SOC or NEE, and its CDR potential via enhanced Ca^{2+} leaching was minimal. Across all treatments, modeled impacts on NPP and R_{eco} were small compare to natural ecosystem variation, underscoring that long-term soil-based CDR is primarily driven by the stability of biochar carbon.

The dominant role of biochar can be explained by its ~ 16 higher CDR potential per unit area compared to rock powder, based on the application rates used. In the modeled idealized scenario, we refer only to changes in specific soil physical and hydrological properties, and do not simulate nutrient dynamics or non-CO_2 GHG emissions. As such, it likely underestimates the full CDR potential of nutrient-rich amendments. Future modeling efforts should incorporate nutrient cycling, land management practices, and empirical data to refine projections and better guide effective soil-based CDR strategies.

Acknowledgments

We would like to thank to ICDC, CEN, University of Hamburg for providing ERA data for running the model. We acknowledge the assistance of AI tools (e.g., OpenAI's ChatGPT, Microsoft Copilot) in refining the publication language and improving the clarity of the manuscript.

The data that support the findings of this study are openly available following an embargo at the following https://zenodo.org/records/16151579.

3.6 Appendix

3.6.1 Model Calibration

For all calibration runs, we use meteorological input from local weather station (Hamburger et al., in prep.). The calibration data are provided with the LiDELSv2 model source in Maslouski and Porada (2025).

Soil Organic Carbon (SOC) estimations

In the LiDELSv2 model, the SOC pool increases through the degradation of labile biochar and vegetation inputs simulated by the litter function. This carbon is subsequently processed by soil microbes, which decompose the litter and release carbon as soil CO_2, eventually emitted through soil respiration.

In the Geisenheim experiment (see Section 3.2.1), no litter input occurred, as the entire plant biomass, including roots, was removed after the experiment. However, microbial activity continued, fueled by available SOC and the degradation of the labile biochar fraction.

Biochar was assumed to be applied to a depth of 25 cm, corresponding to the top two modeled soil layers. This depth aligns with the agricultural definition of topsoil (Poeplau et al., 2020) and matches the pot depth used in the Geisenheim experiment. Carbon release from labile biochar was simulated using a degradation function specific to oak wood biochar produced at 650 °C (Zimmerman, 2010):

$$C(t) = C_{\text{in}} \times \left(1 - \frac{\exp(-5.513)}{-0.679 + 1} \cdot t^{-0.679+1}\right)$$

where C_{in} is the initial amount of biochar. This function provided a good fit ($R = 0.97$ pearson correlation coefficient) to the measured SOC values (Table 3.7) and was applied in the LiDELSv2 simulations. In our research, we selected the oak wood biochar decay function because it best matched the data obtained from the Geisenheim experiment, when compared with decay functions for other 650 °C biochars in Zimmerman (2010) and with the function proposed in the Global Biochar C-Sink Standard 3.1 (Schmidt et al., 2024).

The above function predicts that about 88% of the initially applied oak biochar would remain after 1,000 years. To ensure consistency with the assumed persistent aromatic carbon (PAC) fraction of the (RE-)biochar, we constrained the decay curve such that degradation ceases once the PAC limit is reached, which occurs after approximately 500 years in our simulations.

Table 3.7: Comparison of measured and modeled soil organic carbon (SOC)

Treatment	Measured SOC [%]	Modeled SOC [%]
Control initial	1.24	-
Control final	1.17	1.17
Rock Powder (RP)	1.13	1.21
Wood Biochar (WB)	1.98	1.89
Co-application RP + WB	1.84	1.84
Co-pyrolysis (RE-biochar)	1.96	1.78

Soil Microbial Biomass (MB) as a Function of Soil Organic Carbon (SOC)

An empirical power-law relationship was derived from the data fit, using the functional form and coefficient proposed by Liddle et al. (2020):

$$\text{MB [mg/kg]} = 432 \times 10^{0.00815 \times \text{SOC [g/kg]}}$$

This function was then used to predict MB for the measurement samples based on measured SOC values (Table 3.8). A regression fitted to the measured MB values yielded the following relationship:

$$\text{Measured MB} = 1.5 \times \text{Modeled MB} - 190.05$$

with a Pearson correlation coefficient of $R = 0.93$. Based on this calibration, the final equation used in the model was:

$$\text{MB [mg/kg]} = 648 \times 10^{0.00815 \times \text{SOC [g/kg]}} - 190.05$$

Table 3.8: Measured soil organic carbon (SOC) and microbial biomass (MB) from Ansari et al. (in prep.), compared to modeled MB based on the relationship proposed by Liddle et al. (2020).

Parametr	Measured	Measured	Modeled
Treatment	SOC [g/kg]	MB [mg/kg]	MB [mg/kg]
Control	12	622	539
Rock Powder (RP)	11	589	534
Wood Biochar (WB)	20	754	627
Co-application RP + WB	18	730	611
Co-pyrolysis (RE-biochar)	20	712	624

Net primary production

Net primary production (NPP) in LiDELS is represented as a CO_2 assimilation process, limited by light availability and atmospheric CO_2 concentration. Vegetation growth is also influenced by soil water availability.

In the Geisenheim experiment (see Section 3.2.1), plant yields as well as leaf and root dry biomass were measured (Table 3.9). Modeled NPP accounts for approximately 25% of the measured dry biomass, which is lower than expected based on literature values of $38 - 46\%$ (Pate and Layzell, 1981). Despite a good fit between modeled NPP and measured dry yields ($R = 0.79$, Pearson correlation coefficient), this discrepancy may be explained by the LiDELS model not accounting for the nutrient-enhancing effects of biochar–rock applications, which can significantly promote plant growth. In the Geisenheim experiment, plants were additionally fertilized with both mineral (Ferty 2 Mega) and organic (Vinasse CARBUNA AND) fertilizers – an effect not represented in the model. Furthermore, the vegetation parameters in the model may not be optimized for the specific crop used in the experiment; instead, LiDELS simulates a generic C3 plant rather than the cabbage turnip cultivated in the study.

To assess model dynamics, we calculated the correlation between measured dry yields and the mean soil water content simulated by the model (Table 3.9), which showed a strong relationship ($R = 0.82$, Pearson correlation coefficient). The correlation between modeled NPP and mean soil water content was even higher, with $R = 0.97$.

Table 3.9: Measured dry biomass from Hamburger et al. (in prep.), compared to modeled net primary production (NPP) and modeled mean soil water content in the 25 cm soil column, representing the pot depth used in the lysimeter experiment by Hamburger et al. (in prep.).

Parametr Treatment	Mean soil water content [-]	NPP [g C m^{-2}]	Dry biomass [g m^{-2}]
Control	0.186	313	1170
Rock Powder (RP)	0.190	314	1167
Wood Biochar (WB)	0.205	319	1351
Co-application RP + WB	0.209	321	1301
Co-pyrolysis (RE-biochar)	0.197	316	1203

3.6.2 Supplementary Materials

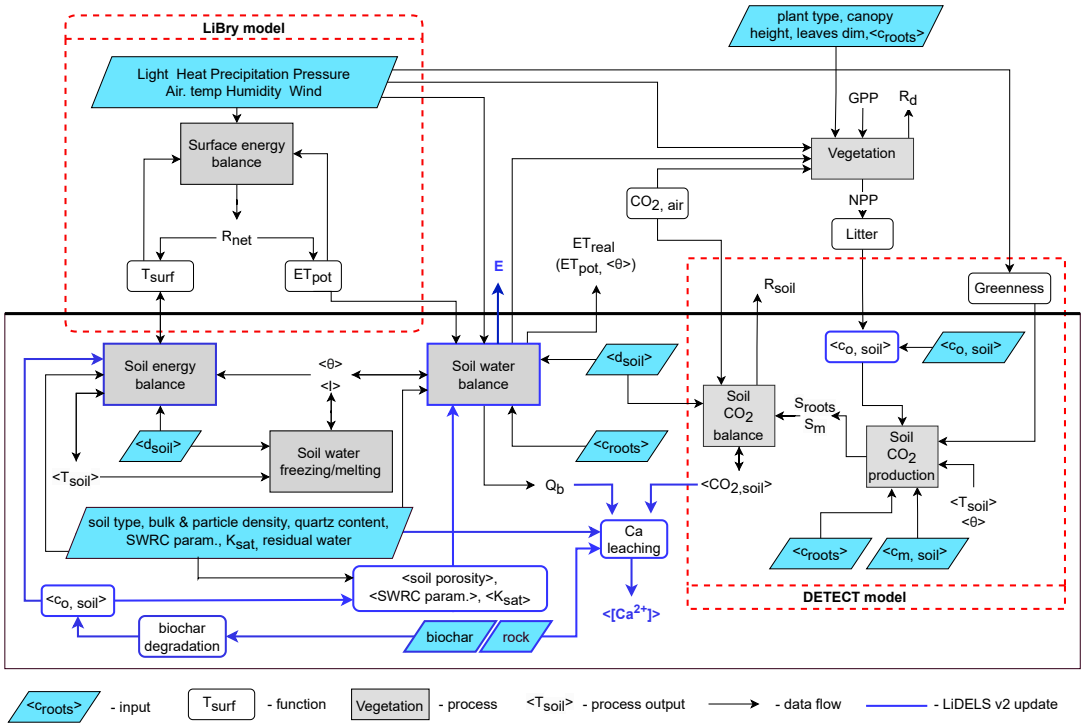

Figure 3.10: Simplified representation of the updated LiDELSv2 model structure. New processes and connections introduced compared to the previous release in Maslouski et al. (2025a) are highlighted in blue. Angle brackets $\langle\rangle$ denote vector-valued variables defined for each soil layer. R_{net} represents net radiation at the soil surface. T indicates temperature at the surface $(_{\text{surf}})$ or within soil layers. ET refers to evapotranspiration, either potential $(_{\text{pot}})$ or actual, while E referes to evaporation. R denotes CO_2 respiration from the entire plant $(_d)$ or from the soil. CO_2 indicates gas concentration in the air or within soil layers. Q_b refers to seepage. θ is the soil water content, and I is the soil ice content. d specifies soil layer thickness. The parameter c describes the vertical distribution of soil organic matter $(_o)$, microbial biomass $(_m)$, or root biomass $(_r)$. $[Ca^{2+}]$ referes to the leaching rate of calcium ions.

Chapter 4

General Conclusions and Outlook

This cumulative dissertation investigated the carbon dioxide removal (CDR) potential of biochar-based Pyrogenic Carbon Capture and Storage (PyCCS) and Enhanced Rock Weathering (ERW) in temperate agricultural soils by developing and applying the LiBry-DETECT Layer Scheme (LiDELS) modeling framework. The work addressed the need for a mechanistic understanding of how soil amendments influence soil physics, microbial activity, and vegetation performance, and how these interactions jointly determine long-term carbon sequestration (Chapter 1). Two peer-reviewed papers presented in this thesis provide complementary perspectives: medium-term soil-vegetation feedbacks following biochar application (Chapter 2) and millennium-scale projections of carbon dynamics under solo, co-application and co-pyrolysis of biochar and silicate rock powder (Chapter 3). Together, these contributions advance both the scientific foundation and practical assessment of land-based CDR strategies.

4.1 Synthesis of main findings

The results presented in this dissertation demonstrate that biochar and basanite rock powder influence carbon cycling through several interconnected pathways. Simulations with LiDELSv1 (Chapter 2) show that biochar amendments consistently improved soil water retention in the root zone, leading to enhanced vegetation productivity. These hydrological improvements strengthened net primary production (NPP) and increased plant-derived carbon inputs to the soil. At the same time, the model predicted only minor increases in soil respiration, resulting in a net gain of soil organic carbon (SOC) in the medium term. The simulations highlight the central role of vegetation responses in shaping the net CDR outcome in amended sandy soils in the medium term, a conclusion that is consistent with the long-term LiDELSv2 results.

Long-term simulations with LiDELSv2 (Chapter 3) revealed that basanite rock powder contributes to inorganic CDR through the release and leaching of calcium ions, with the corresponding bicarbonate export representing a multi-century carbon sink. When

accounting for the assumed amendment rates and changes in specific soil properties, wood biochar remained the amendment with the highest long-term CDR potential, primarily due to its contribution to both total SOC (including the biochar C pool) and the non-biochar SOC pool (excluding biochar) on millennial timescales. Overall, the modeled conditions indicate that biochar is the dominant driver of long-term soil-based CDR. Co-application and co-pyrolysis of biochar and basanite generated slightly synergistic effects by moderating soil hydrology and creating more favorable conditions for vegetation comparing to weathering alone. However, these combinations also led to a moderate reduction in the total long-term CDR relative to biochar alone, primarily due to a dilution effect where the addition of rock powder creates less favorable conditions for the accumulation of SOC. Although changes in NPP and ecosystem respiration are small over most of the 1,000-year simulations, the differences introduced during the first decades to centuries after application can shift SOC accumulation trajectories, and these early divergences persist over millennial timescales. This indicates that biochar-driven long-term CDR in the modeled system arises primarily from the persistence of pyrogenic carbon and its early influence on SOC dynamics, rather than from sustained long-term shifts in biological and geochemical fluxes.

A consistent insight from both chapters is the central importance of soil hydrology in shaping amendment outcomes. Increasing water availability in coarse-textured soils allows biochar to enhance the resilience of agricultural systems (Joseph et al., 2021) by promoting vegetation productivity and microbial activity (Deng et al., 2026; W. Liu et al., 2009). These biological responses regulate ecosystem carbon fluxes and SOC dynamics, which in turn can further modify soil hydrological balance (Vereecken et al., 2010). In LiDELS, this establishes a coupled feedback loop in which amendment-induced changes in soil water availability alter vegetation productivity and microbial respiration, modify CO_2 profiles in the soil column, and thereby influence both SOC dynamics and mineral weathering rates. However, hydrological responses to biochar are not universal and strongly depend on feedstock, particle size, and application rate; at unusually high application rates (Bekchanova et al., 2024) or under conditions that promote hydrophobicity or pore clogging, plant-available water can decrease rather than increase (Vitková et al., 2024; W. Wu et al., 2022).

The weathering module in LiDELSv2, adapted from Arens (2013), depends directly on soil water flow, soil CO_2 concentrations, and mineral content. Because microbial respiration and root-derived CO_2 production are tightly regulated by soil moisture availability, vegetation and microbial processes indirectly influence weathering potential. Results from Oliveira Garcia et al. (2020) indicate that rock powder application has a marginal effect on soil hydraulic properties even at considerably higher application rates than those used in LiDELSv2, while still causing small deviations in plant-available water. LiDELSv2 illustrates how such subtle shifts can propagate through soil-vegetation-microbe feedbacks during the first decades to centuries after application and thereby alter SOC accumu-

lation trajectories, with consequences that remain apparent over millennial timescales, as demonstrated in Chapter 3. Correspondingly, differences in net ecosystem exchange (NEE) are concentrated in the transient period after application, rather than reflecting sustained long-term changes in NPP or ecosystem respiration.

These findings reinforce that hydrology forms the dominant control on both biological and geochemical amendment responses. Because nutrient dynamics are not explicitly represented in the model, the relative importance of hydrological controls may be overestimated. Nevertheless, in water-limited sandy soils, even subtle changes in soil moisture propagate through vegetation productivity, microbial respiration, and weathering microenvironments, ultimately shaping the net long-term CDR potential of both biochar and basanite. The results also demonstrate that vegetation feedbacks play a crucial role in shaping CDR outcomes by regulating carbon inputs to the soil and root-derived CO_2 production, while only modestly altering soil respiration under the modeled conditions. The strongest vegetation responses to a single biochar application are typically observed in the first few years and often weaken thereafter (Safaei Khorram et al., 2020; Song et al., 2016; Yang et al., 2025). In sandy, water-limited systems, vegetation can therefore amplify amendment-induced CDR by increasing carbon inputs during the early post-application phase, and the resulting SOC trajectory can remain shifted long after the initial response has attenuated.

4.2 Evaluation of biochar and basanite (co-)applications

This work provides one of the first mechanistic modeling assessments of combined biochar and basanite rock powder applications over millennial timescales, including co-pyrolyzed systems. Within the specific case-study system, it identifies the hydrological conditions under which co-benefits are maximized and clarifies the relative contributions of organic and inorganic CDR pathways.

The detailed analysis in Chapter 3 shows that, under the temperate sandy soil conditions considered here, combined applications of wood biochar and basanite do not outperform sole wood biochar in terms of long-term CDR. Wood biochar alone produces the largest and most persistent increase in total and non-biochar SOC, and sustains a moderate CO_2 sink over 1,000 years, whereas basanite alone yields only a small additional inorganic CDR flux via Ca^{2+} leaching without improving SOC or NEE relative to the Control. Co-application of biochar and basanite and the use of rock-enhanced biochar lead to intermediate trajectories in SOC and NEE that clearly exceed those of basanite alone, but do not surpass the CDR efficiency of sole biochar, even when evaluated over millennial timescales. In the modeled system, adding basanite to biochar acts primarily as a dilution of the biochar-driven CDR signal rather than creating a strongly synergistic

"super-sink" (see detailed discussion in Section 3.4.2).

These conclusions are, however, conditional on the specific climatic and edaphic setting represented in the LiDELSv2 simulations: a temperate, water-limited, coarse-textured soil receiving amendment rates matching those in the lysimeter experiment – moderate for rock powder and comparatively high for biochar (see detailed discussion in Section 3.4.1). In more humid and warmer climates, higher soil temperatures, greater water fluxes, and enhanced biological activity can substantially accelerate silicate weathering and bicarbonate export (Gurumurthy et al., 2012; P. C. Ryan et al., 2024), increasing the relative importance of the inorganic CDR component from rock powders compared to the temperate case studied here. Similarly, biochar effects on plant productivity and SOC have repeatedly been found to be strongest in coarse-textured, nutrient-poor and water-limited soils, with more variable or weaker responses in fine-textured or already fertile systems (Bekchanova et al., 2024; Blanco-Canqui et al., 2020; X. Liu et al., 2013).

Taken together, this suggests that in other combinations of climate, soil texture, and rock type, the balance between organic and inorganic CDR in combined biochar-rock powder strategies may shift towards a stronger contribution from enhanced weathering or towards additive agronomic co-benefits such as pH buffering and nutrient supply (Amann and Hartmann, 2019; Buss et al., 2022). The site-specific results obtained here therefore argue for treating co-application and co-pyrolysis as context-dependent options that require explicit evaluation across climatic gradients and soil types, which motivates the spatial upscaling and climate-scenario work outlined in Section 4.5.

4.3 Capabilities and limits of the LiDELS model

The LiDELS framework, developed in two iterations (LiDELSv1 and LiDELSv2), provides a lightweight, computationally efficient ecosystem model that couples soil water and heat transport, soil CO_2 production and diffusion, microbial respiration, vegetation carbon assimilation, and a simplified silicate weathering scheme within a one-dimensional soil-plant-atmosphere column. By combining the surface energy and water balance from LiBry with the soil CO_2 production and transport scheme of DETECT through a layered soil representation (for more details of coupling the two models see Sections 2.2 and 3.2.2), the model enables the investigation of feedbacks between soil hydrology, microbial processes, vegetation performance, and carbon cycling that are largely absent from existing biochar or weathering models.

The capabilities of LiDELS are demonstrated in two main contexts. First, LiDELSv1 reproduced key biophysical variables such as soil moisture and soil temperature for a sandy soil in northern Germany, and captured medium-term responses of soil water availability, evapotranspiration, microbial respiration, and vegetation productivity to biochar application (Chapter 2). This indicates that a relatively simple layered representation is sufficient to diagnose how biochar-induced changes in soil properties propagate through

soil-vegetation feedbacks and affect NEE and SOC. Second, LiDELSv2 extended this framework with modules for soil evaporation, silicate weathering (Ca^{2+} leaching), and biochar degradation, and was validated against lysimeter data from the Geisenheim experiment (Chapter 3). The model then enabled millennial-scale simulations of wood biochar, basanite, and their combinations under realistic climate forcing, quantifying long-term organic and inorganic CDR components.

The closest family of models to LiDELS on the soil-physics side are one-dimensional HYDRUS vadose-zone models, which are widely used to simulate variably saturated flow, solute and heat transport, and root water uptake (Simunek et al., 2005). They have also been applied to analyse how biochar modifies soil water retention and plant-available water by adjusting soil hydraulic parameters (for selected applications see Section 2.1), similar to the approach applied in LiDELS. Coupled HYDRUS-PHREEQC models (HPx) additionally resolve aqueous speciation, mineral dissolution, and leaching processes in the vadose zone (Simunek et al., 2012), providing a much more detailed description of biogeochemical reactions than the reduced-form weathering flux implemented in LiDELSv2. However, these frameworks typically treat vegetation only as a sink term for water (and sometimes solutes) and do not represent vegetation carbon assimilation, SOC dynamics, or long-term CDR accounting explicitly. LiDELS occupies a complementary niche by explicitly linking soil hydrology, soil CO_2 dynamics, vegetation productivity, biochar degradation, and simplified silicate weathering in a single framework suitable for long transient simulations.

Relative to widely used soil carbon and crop models, such as RothC (Lefebvre et al., 2020), CENTURY (Dil and Oelbermann, 2014), EPIC (Lychuk et al., 2014) or APSIM (Archontoulis et al., 2016), LiDELS offers a more explicit representation of vertical soil physics and soil CO_2 profiles, but a more schematic treatment of management and nutrient cycling. Many of these models include multiple SOC pools and detailed representations of agricultural practices (harvesting, residue management, fertilisation, tillage) and often explicit nitrogen cycles, which makes them powerful tools for assessing management scenarios at field to regional scale. However, calibration and validation of such models for biochar are often lacking (Ronix et al., 2025). Moreover, these models generally neglect silicate weathering, while most weathering models neglect agricultural processes and management (Taylor et al., 2016). LiDELS helps to bridge part of this gap by explicitly linking amendment-induced changes in soil hydraulic properties to vegetation responses, soil CO_2 dynamics, and a simplified weathering flux.

A key strength of LiDELS is its ability to bridge between detailed soil physics and ecosystem-scale carbon fluxes while remaining computationally tractable. The layer-based structure and limited set of state variables allow for long-term simulations and scenario analyses that would be prohibitively expensive with more complex three-dimensional or fully coupled Earth system models. This makes LiDELS particularly suited as an intermediate-complexity tool: detailed enough to resolve process interactions between soil

hydrology, vegetation, and amendments, yet efficient enough to be applied in sensitivity analyses, parameter explorations, and, in future work, spatial upscaling. Accordingly, the current parameterisation and evaluation are strongest for temperate, coarse-textured agricultural soils, and transfer to other soil-climate contexts should be treated as a hypothesis to be tested.

The specific limitations of LiDELS in its current form are discussed in detail in Section 3.4.3. In short, nutrient cycles, detailed mineralogy and geochemistry, and explicit agricultural management are either absent or represented in highly simplified form. These choices were made to preserve numerical stability and computational efficiency over long-term simulations and in view of future upscaling plans. They imply that LiDELS is best used as a mechanistic testbed for amendment effects on soil hydrology, vegetation, and carbon cycling, and for sensitivity studies, rather than as a fully fledged geochemical or crop model or a replacement for global CDR bookkeeping frameworks. Subsequent development steps, outlined in Section 4.5, aim to connect LiDELS more tightly to both ends of this spectrum.

4.4 Implications for CDR accounting

Scaling combined biochar-basanite applications from field trials to carbon markets requires measurement, reporting, and verification (MRV) that is credible at both site and project scale. Soil-based CDR accounting still faces a practical verification gap: intensive sampling is expensive, soils are highly heterogeneous, and stable carbon pools change slowly enough that clear signals can take decades to emerge (Lotz et al., 2024; P. Smith, 2004; P. Smith et al., 2020). The results of this thesis help structure the MRV problem by separating CDR-relevant outcomes into three connected components: (i) changes in SOC storage, (ii) changes in NEE, and (iii) the potential generation and export of alkalinity from silicate weathering (represented here by Ca^{2+} leaching). Turning these outcomes into climate claims requires a clear accounting boundary and a measurement concept that links observations to modeled state variables over the timescales that matter.

A central accounting challenge is demonstrating additionality: the claimed carbon benefit must be caused by the "intervention" rather than by natural variability (Clarke, 2023; Schmidt et al., 2024; Zakkour and Cook, 2024). For biochar-based pathways, the LiDELS framework supports this attribution because amendment-derived carbon can be tracked separately from changes in native SOC dynamics and plant-derived inputs. This makes a "hybrid" MRV approach more defensible: direct monitoring (e.g., lysimeter networks, targeted soil sampling) provides ground truth at discrete times, while the model provides the continuous context needed to interpret those snapshots and to attribute observed fluxes to specific mechanisms, like shifts in water availability, which affecting plant inputs or microbial activity. Combining monitoring and modeling is therefore not just a convenience; it is necessary if site-level evidence is to be extrapolated across the

soil and climate gradients typical of agricultural landscapes (P. Smith et al., 2020).

One important implication from the modeling results is that interventions can produce offsetting effects within the soil column, including cases of negative additionality. Chapter 3 shows that rock powder applied alone can reduce SOC in sandy soils through hydrological changes. From a MRV perspective, this is a material risk: protocols that focus only on mineral dissolution rates may overstate net climate benefits if concurrent SOC losses are not included in the accounting boundary. The LiDELS simulations provide a way to quantify these trade-offs so that CDR claims reflect the net system balance rather than a single process in isolation. For ERW, another persistent MRV difficulty is that the downstream fate of alkalinity is often not directly observed at the project scale. In this context, Ca^{2+} leaching provides a practical, measurable proxy for mineral dissolution that can be passed to hydrological transport models (e.g., MODFLOW workflows) when the goal is to connect soil signals to catchment-scale export and, ultimately, marine sinks.

The thesis also helps prioritise uncertainties that are likely to dominate long-term CDR estimates and therefore deserve targeted monitoring. Key examples are the multi-decadal degradation kinetics of pyrogenic carbon, the evolution of soil hydraulic properties under repeated amendments, and the stoichiometric conversion of cation export into net CO_2 removal. Treating these as explicit MRV targets clarifies what should be measured, how often, and why. In practical terms, reducing uncertainty will require coordinated datasets that link soil physical monitoring to carbon stocks and chemical export signals over multi-year periods, capturing both early transients and later stabilisation. Improving these constraints is one of the few realistic paths from conservative, high-discount crediting toward higher-confidence, performance-based claims.

Biochar and ERW are also not stand-alone solutions to climate change. Deployment is constrained by resource availability, system capacity, and site suitability, supporting the broader view that meeting Paris Agreement objectives will require a portfolio of CDR options (Zakkour and Cook, 2024). Consortium-scale efforts (e.g. CDRterra) are necessary to test transferability of different CDR approaches across soil and climate gradients, harmonise MRV concepts across sites, and connect process-based modeling with coordinated field evidence. Accounting-consistent MRV is therefore a prerequisite for translating site-level results into robust, comparable CDR claims, and it provides a clear motivation for the model development and evaluation steps described in the following section.

4.5 Future research directions

The development of LiDELS marks a transition toward process-based evaluation of combined CDR strategies, while also highlighting remaining gaps in our ability to simulate the full suite of soil–vegetation–geochemical feedbacks. As the model moves toward broader application, a critical guiding principle must be the maintenance of numerical

efficiency. In this regard, the current one-dimensional architecture provides a computationally efficient representation that can inform or be coupled to larger-scale land surface and Earth system modeling frameworks. Future development should therefore follow a modular architecture, allowing specialized process representations to be activated as needed and matched to the targeted spatial and temporal scale, without unnecessarily increasing model complexity or compromising the feasibility of long-term simulations in appropriate modeling frameworks.

A primary priority for model enhancement is resolving the mechanistic synergies and antagonisms of the combined biochar and rock powder approach, which were part of the original proposed model scheme for the PyMiCCS project (Hartmann et al., 2021, for details see Section 1.1). Currently, the model treats biochar and rock powder largely as additive components, which may underestimate or misrepresent their real-world combined efficiency. This is partly due to the exclusion of explicit nutrient cycling, where fertilization feedbacks on NPP remain indirectly captured. The nutrient cycles for nitrogen and phosphorus can be integrated based on existing modular approaches, such as the model proposed by Goll et al., 2012, using global distribution maps for initial conditions from Gao et al., 2022. Furthermore, to fully represent the co-application effect, future iterations must incorporate simplified aqueous-phase biogeochemistry as proposed by Azeem et al., 2022 and multi-mineral weathering modules (e.g., Bertagni et al., 2025). Moving beyond the current calcium-silicate focus to include a broader suite of base cations and mineral surface area dynamics will allow for a more precise quantification of how biochar-induced pH buffering and moisture retention accelerate mineral dissolution.

Beyond geochemistry, two critical biophysical feedbacks remain missing from the current framework: surface albedo and physical soil organic matter (SOM) stabilization. The application of biochar significantly darkens the soil surface, yet the resulting change in surface reflectance and energy balance (Ahmad Bhat et al., 2022) is not yet resolved in LiDELS. Incorporating an albedo module is essential for determining the net climate forcing of biochar, as increased surface warming could partially offset the benefits of carbon sequestration (Y. Zhang et al., 2018). Additionally, while LiDELS employs biochemical decay functions, it does not yet explicitly account for physical SOM stabilization within biochar micro-pores (Kalu et al., 2024) or via new organo-mineral associations (Guenet et al., 2018; Tang and Riley, 2013). Representing these physical protection mechanisms is a necessary step for moving from theoretical "potential" storage to verifiable long-term sequestration.

Another major frontier is the spatial upscaling of LiDELS from a 1D column model to a global simulation framework. This transition requires the systematic integration of high-resolution global datasets to provide necessary boundary conditions. The SoilGrids database (Poggio et al., 2021) provides a robust foundation for this, offering global maps of the soil physical properties required by the LiDELS hydrology and carbon modules, while mineral distribution data can be integrated from established global simulations (Arens

and Kleidon, 2011). The impact of biochar on soil physical and hydrological parameters can then be incorporated using pedotransfer functions, where biochar is treated as an additional change in SOC parameters (Yu et al., 2025), and rock powder as a shift in soil texture (sand and clay content) (Oliveira Garcia et al., 2020). These modeling frameworks (Arens and Kleidon, 2011; Oliveira Garcia et al., 2020; Yu et al., 2025) could be used to benchmark the individual impacts of biochar and rock powder against LiDELS outputs, allowing for an investigation of their combined potential. By running the upscaled model under varied CMIP6 climate scenarios, future research can identify "CDR hotspots" where the convergence of soil type, mineralogy, and projected precipitation maximizes the efficiency of combined amendments.

Scaling the model to thousands of grid cells necessitates a technical transition to high-performance computing environments. Fortunately, the LiBry model (Porada et al., 2016) – the parent platform from which LiDELS was derived – already possesses a global version equipped with parallel simulation procedures. The technical path forward involves the systematic transfer and optimization of the soil-vegetation-feedback functions developed within LiDELS into this established HPC infrastructure. This transition will not only allow for global spatial coverage but also enable the integration of model outputs into macro-economic assessment frameworks. By providing spatially explicit rates of carbon sequestration and crop yield changes, the upscaled model can inform calculations of the economic feasibility of CDR deployment across different geopolitical regions. Ultimately, these advancements will transform LiDELS from a site-specific research tool into a comprehensive decision-support system for global climate mitigation policy.

Final remarks

In conclusion, this dissertation demonstrates that soil-vegetation-microbe feedbacks are central to understanding the long-term CDR potential of biochar and silicate rock amendments. By combining mechanistic process-based modeling with empirical data, the LiDELS framework provides a foundation for evaluating PyCCS, ERW, and their combination across timescales relevant to climate mitigation. As LiDELS is further refined and upscaled, it will serve as a valuable tool for assessing land-based CDR strategies and informing their integration into climate policy and Earth system modeling.

Funding

This study was conducted as part of the PyMiCCS project (Pyrogenic Carbon and Carbonating Minerals for Enhanced Plant Growth and Carbon Capture and Storage), funded by the Federal Ministry of Education and Research (BMBF) of the Federal Republic of Germany within the CDRterra research program (2022-2025).

Acknowledgments

All the work described above would not have been possible without the support and contributions of colleagues from the University of Hamburg and the PyMiCCS project. I am grateful to my supervisor and co-supervisor for shaping the overall concept of my PhD and to the entire Advisory Panel Team for their guidance and mentoring during our APM meetings. With this, I also would like to thank the SICCS postgraduate school for structuring my PhD.

Both model releases would not have been possible without the data provided for model calibration and validation, including results from the PhD projects of Simon Thomsen and Maria Ansari under the supervision of Annette Eschenbach, as well as the PhD work of Susanne E. Hamburger supervised by Claudia I. Kammann.

I would also like to express my sincere thanks to Nikolas Hagemann, Claudia I. Kammann, Maria Ansari, Joscha N. Becker, Philipp Porada, and Maria-Elena Vorrath for their extensive feedback on the second paper, which I believe significantly improved compared to the first.

My thanks also go to all members of the Ecological Modeling group at IPM who were part of the team during my PhD, and especially to its first PhD graduate, Yunyao Ma, for her invaluable support.

I acknowledge the assistance of AI tools (e.g., OpenAI's ChatGPT, Microsoft Copilot, Google Gemini) in refining the language of this dissertation and improving its clarity.

"Last but not least, I want to thank me... I want to thank me for believing in me, I want to thank me for doing all this hard work. I wanna thank me for having no days off. I wanna thank me ***for never quitting****...."* (Fragment from Snoop Dogg's speech on the day he received his star on the Hollywood Walk of Fame, November 19th, 2018.)

Bibliography

Acharya, Bharat Sharma, Syam Dodla, Jim J Wang, Kiran Pavuluri, Murali Darapuneni, Sanku Dattamudi, Bijesh Maharjan, and Gehendra Kharel (2024). "Biochar impacts on soil water dynamics: knowns, unknowns, and research directions". In: *Biochar* 6.34. DOI: 10.1007/s42773-024-00323-4.

Ahmad Bhat, Shakeel et al. (2022). "Application of biochar for improving physical, chemical, and hydrological soil properties: A systematic review". In: *Sustainability* 14.17, p. 11104. DOI: 10.3390/su141711104.

Alma, Hakkı Mehmet and Alperay Altikat (2024). "Methods of Application and Incorporation of the Biochar into Soil". In: *World Journal of Agriculture and Soil Science* 7.1. DOI: 10.33552/WJASS.2021.07.000653.

Altdorff, Daniel, Lakshman Galagedara, Joinal Abedin, and Adrian Unc (2019). "Effect of biochar application rates on the hydraulic properties of an agricultural-use boreal podzol". In: 3.3, p. 53. DOI: 10.3390/soilsystems3030053.

Amann, Thorben and Jens Hartmann (2019). "Ideas and perspectives: Synergies from co-deployment of negative emission technologies". In: *Biogeosciences* 16.15, pp. 2949–2960. DOI: 10.5194/bg-16-2949-2019.

Ansari, Maria, Svenja Stock, Michaela Dippold, Susanne E. Hamburger, Claudia Kammann, Johannes Meyer zu Drewer, Nikolas Hagemann, Annette Eschenbach, and Joscha N. Becker (in prep.). "Biochar dominated the combined effect of silicate rock powder and biochar application on extracellular enzyme kinetics and nutrient dynamics in a sandy soil". Submitted to Soil and Tillage Research in October 2025.

Antonangelo, Joao Arthur, Steven Culman, and Hailin Zhang (2024). "Comparative analysis and prediction of cation exchange capacity via summation: influence of biochar type and nutrient ratios". In: *Front. Soil Sci.* 4.1371777. DOI: 10.3389/fsoil.2024.1371777.

Archontoulis, Sotirios V, Isaiah Huber, Fernando E Miguez, Peter J Thorburn, Natalia Rogovska, and David A Laird (2016). "A model for mechanistic and system assessments of biochar effects on soils and crops and trade-offs". In: *Glob. Change Biol. Bioenergy* 8.6, pp. 1028–1045. DOI: 10.1111/gcbb.12314.

Arens, Susanne (2013). "Global limits on silicate weathering and implications for the silicate weathering feedback". PhD thesis. Jena: Friedrich-Schiller-Universität Jena. URL: https://www.db-thueringen.de/receive/dbt_mods_00023499.

Arens, Susanne and Axel Kleidon (2008). "Global sensitivity of weathering rates to atmospheric CO_2 under the assumption of saturated river discharge". In: *Mineral. Mag.* 72.1, pp. 301–304. DOI: 10.1180/minmag.2008.072.1.301.

— (2011). "Eco-hydrological versus supply-limited weathering regimes and the potential for biotic enhancement of weathering at the global scale". In: *Appl. Geochem.* 26, S274–S278. DOI: 10.1016/j.apgeochem.2011.03.079.

Azeem, Muhammad, Sajjad Raza, Gang Li, Pete Smith, and Yong-Guan Zhu (2022). "Soil inorganic carbon sequestration through alkalinity regeneration using biologically induced weathering of rock powder and biochar". In: *Soil Ecol. Lett.* 4.4, pp. 293–306. DOI: 10.1007/s42832-022-0136-4.

Baronti, S, R Magno, A Maienza, A Montagnoli, F Ungaro, and F P Vaccari (2022). "Long term effect of biochar on soil plant water relation and fine roots: Results after 10 years of vineyard experiment". In: *Sci. Total Environ.* 851.Pt 1, p. 158225. DOI: 10.1016/j.scitotenv.2022.158225.

Beegum, Sahila, Wenguang Sun, Dennis Timlin, Zhuangji Wang, David Fleisher, Vangimalla R Reddy, and Chittaranjan Ray (2023). "Incorporation of carbon dioxide production and transport module into a Soil-Plant-Atmosphere continuum model". In: *Geoderma* 437, p. 116586. DOI: 10.1016/j.geoderma.2023.116586.

Beerling, David J et al. (2020). "Potential for large-scale CO_2 removal via enhanced rock weathering with croplands". In: *Nature* 583.7815, pp. 242–248. DOI: 10.1038/s41586-020-2448-9.

Bekchanova, Madina, Luca Campion, Stephan Bruns, Tom Kuppens, Johannes Lehmann, Marijke Jozefczak, Ann Cuypers, and Robert Malina (2024). "Biochar improves the nutrient cycle in sandy-textured soils and increases crop yield: a systematic review". In: *Environ. Evid.* 13.1, p. 3. DOI: 10.1186/s13750-024-00326-5.

Bernacchi, C J, C Pimentel, and Stephen P Long (2003). "In vivo temperature response functions of parameters required to model RuBP-limited photosynthesis". In: *Plant, Cell & Environment* 26.9, pp. 1419–1430. DOI: 10.1046/j.0016-8025.2003.01050.x.

Bernacchi, C J, EL Singsaas, C Pimentel, AR Portis Jr, and Stephen P Long (2001). "Improved temperature response functions for models of Rubisco-limited photosynthesis". In: *Plant, Cell & Environment* 24.2, pp. 253–259. DOI: 10.1111/j.1365-3040.2001.00668.x.

Bertagni, Matteo B, Salvatore Calabrese, Giuseppe Cipolla, Leonardo V Noto, and Amilcare Porporato (2025). "Advancing Enhanced Weathering modeling in soils: Critical comparison with experimental data". In: *J. Adv. Model. Earth Syst.* 17.1. DOI: 10.1029/2024MS004224.

Blanco-Canqui, Humberto (2017). "Biochar and soil physical properties". en. In: *Soil Sci. Soc. Am. J.* 81.4, pp. 687–711. DOI: 10.2136/sssaj2017.01.0017.

— (2021). "Does Biochar Improve All Soil Ecosystem Services?" In: *GCB Bioenergy* 13.2, pp. 291–304. DOI: 10.1111/gcbb.12783.

Blanco-Canqui, Humberto, David A Laird, Emily A Heaton, Samuel Rathke, and Bharat Sharma Acharya (2020). "Soil carbon increased by twice the amount of biochar carbon applied after 6 years: Field evidence of negative priming". In: *Glob. Change Biol. Bioenergy* 12.4, pp. 240–251. DOI: 10.1111/gcbb.12665.

Bohara, Hari, Syam Dodla, Jim Jian Wang, Murali Darapuneni, Bharat Sharma Acharya, Selim Magdi, and Kiran Pavuluri (2019). "Influence of poultry litter and biochar on soil water dynamics and nutrient leaching from a very fine sandy loam soil". In: *Soil and Tillage Research* 189, pp. 44–51. ISSN: 0167-1987. DOI: 10.1016/j.still.2019.01.001.

Bonan, Gordon (2019). *Climate change and terrestrial ecosystem modeling*. Cambridge University Press. DOI: 10.1017/9781107339217.

Buss, Wolfram, Heath Hasemer, Noah W Sokol, Eelco J Rohling, and Justin Borevitz (2024). "Applying minerals to soil to draw down atmospheric carbon dioxide through synergistic organic and inorganic pathways". In: *Commun. Earth Environ.* 5.1. DOI: 10.1038/s43247-024-01771-3.

Buss, Wolfram, Christian Wurzer, David A C Manning, Eelco J Rohling, Justin Borevitz, and Ondřej Mašek (2022). "Mineral-enriched biochar delivers enhanced nutrient recovery and carbon dioxide removal". In: *Commun. Earth Environ.* 3.1. DOI: 10.1038/s43247-022-00394-w.

Calvin, Katherine et al. (2023). "IPCC, 2023: Climate Change 2023: Synthesis Report, summary for Policymakers. Contribution of working groups I, II and III to the Sixth Assessment Report of the Intergovernmental Panel on Climate Change". In: pp. 1–34. DOI: 10.59327/ipcc/ar6-9789291691647.001.

Campbell, Gaylon S (1985). *Soil physics with BASIC: transport models for soil-plant systems*. Elsevier. ISBN: 9780080869827.

Cayuela, M L, L van Zwieten, B P Singh, S Jeffery, A Roig, and M A Sánchez-Monedero (2014). "Biochar's role in mitigating soil nitrous oxide emissions: A review and meta-analysis". In: *Agric. Ecosyst. Environ.* 191, pp. 5–16. DOI: 10.1016/j.agee.2013.10.009.

Chiaravalloti, Isabella, Nicolas Theunissen, Shuang Zhang, Jiuyuan Wang, Fengchao Sun, Ayesha A Ahmed, Evelin Pihlap, Christopher T Reinhard, and Noah J Planavsky (2023). "Mitigation of soil nitrous oxide emissions during maize production with basalt amendments". In: *Front. Clim.* 5. DOI: 10.3389/fclim.2023.1203043.

Ciais, P et al. (2010). "The European carbon balance. Part 2: croplands". In: *Glob. Chang. Biol.* 16.5, pp. 1409–1428. DOI: 10.1111/j.1365-2486.2009.02055.x.

Clarke, Lionel (2023). *Distributed Biochar Methodology Foundation v1.0: Digital MRV for distributed Biochar production and Carbon Dioxide removal (CDR) system*. Methodology Foundation. Version 1.0. Haarlem, Netherlands: I-TRACK Foundation. URL:

https://www.trackingstandard.org/wp-content/uploads/Distributed_Biochar_Methodology_Foundation_v1.0.pdf.

Deng, Mingshan, Xianhong Meng, Rebecca J Oliver, Yaqiong Lu, Bo Feng, and Xuan Gui (2026). "Enhanced water stress on vegetation productivity with climate warming over the Northern Hemisphere". In: *Atmos. Res.* 331.108639, p. 108639. DOI: 10.1016/j.atmosres.2025.108639.

Dietzen, Christiana, Robert Harrison, and Stephani Michelsen-Correa (2018). "Effectiveness of enhanced mineral weathering as a carbon sequestration tool and alternative to agricultural lime: An incubation experiment". In: *Int. J. Greenhouse Gas Control* 74, pp. 251–258. DOI: 10.1016/j.ijggc.2018.05.007.

Dil, Matthew and Maren Oelbermann (2014). "Chapter 13. Evaluating the long-term effects of pre-conditioned biochar on soil organic carbon in two southern Ontario soils using the century model". In: pp. 249–268. ISBN: 978-90-8686-235-1. DOI: 10.3920/978-90-8686-788-2_13.

Dupla, Xavier, Romane Claustre, Emma Bonvin, Iris Graf, Renée-Claire Le Bayon, and Stéphanie Grand (2024). "Let the dust settle: Impact of enhanced rock weathering on soil biological, physical, and geochemical fertility". In: *Sci. Total Environ.* 954.176297, p. 176297. DOI: 10.1016/j.scitotenv.2024.176297.

Dupla, Xavier, Benjamin Möller, Philippe C Baveye, and Stéphanie Grand (2023). "Potential accumulation of toxic trace elements in soils during enhanced rock weathering". In: *Eur. J. Soil Sci.* 74.1. DOI: 10.1111/ejss.13343.

DWD (n.d.). *Open Data Server of the German Meteorological Service (DWD)*. Accessed: 2024-01-01. URL: https://opendata.dwd.de/climate%5C_environment/CDC/observations%5C_germany/climate/hourly/.

Elnashar, Abdelrazek, Linjiang Wang, Bingfang Wu, Weiwei Zhu, and Hongwei Zeng (2021). "Synthesis of global actual evapotranspiration from 1982 to 2019". In: *Earth System Science Data* 13.2, pp. 447–480. DOI: 10.5194/essd-13-447-2021.

Entekhabi, Dara and Peter S Eagleson (1989). "Land surface hydrology parameterization for atmospheric general circulation models including subgrid scale spatial variability". In: *Journal of climate* 2.8, pp. 816–831.

Fang, C. and John.B. Moncrieff (1999). "A model for soil CO2 production and transport 1:: Model development". In: *Agricultural and Forest Meteorology* 95.4, pp. 225–236. ISSN: 0168-1923. DOI: 10.1016/S0168-1923(99)00036-2.

Farquhar, G D, S von Caemmerer, and J A Berry (1980). "A biochemical model of photosynthetic CO_2 assimilation in leaves of C3 species". In: *Planta* 149.1, pp. 78–90. DOI: 10.1007/bf00386231.

Filipović, Vilim et al. (2020). "Modeling Water Flow and Phosphorus Sorption in a Soil Amended with Sewage Sludge and Olive Pomace as Compost or Biochar". In: *Agronomy* 10.8. ISSN: 2073-4395. DOI: 10.3390/agronomy10081163.

Friedlingstein, Pierre et al. (2025). "Global carbon budget 2024". In: *Earth Syst. Sci. Data* 17.3, pp. 965–1039. DOI: 10.5194/essd-17-965-2025.

Fuhrman, Jay, Haewon McJeon, Scott C Doney, William Shobe, and Andres F Clarens (2019). "From zero to hero?: Why integrated assessment modeling of negative emissions technologies is hard and how we can do better". In: *Front. Clim.* 1. DOI: 10.3389/fclim.2019.00011.

Gao, Decai, Edith Bai, Siyu Wang, Shengwei Zong, Ziping Liu, Xianlei Fan, Chunhong Zhao, and Frank Hagedorn (2022). "Three-dimensional mapping of carbon, nitrogen, and phosphorus in soil microbial biomass and their stoichiometry at the global scale". In: *Glob. Chang. Biol.* 28.22, pp. 6728–6740. DOI: DOI:10.1111/gcb.16374.

Ghanem, Kholoud Z, Mostafa M A Hasham, Abdel-Nasser A El-Sheshtawy, Rasha S El-Serafy, and Mohamed H Sheta (2022). "Biochar stimulated actual evapotranspiration and wheat productivity under water deficit conditions in sandy soil based on non-weighing lysimeter". In: *Plants* 11.23, p. 3346. DOI: 10.3390/plants11233346.

Al-Ghussain, Loiy (2019). "Global warming: review on driving forces and mitigation". In: *Environ. Prog. Sustain. Energy* 38.1, pp. 13–21. DOI: 10.1002/ep.13041.

Głab, Tomasz, Joanna Palmowska, Tomasz Zaleski, and Krzysztof Gondek (2016). "Effect of biochar application on soil hydrological properties and physical quality of sandy soil". In: *Geoderma* 281, pp. 11–20. DOI: 10.1016/j.geoderma.2016.06.028.

Goll, D S, V Brovkin, B R Parida, C H Reick, J Kattge, P B Reich, P M van Bodegom, and Ü Niinemets (2012). "Nutrient limitation reduces land carbon uptake in simulations with a model of combined carbon, nitrogen and phosphorus cycling". In: *Biogeosciences* 9.9, pp. 3547–3569. DOI: 10.5194/bg-9-3547-2012.

Grafmüller, Jannis, Jens Möllmer, Claudia I Muehe E Marieand Kammann, Daniel Kray, Hans-Peter Schmidt, and Nikolas Hagemann (2024). "Granulation compared to co-application of biochar plus mineral fertilizer and its impacts on crop growth and nutrient leaching". In: *Sci. Rep.* 14.1, p. 16555. DOI: 10.1038/s41598-024-66992-0.

Gross, Arthur, Tobias Bromm, and Bruno Glaser (2021). "Soil organic carbon sequestration after biochar application: A global meta-analysis". In: *Agronomy (Basel)* 11.12, p. 2474. DOI: 10.3390/agronomy11122474.

Gross, Arthur, Tobias Bromm, Steven Polifka, Daniel Fischer, and Bruno Glaser (2024). "Long-term biochar and soil organic carbon stability - Evidence from field experiments in Germany". In: *Sci. Total Environ.* 954.176340, p. 176340. DOI: 10.1016/j.scitotenv.2024.176340.

Guenet, Bertrand, Marta Camino-Serrano, Philippe Ciais, Marwa Tifafi, Fabienne Maignan, Jennifer L Soong, and Ivan A Janssens (2018). "Impact of priming on global soil carbon stocks". In: *Glob. Chang. Biol.* 24.5, pp. 1873–1883. DOI: 10.1111/gcb.14069.

Guo, Fenglei, Chen Wang, Shuang Wang, Xiaorong Zhao, Guitong Li, and Zhencai Sun (2024). "The native SOC increase in woodland and lawn soil amended with biochar

surpassed greenhouse - A seven-year field trial". In: *Sci. Total Environ.* 907.167924, p. 167924. DOI: 10.1016/j.scitotenv.2023.167924.

Gurumurthy, G P, K Balakrishna, Jean Riotte, Jean-Jacques Braun, Stéphane Audry, H N Udaya Shankar, and B R Manjunatha (2012). "Controls on intense silicate weathering in a tropical river, southwestern India". In: *Chem. Geol.* 300-301, pp. 61–69. DOI: 10.1016/j.chemgeo.2012.01.016.

Hagemann, Nikolas, Hans-Peter Schmidt, Thomas D Bucheli, Jannis Grafmüller, Silvio Vosswinkel, Volker Herdegen, William Meredith, Clement N Uguna, and Colin E Snape (2025). "Proxies for use in biochar decay models: Hydropyrolysis, electric conductivity, and H/Corg molar ratio". In: *PLoS One* 20.9. DOI: 10.1371/journal.pone.0330206.

Halder, Suman, Susanne K M Arens, Kai Jensen, Tais W Dahl, and Philipp Porada (2022). "A dynamic local-scale vegetation model for lycopsids (LYCOm v1.0)". In: *Geoscientific Model Development* 15.5, pp. 2325–2343. DOI: 10.5194/gmd-15-2325-2022.

Hamburger, Susanne E., Carolyn-M. Görres, Nikolas Hagemann, Johannes Meyer zu Drewer, Maria Ansari, Christof-M. Geilfus, and Claudia Kammann (in prep.). "The effects of biochar in combined application with rock powder on agricultural parameters and on soil greenhouse gas emission".

Han, Mengjie et al. (2024). "Modeling biochar effects on soil organic carbon on croplands in a microbial decomposition model (MIMICS-BC_v1.0)". In: 17.12, pp. 4871–4890. DOI: 10.5194/gmd-17-4871-2024.

Hartmann, Jens, Annette Eschenbach, Christian Beer, Philipp Porada, Joscha N. Becker, Hans-Peter Schmidt, Nikolas Hagemann, Claudia I Kammann, and Alexander Popp (2021). *Pyrogenic carbon and carbonating minerals (PyMiCCS) for enhanced plant growth and carbon capture and storage*. BMBF Proposal to application call: CDR - Carbon Dioxide Removal.

Hartmann, Jens, A Joshua West, Phil Renforth, Peter Köhler, Christina L De La Rocha, Dieter A Wolf-Gladrow, Hans H Dürr, and Jürgen Scheffran (2013). "Enhanced chemical weathering as a geoengineering strategy to reduce atmospheric carbon dioxide, supply nutrients, and mitigate ocean acidification". In: *Rev. Geophys.* 51.2, pp. 113–149. DOI: 10.1002/rog.20004.

He, Yanghui et al. (2017). "Effects of biochar application on soil greenhouse gas fluxes: A meta-analysis". In: *Gcb Bioenergy* 9.4, pp. 743–755. DOI: 10.1111/gcbb.12376.

Hersbach, Hans et al. (2020). "The ERA5 global reanalysis". In: *Quarterly Journal of the Royal Meteorological Society* 146.730. Accessed: 2020-12-01, pp. 1999–2049.

Honvault, Nicolas, Marie-Laure Tiouchichine, Joana Sauze, Clément Piel, Damien Landais, Sébastien Devidal, Emmanuel Gritti, Delphine Bosch, and Alexandru Milcu (2024). "Additive effects of basalt enhanced weathering and biochar co-application on carbon

sequestration, soil nutrient status and plant performance in a mesocosm experiment". In: *Appl. Geochem.* 169.106054, p. 106054. DOI: 10.1016/j.apgeochem.2024.106054.

Horel, Ágota, Eszter Tóth, Györgyi Gelybó, Márton Dencső, and Csilla Farkas (2019). "Biochar Amendment Affects Soil Water and CO2 Regime during Capsicum Annuum Plant Growth". In: *Agronomy* 9.2. ISSN: 2073-4395. DOI: 10.3390/agronomy9020058.

Howell, Alexandra, Sophia Helmkamp, and Erica Belmont (2022). "Stable polycyclic aromatic carbon (SPAC) formation in wildfire chars and engineered biochars". In: *Sci. Total Environ.* 849.157610, p. 157610. DOI: 10.1016/j.scitotenv.2022.157610.

Huang, Xiang, Charles J Abolt, and Katrina E Bennett (2023). "Brief Communication: Effects of different saturation vapor pressure calculations on simulated surface-subsurface hydrothermal regimes at a permafrost field site". In: *The Cryosphere Discussions* 2023, pp. 1–15. DOI: 10.5194/tc-2023-8.

Jesus Paula, Rafaela de et al. (2025). "Pyrolysis converts urban pruning waste into biochar with soil and climate benefits". In: *Sci. Rep.* 15.1, p. 45071. DOI: 10.1038/s41598-025-32360-9.

Jiang, Zhen, Shuang Huang, and Zhuowen Meng (2025). "Long-term effects of biochar on the hydraulic properties of soil: A meta-analysis based on 1–10 years field experiments". In: *Geoderma* 458.117318, p. 117318. DOI: 10.1016/j.geoderma.2025.117318.

Jiang, Zhixiang, Fei Lian, Zhenyu Wang, and Baoshan Xing (2019). "The role of biochars in sustainable crop production and soil resiliency". In: *Journal of Experimental Botany* 71.2, pp. 520–542. ISSN: 0022-0957. DOI: 10.1093/jxb/erz301.

Joseph, Stephen et al. (2010). "An investigation into the reactions of biochar in soil". In: *Soil Res.* 48.7, p. 501. DOI: 10.1071/SR10009.

Joseph, Stephen et al. (2021). "How biochar works, and when it doesn't: A review of mechanisms controlling soil and plant responses to biochar". In: *Glob. Change Biol. Bioenergy* 13.11, pp. 1731–1764. DOI: 10.1111/gcbb.12885.

Kalu, Subin, Aino Seppänen, Kevin Z Mganga, Outi-Maaria Sietiö, Bruno Glaser, and Kristiina Karhu (Jan. 2024). "Biochar reduced the mineralization of native and added soil organic carbon: evidence of negative priming and enhanced microbial carbon use efficiency". In: *Biochar* 6.1. DOI: 10.1007/s42773-023-00294-y.

Keerthi, Murugesan Mohana (2024). "Innovative approaches to carbon sequestration emerging technologies and global impacts on climate change mitigation". In: *Environmental Reports* 6.2, pp. 15–18. DOI: 10.51470/er.2024.6.2.15.

Kujawska, Justyna (2023). "Content of heavy metals in various biochar and assessment environmental risk". In: *Journal of Ecological Engineering* 24.8, pp. 287–295. DOI: 10.12911/22998993/166557.

Lawrence, David M and Andrew G Slater (2008). "Incorporating organic soil into a global climate model". In: *Clim. Dyn.* 30.2-3, pp. 145–160. DOI: 10.1007/s00382-007-0278-1.

Lee, Ming-Hsi, Ed-Haun Chang, Chia-Hsing Lee, Jyun-Yuan Chen, and Shih-Hao Jien (2021). "Effects of biochar on soil aggregation and distribution of organic carbon fractions in aggregates". In: *Processes (Basel)* 9.8, p. 1431. DOI: 10.3390/pr9081431.

Lefebvre, David, Anna Williams, Jeroen Meersmans, and et al. (2020). "Modelling the Potential for Soil Carbon Sequestration Using Biochar from Sugarcane Residues in Brazil". In: *Scientific Reports* 10, p. 19479. DOI: 10.1038/s41598-020-76470-y.

Lehmann, Johannes, Annette Cowie, Caroline A Masiello, Claudia Kammann, Dominic Woolf, James E Amonette, Maria L Cayuela, Marta Camps-Arbestain, and Thea Whitman (2021). "Biochar in climate change mitigation". In: *Nat. Geosci.* 14.12, pp. 883–892. DOI: 10.1038/s41561-021-00852-8.

Li, Chaojun et al. (2022). "High-resolution mapping of the global silicate weathering carbon sink and its long-term changes". In: *Glob. Chang. Biol.* 28.14, pp. 4377–4394. DOI: 10.1111/gcb.16186.

Li, Zhi-Long et al. (2021). "Changes in net ecosystem exchange of CO_2 in Arctic and their relationships with climate change during 2002–2017". In: *Adv. Clim. Chang. Res.* 12.4, pp. 475–481. DOI: 10.1016/j.accre.2021.06.004.

Liddle, Kaylin, Terence McGonigle, and Alexander Koiter (2020). "Microbe biomass in relation to organic carbon and clay in soil". In: *Soil Syst.* 4.3, p. 41. DOI: 10.3390/soilsystems4030041.

Liu, Shuwei, Yaojun Zhang, Yajie Zong, Zhiqiang Hu, Shuang Wu, JIE Zhou, Yaguo Jin, and Jianwen Zou (2016). "Response of soil carbon dioxide fluxes, soil organic carbon and microbial biomass carbon to biochar amendment: a meta-analysis". In: *Gcb Bioenergy* 8.2, pp. 392–406. DOI: 10.1111/gcbb.12265.

Liu, Weixing, Zhe Zhang, and Shiqiang Wan (Jan. 2009). "Predominant role of water in regulating soil and microbial respiration and their responses to climate change in a semiarid grassland". In: *Glob. Chang. Biol.* 15.1, pp. 184–195. DOI: 10.1111/j.1365-2486.2008.01728.x.

Liu, Xiaoyu, Afeng Zhang, Chunying Ji, Stephen Joseph, Rongjun Bian, Lianqing Li, Genxing Pan, and Jorge Paz-Ferreiro (2013). "Biochar's effect on crop productivity and the dependence on experimental conditions—a meta-analysis of literature data". In: *Plant Soil* 373.1-2, pp. 583–594. DOI: 10.1007/s11104-013-1806-x.

Lotz, Simon, Thomas D Bucheli, Hans-Peter Schmidt, and Nikolas Hagemann (2024). "Quantification of soil organic carbon: the challenge of biochar-induced spatial heterogeneity". In: *Front. Clim.* 6. DOI: 10.3389/fclim.2024.1344524.

Lychuk, Taras, Roberto Izaurralde, Robert Hill, William Mcgill, and Jimmy Williams (2014). "Biochar as a global change adaptation: predicting biochar impacts on crop productivity and soil quality for a tropical soil with the Environmental Policy Integrated Climate (EPIC) model". In: *Mitigation and Adaptation Strategies for Global Change* 20, pp. 1437–1458. DOI: 10.1007/s11027-014-9554-7.

Ma, Liwei (2020). "Effects of spatial-temporal land cover distribution on gross primary production and net primary production in Schleswig-Holstein, northern Germany". In: *Carbon Balance Manag.* 15.1, p. 3. DOI: 10.1186/s13021-020-00138-3.

Ma, Yunyao, Maaike Y Bader, Imke Petersen, and Philipp Porada (2024). "Quantifying the effect of competition on the functional assembly of bryophyte and lichen communities: A process-based model analysis". In: *Journal of Ecology* 112.5, pp. 998–1012. DOI: 10.1111/1365-2745.14279.

Maaroufi, Nadia (2016). "The effect of simulated anthropogenic nitrogen deposition on the net carbon balance of boreal soils". PhD thesis. Acta Universitatis agriculturae Sueciae.

Major, Julie (2010). *Guidelines on Practical Aspects of Biochar Application to Field Soil in Various Soil Management Systems*. Tech. rep.

Manickam, Theeba, Gerard Cornelissen, Robert Bachmann, Illani Ibrahim, Jan Mulder, and Sarah Hale (2015). "Biochar application in Malaysian sandy and acid sulfate soils: Soil amelioration effects and improved crop production over two cropping seasons". In: *Sustainability* 7.12, pp. 16756–16770. DOI: 10.3390/su71215842.

Marazza, Diego, Simone Pesce, Nicolas Greggio, Francesco Primo Vaccari, Enrico Balugani, and Alessandro Buscaroli (2022). "The long-term experiment platform for the study of agronomical and environmental effects of the biochar: Methodological framework". In: *Agriculture* 12.8, p. 1244. DOI: 10.3390/agriculture12081244.

Maslouski, Mikita, Annette Eschenbach, Christian Beer, Simon Thomsen, and Philipp Porada (2025a). "Soil and vegetation responses to biochar application in terms of its feedback on carbon sequestration under different environmental conditions - LiDELS model overview". In: *Environ. Res. Lett.* DOI: 10.1088/1748-9326/adbfa6.

Maslouski, Mikita and Philipp Porada (2024). *LiBry-DETECT Layer Scheme model*. DOI: 10.5281/zenodo.14849558.

— (2025). *LiBry-DETECT Layer Scheme model v2*. DOI: 10.5281/zenodo.16151579.

Maslouski, Mikita et al. (2025b). "Long-term carbon dioxide removal potential from the application of wood biochar and basanite rock powder in sandy soil using the LiDELSv2 process-based modeling approach". In: *Environ. Res. Lett.* DOI: 10.1088/1748-9326/ae21f6.

Meyer zu Drewer, Johannes and Nikolas Hagemann (2025). *Industrial production and characterization of biochar and rock-enhanced biochar [Data set]*. DOI: 10.5281/zenodo.15840176.

Meyer zu Drewer, Johannes et al. (2025). "Pyrogenic Carbon and Carbonating Minerals for Carbon Capture and Storage (PyMiCCS) Part I: Production, Physico-Chemical Characterization and C-Sink Potential". In: *Frontiers in Climate* 7. DOI: 10.3389/fclim.2025.1631368.

Mia, S, F A Dijkstra, and B Singh (2017). "Long-term aging of biochar". In: *Advances in Agronomy* series, pp. 1–51. DOI: 10.1016/bs.agron.2016.10.001.

Miralles, Diego G et al. (2025). "GLEAM4: global land evaporation and soil moisture dataset at 0.1 resolution from 1980 to near present". In: *Sci. Data* 12.1, p. 416. DOI: 10.1038/s41597-025-04610-y.

Mollinedo, Javier, Thomas E. Schumacher, and Rajesh Chintala (2015). "Influence of feedstocks and pyrolysis on biochar's capacity to modify soil water retention characteristics". In: *Journal of Analytical and Applied Pyrolysis* 114, pp. 100–108. ISSN: 0165-2370. DOI: 10.1016/j.jaap.2015.05.006.

Monteith, J. L. (1981). "Evaporation and Surface Temperature". In: *Quarterly Journal of the Royal Meteorological Society* 107.451, pp. 1–27. DOI: 10.1002/qj.49710745102.

El-Naggar, Ahmed H., Adel R.A. Usman, Abdulrasoul Al-Omran, Yong Sik Ok, Mahtab Ahmad, and Mohammad I. Al-Wabel (2015). "Carbon mineralization and nutrient availability in calcareous sandy soils amended with woody waste biochar". In: *Chemosphere* 138, pp. 67–73. ISSN: 0045-6535. DOI: 10.1016/j.chemosphere.2015.05.052.

Nockolds, S R (1954). "Average chemical compositions of some igneous rocks". In: *Geol. Soc. Am. Bull.* 65.10, p. 1007. DOI: 10.1130/0016-7606(1954)65[1007:ACCOSI]2.0.CO;2.

Obia, Alfred, Trond Børresen, Vegard Martinsen, Gerard Cornelissen, and Jan Mulder (2017). "Effect of biochar on crust formation, penetration resistance and hydraulic properties of two coarse-textured tropical soils". In: *Soil Tillage Res.* 170, pp. 114–121. DOI: 10.1016/j.still.2017.03.009.

Oliveira Garcia, Wagner de, Thorben Amann, Jens Hartmann, Kristine Karstens, Alexander Popp, Lena R Boysen, Pete Smith, and Daniel Goll (2020). "Impacts of enhanced weathering on biomass production for negative emission technologies and soil hydrology". In: *Biogeosciences* 17.7, pp. 2107–2133. DOI: 10.5194/bg-17-2107-2020.

Pan, Shufen et al. (2020). In: *Hydrology and Earth System Sciences* 24.3, pp. 1485–1509. DOI: 10.5194/hess-24-1485-2020.

Pate, John S and David B Layzell (1981). "Carbon and nitrogen partitioning in the whole plant — A thesis based on empirical modeling". In: *Nitrogen and Carbon Metabolism*. Dordrecht: Springer Netherlands, pp. 94–134. DOI: 10.1007/978-94-009-8267-3_4.

Poeplau, Christopher et al. (2020). "Stocks of organic carbon in German agricultural soils—Key results of the first comprehensive inventory". In: *J. Plant Nutr. Soil Sci.* 183.6, pp. 665–681. DOI: 10.1002/jpln.202000113.

Poggio, Laura, Luis M de Sousa, Niels H Batjes, Gerard B M Heuvelink, Bas Kempen, Eloi Ribeiro, and David Rossiter (2021). "SoilGrids 2.0: producing soil information for the globe with quantified spatial uncertainty". In: *SOIL* 7.1, pp. 217–240. DOI: 10.5194/soil-7-217-2021.

Porada, Philipp, T. M. Lenton, A. Pohl, B. Weber, L. Mander, Y. Donnadieu, C. Beer, U. Pöschl, and A. Kleidon (2016). "High potential for weathering and climate effects of non-vascular vegetation in the Late Ordovician". In: *Nature Communications* 7, p. 12113. DOI: 10.1038/ncomms12113.

Porada, Philipp, B Weber, W Elbert, U Pöschl, and Axel Kleidon (2013). "Estimating global carbon uptake by lichens and bryophytes with a process-based model". In: *Biogeosciences* 10.11, pp. 6989–7033. DOI: 10.5194/bg-10-6989-2013.

Poyda, Arne, Thorsten Reinsch, Christof Kluß, Ralf Loges, and Friedhelm Taube (2016). "Greenhouse gas emissions from fen soils used for forage production in northern Germany". In: *Biogeosciences* 13.18, pp. 5221–5244. DOI: 10.5194/bg-13-5221-2016.

Renforth, P and J S Campbell (2021). "The role of soils in the regulation of ocean acidification". In: *Philos. Trans. R. Soc. Lond. B Biol. Sci.* 376.1834, p. 20200174. DOI: 10.1098/rstb.2020.0174.

Renforth, Phil and Gideon Henderson (2017). "Assessing ocean alkalinity for carbon sequestration". In: *Rev. Geophys.* 55.3, pp. 636–674. DOI: 10.1002/2016RG000533.

Risk, David, Lisa Kellman, and Hugo Beltrami (2002). "Carbon dioxide in soil profiles: production and temperature dependence". In: *Geophysical research letters* 29.6, pp. 11–1. DOI: 10.1029/2001GL014002.

Rohling, Eelco J, Ivan D Haigh, Gavin L Foster, Andrew P Roberts, and Katharine M Grant (2013). "A geological perspective on potential future sea-level rise". In: *Sci. Rep.* 3.1, p. 3461. DOI: 10.1038/srep03461.

Ronix, Amanda, Eduardo Carvalho da Silva Neto, Carlos Eduardo Pellegrino Cerri, Agnieszka Ewa Latawiec, and João Luís Nunes Carvalho (2025). "Incorporating biochar into biogeochemical models: Achievements and challenges". In: 17.5. DOI: 10.1111/gcbb.70037.

Ryan, Edmund M, Kiona Ogle, Heather Kropp, Kimberly E Samuels-Crow, Yolima Carrillo, and Elise Pendall (2018). "Modeling soil CO_2 production and transport with dynamic source and diffusion terms: testing the steady-state assumption using DETECT v1.0". In: *Geosci. Model Dev.* 11.5, pp. 1909–1928. DOI: 10.5194/gmd-11-1909-2018.

Ryan, Peter C. et al. (2024). "The potential for carbon dioxide removal by enhanced rock weathering in the tropics: An evaluation of Costa Rica". In: *Sci. Total Environ.* 927.172053, p. 172053. DOI: 10.1016/j.scitotenv.2024.172053.

Safaei Khorram, Mahdi, Gan Zhang, Akram Fatemi, Rudolf Kiefer, Adeel Mahmood, Sasan Jafarnia, Mohammad Pauzi Zakaria, and Gang Li (2020). "Effect of walnut shell biochars on soil quality, crop yields, and weed dynamics in a 4-year field experiment". In: *Environ. Sci. Pollut. Res. Int.* 27.15, pp. 18510–18520. DOI: 10.1007/s11356-020-08335-w.

Sagrilo, Edvaldo, Simon Jeffery, Ellis Hoffland, and Thomas W Kuyper (2015). "Emission of CO 2 from biochar-amended soils and implications for soil organic carbon". In: *Gcb Bioenergy* 7.6, pp. 1294–1304. DOI: 10.1111/gcbb.12234.

Samuels-Crow, Kimberly E, Edmund Ryan, Elise Pendall, and Kiona Ogle (2018). "Temporal Coupling of Subsurface and Surface Soil CO2 Fluxes: Insights From a Nonsteady

State Model and Cross-Wavelet Coherence Analysis". In: *Journal of Geophysical Research: Biogeosciences* 123.4, pp. 1406–1424. DOI: 10.1002/2017JG004207.

Schaap, Marcel G, Feike J Leij, and Martinus Van Genuchten (2001). "Rosetta : A computer program for estimating soil hydraulic parameters with hierarchical pedotransfer functions". In: *Journal of Hydrology* 251.3, pp. 163–176. ISSN: 0022-1694. DOI: 10.1016/S0022-1694(01)00466-8.

Schmidt, Hans-Peter, Andrés Anca-Couce, Nikolas Hagemann, Constanze Werner, Dieter Gerten, Wolfgang Lucht, and Claudia Kammann (2019). "Pyrogenic carbon capture and storage". In: *Glob. Change Biol. Bioenergy* 11.4, pp. 573–591. DOI: 10.1111/gcbb.12553.

Schmidt, Hans-Peter, Claudia Kammann, and Nikolas Hagemann (2024). *Global Biochar C-Sink Standard*. https://www.carbon-standards.com/docs/transfer/4000039EN.pdf. online; accessed 1 April 2025.

Schmidt, Hans-Peter, Claudia Kammann, Nikolas Hagemann, Jens Leifeld, Thomas D Bucheli, Miguel Angel Sánchez Monedero, and Maria Luz Cayuela (2021). "Biochar in agriculture – A systematic review of 26 global meta-analyses". In: *Glob. Change Biol. Bioenergy* 13.11, pp. 1708–1730. DOI: 10.1111/gcbb.12889.

Simunek, Jiri, Diederik Jacques, Miroslav Šejna, and Martinus Van Genuchten (2012). *The HP2 Program for HYDRUS (2D/3D) A Coupled Code for Simulating Two-Dimensional Variably- Saturated Water Flow, Head Transport, Solute Transport and Biogeochemistry in Porous Media (HYDRUS + PHREEQC + 2D)*. Tech. rep. Version 1.0, p. 76. URL: https://www.pc-progress.com/Documents/HYDRUS3D_HP2_Manual.pdf.

Simunek, Jiri, M Th Van Genuchten, and M Sejna (2005). "The HYDRUS-1D software package for simulating the one-dimensional movement of water, heat, and multiple solutes in variably-saturated media". In: *University of California-Riverside Research Reports* 3, pp. 1–240.

Skaggs, Todd and Ehsan Ghane (2017). *Rosetta model*. Accessed: 2024-10-24. URL: https://www.handbook60.org/rosetta/.

Skov, Kirstine et al. (2024). "Initial agronomic benefits of enhanced weathering using basalt: A study of spring oat in a temperate climate". In: *PLoS One* 19.3, e0295031. DOI: 10.1371/journal.pone.0295031.

Smith, Pete (2004). "How long before a change in soil organic carbon can be detected?" In: *Glob. Chang. Biol.* 10.11, pp. 1878–1883. DOI: 10.1111/j.1365-2486.2004.00854.x.

Smith, Pete et al. (2020). "How to measure, report and verify soil carbon change to realize the potential of soil carbon sequestration for atmospheric greenhouse gas removal". In: *Glob. Chang. Biol.* 26.1, pp. 219–241. DOI: 10.1111/gcb.14815.

Smith, S M et al. (2024). "The state of carbon dioxide removal - 2nd edition". In: *The State of Carbon Dioxide Removal*. DOI: 10.17605/OSF.IO/F85QJ.

Song, Xinzhang, Genxing Pan, Chao Zhang, Lu Zhang, and Hailong Wang (2016). "Effects of biochar application on fluxes of three biogenic greenhouse gases: a meta-analysis". In: *Ecosyst. Health Sustain.* 2.2, e01202. DOI: 10.1002/ehs2.1202.

Stylianou, Marios, Apostolos Christou, Panagiotis Dalias, Christakis Polycarpou, Philip Michael, Athos Agapiou, Panayiotis Papanastasiou, and Despo Fatta-Kassinos (2021). "Assessing the influence of biochars on the hydraulic properties of a loamy sand soil". In: *Biomass Conversion and Biorefinery* 11, pp. 2191–2207. DOI: 10.1007/s13399-020-01114-0.

Šurda, Peter, Justína Vitková, L'ubomír Lichner, Natália Botková, and Lucia Toková (2024). "Effect of wettable and hydrophobic biochar addition on properties of sandy soil". In: *Biologia*, pp. 1–12. DOI: 10.1007/s11756-024-01702-9.

Swoboda, Philipp, Thomas F Döring, and Martin Hamer (2022). "Remineralizing soils? The agricultural usage of silicate rock powders: A review". In: *Sci. Total Environ.* 807.Pt 3, p. 150976. DOI: 10.1016/j.scitotenv.2021.150976.

Tang, J Y and W J Riley (2013). "A total quasi-steady-state formulation of substrate uptake kinetics in complex networks and an example application to microbial litter decomposition". In: *Biogeosciences* 10.12, pp. 8329–8351. DOI: 10.5194/bg-10-8329-2013.

Taylor, Lyla L, Steve A Banwart, J Leake, and David J Beerling (2011). "Modeling the evolutionary rise of ectomycorrhiza on sub-surface weathering environments and the geochemical carbon cycle". In: *Am. J. Sci.* 311.5, pp. 369–403. DOI: 10.2475/05.2011.01.

Taylor, Lyla L, David J Beerling, Shaun Quegan, and Steven A Banwart (2017). "Simulating carbon capture by enhanced weathering with croplands: an overview of key processes highlighting areas of future model development". In: *Biol. Lett.* 13.4, p. 20160868. DOI: 10.1098/rsbl.2016.0868.

Taylor, Lyla L, Joe Quirk, Rachel M S Thorley, Pushker A Kharecha, James Hansen, Andy Ridgwell, Mark R Lomas, Steve A Banwart, and David J Beerling (2016). "Enhanced weathering strategies for stabilizing climate and averting ocean acidification". In: *Nat. Clim. Chang.* 6.4, pp. 402–406. DOI: 10.1038/nclimate2882.

Thao, Touyee, Bhavna Arora, and Teamrat A. Ghezzehei (2023). "Impact of biochar amendments on soil water and plant uptake dynamics under different cropping systems". In: *Vadose Zone Journal*, e20266. DOI: 10.1002/vzj2.20266.

Thomsen, Simon (2018). "Impact of soil water availability and local climate in urban environments on water use of mature pedunculate oaks (Quercus robur L.)" PhD thesis. Staats-und Universitätsbibliothek Hamburg Carl von Ossietzky.

Tomczyk, Agnieszka, Zofia Sokołowska, and Patrycja Boguta (2020). "Biochar physicochemical properties: pyrolysis temperature and feedstock kind effects". In: *Rev. Environ. Sci. Biotechnol.* 19.1, pp. 191–215. DOI: 10.1007/s11157-020-09523-3.

Usowicz, Bogusław, Jerzy Lipiec, Mateusz Łukowski, Wojciech Marczewski, and Jerzy Usowicz (2016). "The effect of biochar application on thermal properties and albedo of loess soil under grassland and fallow". In: *Soil and Tillage Research* 164. Current and future challenges in biochar research, pp. 45–51. ISSN: 0167-1987. DOI: 10.1016/j.still.2016.03.009.

Van Genuchten, Martinus (1980). "A Closed-form Equation for Predicting the Hydraulic Conductivity of Unsaturated Soils1". In: *Soil Science Society of America Journal* 44. DOI: 10.2136/sssaj1980.03615995004400050002x.

Vereecken, H, M Weynants, M Javaux, Y Pachepsky, M G Schaap, and M Th van Genuchten (2010). "Using pedotransfer functions to estimate the van Genuchten–Mualem soil hydraulic properties: A review". In: *Vadose Zone J.* 9.4, pp. 795–820. DOI: 10.2136/vzj2010.0045.

Vienne, Arthur, Silvia Poblador, Miguel Portillo-Estrada, Jens Hartmann, Samuel Ijiehon, Peter Wade, and Sara Vicca (2022). "Enhanced weathering using basalt rock powder: Carbon sequestration, co-benefits and risks in a mesocosm study with Solanum tuberosum". In: *Front. Clim.* 4. DOI: 10.3389/fclim.2022.869456.

Vitková, Justína, Peter Šurda, Ľubomír Lichner, and Roman Výleta (2024). "Influence of biochar application rate, particle size, and pyrolysis temperature on hydrophysical parameters of sandy soil". In: *Appl. Sci. (Basel)* 14.8, p. 3472. DOI: 10.3390/app14083472.

Vorrath, Maria-Elena et al. (2025). "Pyrogenic Carbon and Carbonating Minerals for Carbon Capture and Storage (PyMiCCS) Part II: Organic and Inorganic Carbon Dioxide Removal in an Oxisol." In: *Frontiers in Climate* 7. DOI: 10.3389/fclim.2025.1592454.

Wang, Jinyang, Zhengqin Xiong, and Yakov Kuzyakov (2016). "Biochar stability in soil: meta-analysis of decomposition and priming effects". In: *Glob. Change Biol. Bioenergy* 8.3, pp. 512–523. DOI: 10.1111/gcbb.12266.

Wang, Tongtong, Catherine E Stewart, Jiangbo Ma, Jiyong Zheng, and Xingchang Zhang (2017). "Applicability of five models to simulate water infiltration into soil with added biochar". In: *Journal of Arid Land* 9, pp. 701–711. DOI: 10.1007/s40333-017-0025-3.

Weber, Kathrin and Peter Quicker (2018). "Properties of biochar". In: *Fuel (Lond.)* 217, pp. 240–261. DOI: 10.1016/j.fuel.2017.12.054.

Weng, Zhe Han et al. (2022). "Microspectroscopic visualization of how biochar lifts the soil organic carbon ceiling". In: *Nat. Commun.* 13.1, p. 5177. DOI: 10.1038/s41467-022-32819-7.

Wild, Bastien, Ruben Gerrits, and Steeve Bonneville (2022). "The contribution of living organisms to rock weathering in the critical zone". In: *Npj Mater. Degrad.* 6.1. DOI: 10.1038/s41529-022-00312-7.

Wordell-Dietrich, Patrick, Anja Wotte, Janet Rethemeyer, Jörg Bachmann, Mirjam Helfrich, Kristina Kirfel, Christoph Leuschner, and Axel Don (2020). "Vertical partitioning of CO_2 production in a forest soil". In: *Biogeosciences* 17.24, pp. 6341–6356. DOI: 10.5194/bg-17-6341-2020.

Wu, Wenao et al. (2022). "Impact of biochar amendment on soil hydrological properties and crop water use efficiency: A global meta-analysis and structural equation model". In: *Glob. Change Biol. Bioenergy* 14.6, pp. 657–668. DOI: 10.1111/gcbb.12933.

Wu, Y, A Yang, Y Zhao, and Z Liu (2019). "Simulation of soil water movement under biochar application based on the hydrus-1D in the black soil region of China". In: *Applied Ecology and Environmental Research* 17, pp. 4183–4192. DOI: 10.15666/aeer/1702_41834192.

Xiong, Kun, Yuqing Feng, Hua Jin, Sihai Liang, Kaining Yu, Xingxing Kuang, and Li Wan (2023). "A new model to predict soil thermal conductivity". In: *Scientific Reports* 13.1, p. 10684. DOI: 10.1038/s41598-023-37413-5.

Yang, Jingrui et al. (2025). "Sustained benefits of long-term biochar application for food security and climate change mitigation". In: *Proc. Natl. Acad. Sci. U. S. A.* 122.33, e2509237122. DOI: 10.1073/pnas.2509237122.

Ye, Lili, Marta Camps-Arbestain, Qinhua Shen, Johannes Lehmann, Balwant Singh, and Muhammad Sabir (2020). "Biochar effects on crop yields with and without fertilizer: A meta-analysis of field studies using separate controls". In: *Soil Use Manag.* 36.1, pp. 2–18. DOI: 10.1111/sum.12546.

Yu, Lin, Thomas Kleinen, Min Jung Kwon, Christian Knoblauch, and Christian Beer (2025). "Biochar-induced soil property changes may reduce temperature and precipitation extremes: Insights from Earth system model experiments". DOI: 10.5194/egusphere-2025-4648.

Zakkour, Paul and Greg Cook (2024). *Measurement, reporting and verification (MRV) and accounting for carbon dioxide removal (CDR) in the context of both project-based approaches and national greenhouse gas inventories (NGHGI)*. Technical Report. Cheltenham, UK: IEA Greenhouse Gas R&D Programme (IEAGHG). URL: https://publications.ieaghg.org/technicalreports/2024-09%20Measurement,%20reporting%20and%20verification%20of%20CDR.pdf.

Zhang, Qingzhong, Yiding Wang, Yongfeng Wu, Xiahui Wang, Zhangliu Du, Xingren Liu, and Jiqing Song (2013). "Effects of biochar amendment on soil thermal conductivity, reflectance, and temperature". In: *Soil Science Society of America Journal* 77.5, pp. 1478–1487. DOI: 10.2136/sssaj2012.0180.

Zhang, Yangyang, Xueyu Hu, Juan Zou, Di Zhang, Wei Chen, Yang Liu, Yaojun Chen, and Xiangqian Wang (2018). "Response of surface albedo and soil carbon dioxide fluxes to biochar amendment in farmland". In: *J. Soils Sediments* 18.4, pp. 1590–1601. DOI: 10.1007/s11368-017-1889-8.

Zimmerman, Andrew R (2010). "Abiotic and microbial oxidation of laboratory-produced black carbon (biochar)". In: *Environ. Sci. Technol.* 44.4, pp. 1295–1301. DOI: 10.1021/es903140c.

Zong, Yutong, Qing Xiao, and Shenggao Lu (2016). "Acidity, water retention, and mechanical physical quality of a strongly acidic Ultisol amended with biochars derived from different feedstocks". In: *J. Soils Sediments* 16.1, pp. 177–190. DOI: 10.1007/s11368-015-1187-2.